RADIO-ECHO LAYERING IN POLAR ICE SHEETS

DAVID HUGH MACFARLANE MILLAR

A dissertation submitted for the degree of

Doctor of Philosophy

in the University of Cambridge

Darwin College,
Cambridge.
November 1981

PREFACE

This dissertation is an account of work carried out by the author at the Scott Polar Research Institute during the last three years under the direction of Dr. G.de Q.Robin.

The dissertation does not exceed the regulations in length, and has not been submitted for a degree at any other university. Although the data collection necessarily involved team-work, all other work is the original work of the author, unless otherwise stated.

SUMMARY

This thesis is concerned with layered reflections observed in the Antarctic and Greenland ice sheets during radio-echo sounding. It describes in detail layering seen with 60 and 300 MHz equipment in the Antarctic ice sheet during three field seasons between 1974 and 1979, and discusses the effects of glaciological and equipment factors, particularly radio pulse length. The effects of changing pulse length and accumulation rate on layer echo separation are analysed, and the importance of closely spaced groups of reflectors assessed.

Reflection coefficient vs depth profiles are presented for layering observed at nearly twenty sites in the Antarctic and Greenland, and are used to demonstrate the existence of two separate reflection mechanisms: changes in (a) ice density, and (b) loss tangent. Supporting density and conductivity data from ice cores are summarised. It is concluded that most layer echoes arise from layers of ice containing acidic impurities of volcanic origin.

Layer reflectivity variations are observed over distances of tens of kilometres. Short-period fading is also observed, from which estimates of layer reflector roughness are made using the autocorrelation function and variance of the received power. The roughness estimates are shown to be consistent with a depositional origin for the surfaces.

Relevant theory is summarised and a procedure developed for the remote estimation of elevated acidity levels in ice from radio-echo sounding. Such estimates are shown to compare well with direct ice core measurements. The method is used to present estimated elevated acidity profiles for the Antarctic (to ~100 kaBP) and Greenland (to ~30 kaBP), which are interpreted in terms of variations in the input of volcanogenic acid impurities to the ice sheets.

The use of layering as isochronous horizons in ice flow studies is discussed in the light of new measurements, with particular emphasis on the zone close to bedrock.

ACKNOWLEDGEMENTS

I should like to thank my supervisor, Dr. G.de Q.Robin, for his generous help and encouragement during the last three years.

I have also benefited from discussions with colleagues at SPRI, particularly Dr. D.J.Drewry, Dr. E.J.Jankowski, and Dr. C.S.Neal, whom I warmly thank. I am especially grateful to Dr. J.G.Paren of the British Antarctic Survey for his stimulating comments, and to Dr. S.Overgaard of the Technical University of Denmark, for kindly providing radio-echo sounding data from Greenland.

The Antarctic field season in which I participated was carried out under the auspices of the US National Science Foundation. The Natural Environment Research Council provided a Research Studentship for three years. I would like to express my gratitude to both these bodies.

CONTENTS

List of variables

A'	effective area of antenna = $G^{\frac{1}{2}}\lambda^2/4\pi$
c	impurity concentration in ice
e	electronic charge = 1.6×10^{-19} C
G	mean square forward antenna gain
f	echo sounding frequency
h	depth of internal layer
$J_{\pm}$	effective charge on impurity ion
ℓ	thickness of thin reflecting layer
L	autocorrelation length of power returned from a surface
n	refractive index of ice = 1.78
N_A	Avogadro's number = 6.01×10^{23}
p	radio pulse length
$\langle P\rangle = P_r/P_t$	= received power relative to transmitted power
r	effective range of surface = $r_o + h/n$
r_o	terrain clearance
R	power reflection coefficient
R'	power reflection coefficient of thin layer
$\tan\delta$	loss tangent of ice
V_p	variance of power returned from a surface
β_o	RMS slope of a surface
ε	permittivity of ice
ε_o	permittivity of free space
λ	radio wavelength in ice = λ_o/n
λ_o	radio wavelength in air
μ_+	mobility of impurity ions in ice
ρ	ice density
ρ_p	autocorrelation function of received power
σ	RMS vertical deviation from mean horizontal plane of a surface
σ_∞	high frequency conductivity of ice
σ_o	static conductivity of ice
ϕ_o	RMS phase shift imposed by a surface on the received power

Chapter 1

RADIO-ECHO SOUNDING AND LAYER ECHOES IN POLAR ICE SHEETS

1.1 Introduction

Radio-echo sounding (RES) techniques for measuring the thickness of large ice masses have been developed since the early sixties (Evans 1963), and have now largely superceded other methods of depth profiling polar ice sheets and glaciers. The method relies upon the radio frequency transparency of the cold and chemically ultra-pure ice of polar glaciers; reflections are to be expected only from the surface and basal interfaces of the ice mass. The first, unexpected, observations of echoes from reflecting horizons within the ice mass itself were made in the summer of 1964 during a traverse along the Thule peninsula in NW Greenland (Robin and others 1969), and were followed by similar observations by the University of Wisconsin in the following year at South Pole and Byrd Stations in the Antarctic and over a large area of east Antarctica during airborne work conducted by the Scott Polar Research Institute and the US National Science Foundation in 1967. Subsequent work in the Antarctic and Greenland has confirmed the very widespread observation with radio-echo sounding equipment of stratified (layer) echoes from surfaces within the ice sheet.

Robin and others (1969) concluded that the probable cause of the internal reflections was variations in density or in other properties influencing the dielectric properties of the deposited snow. These variations would be preserved in the polar ice after compression and burial. Observations of density variations along ice cores, and a close agreement between observed layer depths and calculated isochronous surfaces added weight to these ideas. However, below about 1000 m, density fluctuations in polar ice sheets are too small to be responsible for

Chapter 1

RADIO-ECHO SOUNDING AND LAYER ECHOES IN POLAR ICE SHEETS

1.1 Introduction

Radio-echo sounding (RES) techniques for measuring the thickness of large ice masses have been developed since the early sixties (Evans 1963), and have now largely superceded other methods of depth profiling polar ice sheets and glaciers. The method relies upon the radio frequency transparency of the cold and chemically ultra-pure ice of polar glaciers; reflections are to be expected only from the surface and basal interfaces of the ice mass. The first, unexpected, observations of echoes from reflecting horizons within the ice mass itself were made in the summer of 1964 during a traverse along the Thule peninsula in NW Greenland (Robin and others 1969), and were followed by similar observations by the University of Wisconsin in the following year at South Pole and Byrd Stations in the Antarctic and over a large area of east Antarctica during airborne work conducted by the Scott Polar Research Institute and the US National Science Foundation in 1967. Subsequent work in the Antarctic and Greenland has confirmed the very widespread observation with radio-echo sounding equipment of stratified (layer) echoes from surfaces within the ice sheet.

Robin and others (1969) concluded that the probable cause of the internal reflections was variations in density or in other properties influencing the dielectric properties of the deposited snow. These variations would be preserved in the polar ice after compression and burial. Observations of density variations along ice cores, and a close agreement between observed layer depths and calculated isochronous surfaces added weight to these ideas. However, below about 1000 m, density fluctuations in polar ice sheets are too small to be responsible for

echoes of the magnitudes generally observed, and other types of dielectric discontinuity must therefore be responsible for the deeper echoes. Paren & Robin (1975) have shown that small changes in the loss tangent of ice can cause detectable radio reflections, but the cause of these changes, if they exist, was not identified.

The use of internal layering (assumed to be isochronous surfaces) in modelling the flow of ice sheets has been suggested by Robin and others (1969). If such an approach is valid then it is clearly a unique method of studying the dynamics of the ice sheet at depth over wide areas. A good example of an analysis of this type is the work by Whillans (1976) along the flowline above Byrd Station, West Antarctica.

The present work is mainly based upon the results of the 1974-75, 1977-78 and 1978-79 Antarctic field seasons of the airborne RES programme conducted jointly by the US National Science Foundation (NSF), the Scott Polar Research Institute (SPRI) and the Electromagnetics Institute of the Technical University of Denmark (TUD), of which the author took part in the last season. This survey covers about half of the Antarctic continent with 60 and 300 MHz sounding lines at 50-100 km spacings, and is the largest such RES survey to have been undertaken. Making use of this large amount of data (and some similar results from Greenland) the geographical distribution, spacing and horizontal continuity of layer echoes has been studied, and in particular returned power levels have been measured and analysed at many sites.

These results have been used to improve understanding of reflection mechanisms, to examine changes in ice density and to make estimates of acidity changes within the ice mass. Acidic impurities in the ice sheets have an important effect on the electrical properties of polar ice, and varying acid concentrations will be concluded to be the prime cause of the deeper layer reflections. A method of estimating acidity levels from radio-echo sounding measurements is developed here, and the results

discussed with reference to the detailed chemical analyses of ice cores now becoming available. In the light of a better understanding of the causes of radio-echo layering, the last chapter of the thesis is concerned with the use of radio-echo layering in studying ice dynamics, and its relevance in ice core chronology.

1.2 Radio-echo sounding equipment and data recording

The echo sounder used for the majority of this work was the Technical University of Denmark 60 MHz system (Skou & Sondergaard 1976), but recordings obtained with the SPRI Mk IV 60 MHz system (Evans & Smith 1969) and the TUD 300 MHz system (Christensen 1970) have also been studied. The antenna array of the TUD 60 MHz system consists of four collinear dipoles mounted one quarter-wavelength beneath the starboard wing of a specially adapted Lockheed C-130 (Hercules) aircraft. This arrangement gives an elliptical radiation pattern with a half power beamwidth of 120° fore-and-aft and 20° side-to-side. The system was usually employed with a 250 ns nominally square pulse and a peak output power of 10 kW, in which mode the calculated system performance (including antenna gain and cable losses, etc.) is 176 dB. Other pulse lengths available with the system were 60, 125, 500 and 1000 ns, and a lower output power of 1 kW could also be selected. The system performance with a 60 ns pulse at 1 kW power output has been measured by Neal (1977) to be 159.5±3 dB, in good agreement with the calculated value of 161 dB. Difficulty in tracing layers on the undifferentiated Z-scope output of the SPRI Mk IV system, together with infrequently recorded A-scope displays, make the data from this equipment less suitable for studying layers than the TUD 60 MHz system. The power received by the 300 MHz TUD equipment has not been accurately calibrated, making it of limited use for the present purpose.

Several methods of recording the received signal were used. For the primary purpose of depth profiling of the ice sheet and ice shelves, a 'Z-

scope' representation was used, i.e. a continuous record of the differentiated, intensity-modulated return against time. This format facilitates the recognition of horizontally continuous surfaces, and enables changes in surface and bedrock reflection characteristics to be seen more easily. This was displayed on a Tektronix 465 oscilloscope and recorded on 35 mm photographic film and also (during the 1977-78 and 1978-79 seasons) with a Honeywell 1856A fibre-optic oscillograph. To study returned power levels 'A-scope' recordings were made, i.e. a display of returned power (on an approximately logarithmic scale) vs time range. These displays were recorded both on 35 mm film at every CBD (the time unit used by the TUD system, equal to 20 s during the 1974-75 season, and 15 s in later seasons) which is roughly every 2 km along the flight-track, and also on 8 mm film with a Leicina Super 8 cine camera operating at 54 frames per second for 'bursts' of up to 20 s duration (1974-75 and 1977-78 seasons only). Such bursts were recorded automatically every fifty CBDs, and manually at places of interest during the flight. The horizontal spacing of the Super 8 recordings is approximately 2 m. Finally, continuous power profiling of the bedrock signal was conducted using an echo strength measurement (ESM) device (Neal 1976). This recording format is particularly useful in locating areas of similar basal roughness and in detecting changes in basal reflection coefficient. The device can be set to record the peak power returned within any time window, and was normally employed recording the bedrock signal, but has also been used experimentally on internal echoes and the surface of the Ross Ice Shelf - enabling useful comparisons to be made of the reflection characteristics of internal layers and other surfaces. Examples of the various formats are to be found in figs. 2.1 (Z-scope), 2.7 (A-scope) and 3.5 (ESM).

The following chapter describes the internal layering observed in the Antarctic and the effect of ice flow and of equipment parameters on its appearance. Later chapters report measurements of layer reflection coefficient and roughness, discuss reflection mechanisms, and use the measurements to make estimates of acidity levels in the Antarctic and

Greenland ice sheets. Finally, internal horizons are used to provide information about the flow of ice, particularly near to the base and in the vicinity of bedrock obstacles.

Note that in this thesis the phrases 'stratification echo', 'layer echo' and 'layering' are synonymous and refer to the observed echoes. 'Internal horizon' or 'surface' are used to refer to the reflecting surface giving rise to the echo.

Chapter 2

FACTORS INFLUENCING THE APPEARANCE OF STRATIFICATION ECHOES

2.1 The effect of ice flow on layering

Stratification echoes have been observed in both of the polar ice sheets with a variety of RES equipment (Table 2.1). These internal horizons appear to follow isochronous surfaces within the ice mass (Robin and others 1969; Whillans 1976). Individual reflections are sometimes traceable for several hundred kilometres along flight-tracks, the horizontal continuity apparently depending on bedrock roughness, ice velocity and age. Reflections are characteristic of specular surfaces, returned power falling off sharply with increasing angle of incidence (this is very noticeable when the sounding aircraft banks, for example), and generally have power reflection coefficients (PRCs) in the range -60 to -80 dB.

Fig. 2.1 shows three examples of layering recorded with the 60 MHz equipment in the Antarctic, and illustrates that the appearance of layers is influenced by ice movement (further examples of Z-scope records can be found in Chapter 6). The deformation of the layers caused by the movement of the ice may be greatly exaggerated by convolution of the signal (e.g. in fig. 2.1(c)) which occurs if the reflecting surfaces have a centre of curvature near to or below the altitude of the aircraft (Harrison 1971). This type of feature is often seen in areas with rough bedrock topography. Even in areas with relatively smooth bedrock and parallel layering, the detailed appearance of the layers may become unclear and individual echoes no longer unambiguously followable, although the general sense of the stratification remains visible.

TABLE 2.1 REPORTED OBSERVATIONS OF LAYER ECHOES IN POLAR ICE SHEETS

Date of obsvn.	Reference	Site	Depth (m)	R (dB)	F'cy (MHz)	Remarks
1964	Bailey et al (1964); Robin et al (1969)	*Tuto-Camp Century	420-610	-43 to -70	35	SPRI MkII, 240ns, 50W
		*near Camp Century	410-455	-72 to -80	35	do. "AD 957" layer
1964/65	Jiracek (1967)	Skelton Glacier	<570	-	30	US Army radar, 500ns, 300W;
		Roosevelt Island	300	-	30	polarisation & wide angle
		South Pole Sta.	650,1020	-	30	reflection measurements
1965/66	Fedorov (1967)	Mirny-Pioneerskaya	<700	-	440	
1965/66, 1967/68	Clough & Bentley (1970)	South Pole-Queen Maud Land Trav. II	250-1250	-	30	US Army radar
1967	Robin et al (1970)	Byrd Station	1250	-69	35	SPRI MkII, 240ns, 500W
		Sovetskaya	<2200	-76	35	do.
1967, 1973	Ackley & Keliher (1979)	Cape Folger	177,228	-	35,100	ANARE Traverse
1969/70, 1971/72	Harrison (1972)	Vostok-Dome C	2000-3000	-79 to -83	60	SPRI MkIV, 200ns, 800W
		do.	do.	-60 to -80	60	do., but 1000ns
		South Pole	-	-75	60	do.
1969-74	Gudmandsen (1975)	*Crête	2300-2500	-70 to -75	60	TUD radar, 250ns, 10kW
1970	Clough (1977)	Byrd Station	<1000	-	50	modified SPRI MkII, polar-
		South Pole Sta.	<850	-	50	isation & wide angle reflection measurements
1974/75	Whillans (1976)	near Byrd Sta.	-	-	60	TUD radar, 250ns, 10kW
	Robin et al (1977)	east Antarctica	-	-	60,300	do.
1975	Sondergaard (1975)	*DYE-3	700-1500	-	60	do.
	Hargreaves (1977)	do.	<1500	-	300	do.
1977/78	Drewry & Meldrum (1978)	Dome C	<2600	-	60,300	do.
1979/80	Shabtaie et al (1981)	do.	<2400	-	35	modified SPRI MkIV radar

*Greenland site; all others in Antarctica.

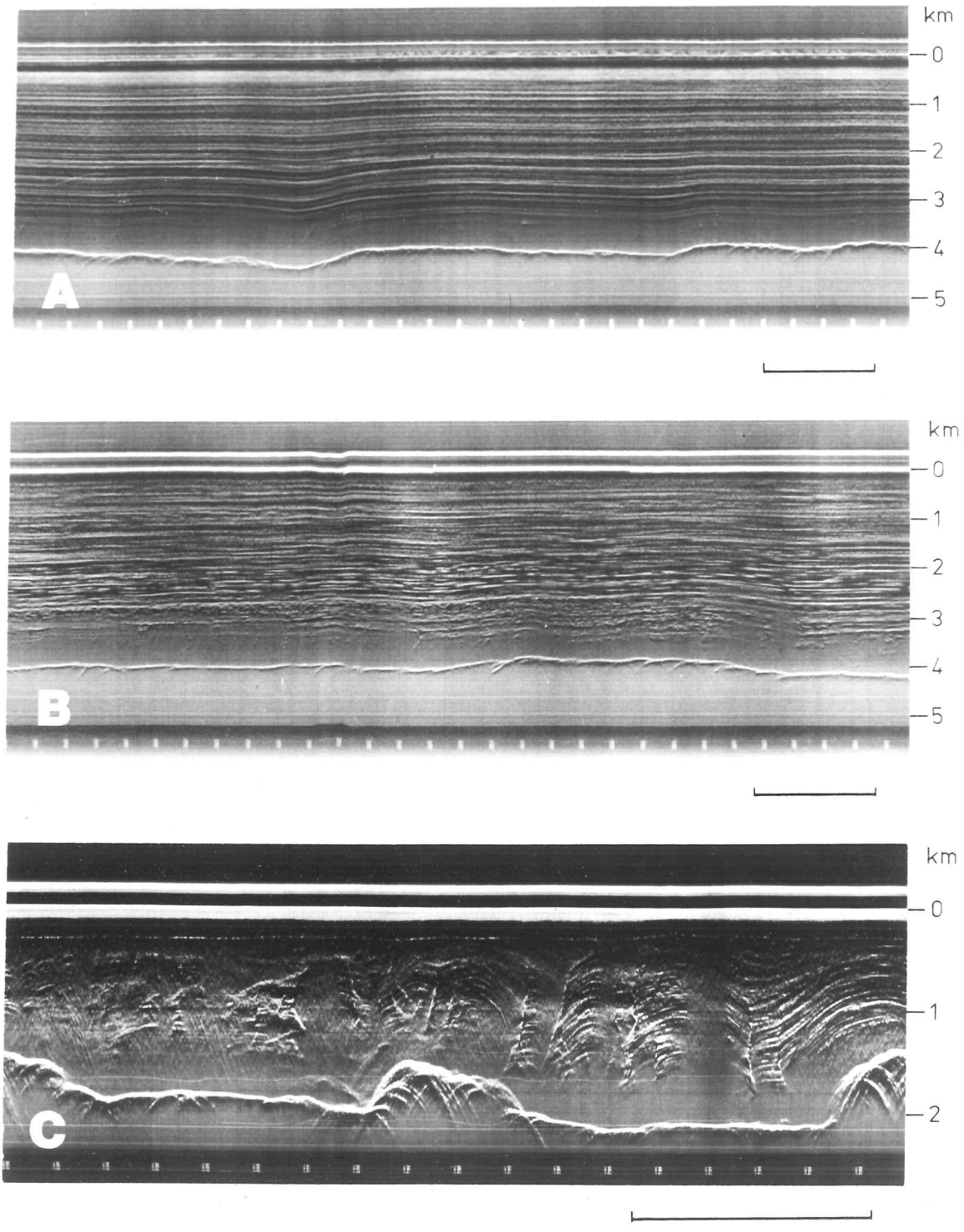

Fig. 2.1 Examples of the different appearances of internal layer echoes in the Antarctic.
60 MHz radar, 250 ns pulse length. Scale bar = 10 km.

There is a useful distinction to be made between these varieties of layering; layering in which individual reflections are clearly visible is of greater use in defining isochronous surfaces and in studies of the nature of the reflecting surfaces themselves. It would be useful to know: (i) the relationship between flow conditions in the ice and the appearance of layers, and (ii) the distribution of layering with different appearances. Because there are many layers visible in the ice column at any one place, it is difficult to make a strict classification of the appearance and continuity of the layering as a whole at a particular site, and more importantly such a classification would vary with the type of RES equipment used. Instead, the following empirical classifications have been used, of which the examples in fig. 2.1 are illustrations:

A good continuity - some layers >100 km long, layers appear smooth and parallel on Z-film.

B moderate continuity - some layers >10 km long, layers show a generally stratified appearance but individual layers usually not resolved. Focussing (convolution) effects occasionally seen.

C poor continuity - internal reflections no longer possess a stratified structure (few layers traceable for >1 km). Focussing effects very common, layering often appears 'turbulent'.

These classifications are intended to be applied to the layering on a representative scale (several ice thicknesses in extent), so that local anomalies are ignored. The distribution of these categories of layering has been mapped for the part of the Antarctic covered by the NSF-TUD-SPRI survey, and the results shown on fig. 2.2. All observations refer to the 60 MHz system operating with a pulse length of 250 ns, a bandwidth of 4 MHz and a nominal output power of 10 kW.

By comparing the layer appearance distribution map with a surface contour map one can see that the more continuous (type A) layering is mainly found near centres of outflow and ice divides, where the ice has not

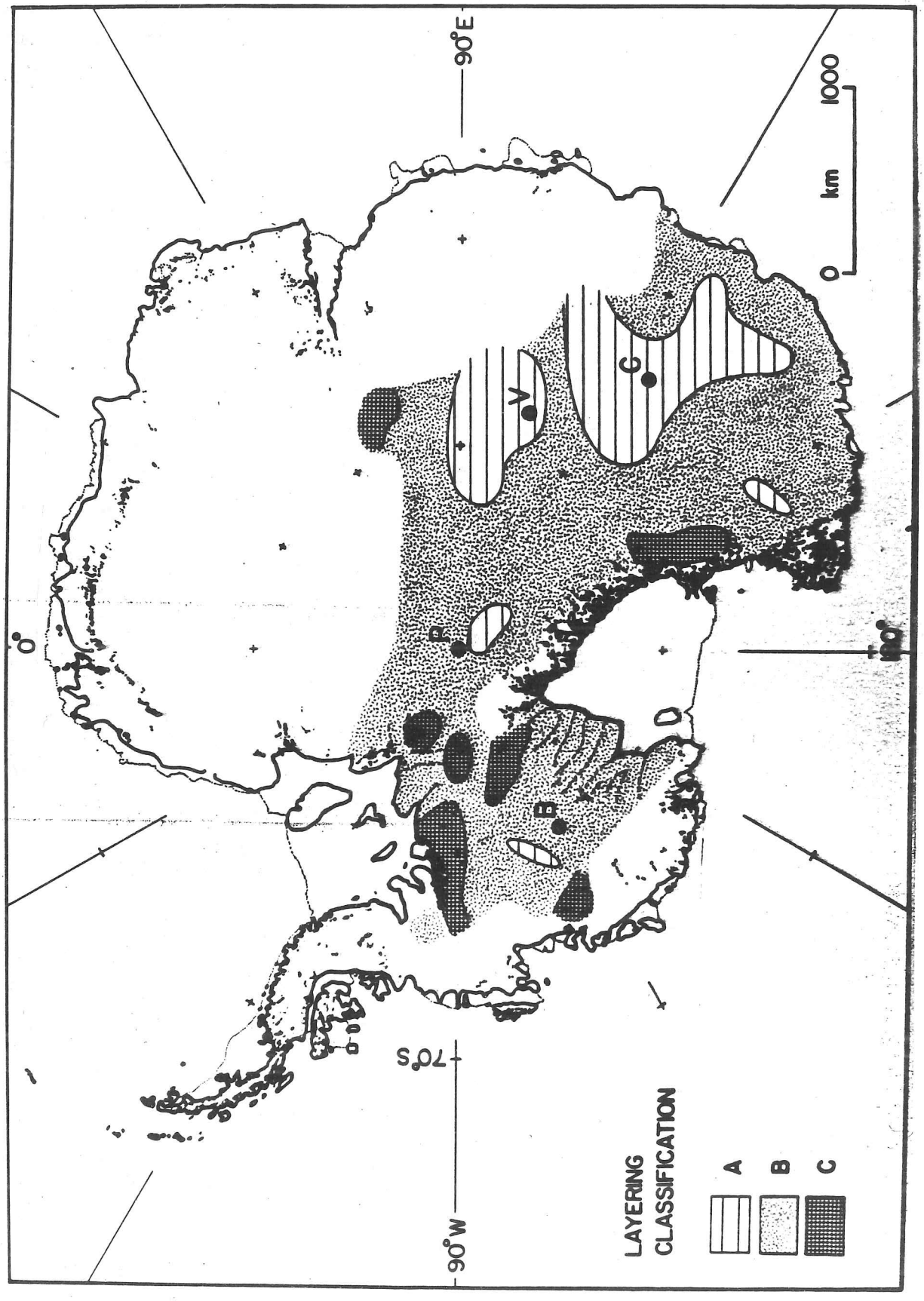

Fig. 2.2 Distribution of layering types in the Antarctic.

moved any great distance horizontally since its deposition. In such areas the principal motion of the ice layers is downwards into the ice mass, with little of the deformation caused by horizontal movement over bedrock irregularities. Discontinuous (type C) layering, by contrast, is found only in areas with very rough bedrock topography, and presumably results from the deformation of the ice over the complicated bedrock form. The frequent focussing effects observed show that the reflecting surfaces from which the layer echoes originate have relatively large curvatures, and usually the layering is too confused to allow deconvolution. In areas with clearer layering a quantitative comparison may be made between observed layer positions and those predicted with the aid of flow models. In many areas an echo-free zone has been observed near to bedrock, which is believed to be caused by complex three-dimensional ice flow over rough terrain. These two topics are covered in greater detail in Chapter 6.

To summarise, the appearance of the layering on the Z-scope record may be a qualitative indicator of the nature of the ice flow at depth. Three types of layering have been illustrated and their occurrence in the Antarctic mapped. The clearest layering (type A) is preferred here to define isochronous horizons and to study reflection mechanisms.

2.2 Influence of sounding frequency and antenna design

There are three main equipment parameters that affect the appearance of layer echoes on the Z-scope record - carrier frequency, radiation pattern and pulse length. The last of these is of particular interest because of the problems that have been encountered as a result of using long pulse lengths, and this will therefore be discussed separately in the next section.

Laboratory measurements show that within the commonly-used band of frequencies for radio-echo sounding (20-500 MHz), there is only a slight

change in dielectric attenuation by the ice (Evans 1965). Factors which are frequency-dependent are the reflection coefficient of thin reflecting layers (eqn. [4.8]), and scattering from small inclusions within the ice (eqn. [4.21]).

Simultaneous records from the 60 and 300 MHz systems generally show several differences (fig. 2.3):

(i) apparently shallower penetration by the 300 MHz equipment
(ii) lack of layering structure in the upper part of the ice at 300 MHz
(iii) 'interference' effects at 300 MHz

Because the two TUD systems have different radiation patterns as well as different frequencies, it is difficult to identify an unambiguous cause for the observed differences. The 60 MHz equipment employs four dipoles giving a radiation pattern with an elliptical footprint whereas the 300 MHz equipment uses a backfire antenna array giving a narrower conical beam with a half-power angle of approximately 20°. The principal result of this is that the 300 MHz system is much less sensitive to echoes returned at a wide angle from the vertical than is the 60 MHz system; this enables the 300 MHz system to achieve better penetration in areas with many scattering objects on the surface, such as crevasses. The 'interference' effect is believed to be an equipment artifact, caused by beating (Sondergaard, personal communication), although since it is seen intermittently the possibility remains that it is related to the spacing of reflectors within the ice.

It seems possible that the lack of layering structure in the upper part of the ice is caused by greater scattering within the ice at 300 MHz. Although the loss to the forward beam due to scattering from small objects within the firn layer is negligible at frequencies below 1 GHz, density fluctuations a few centimetres in extent in the near-surface layers of the

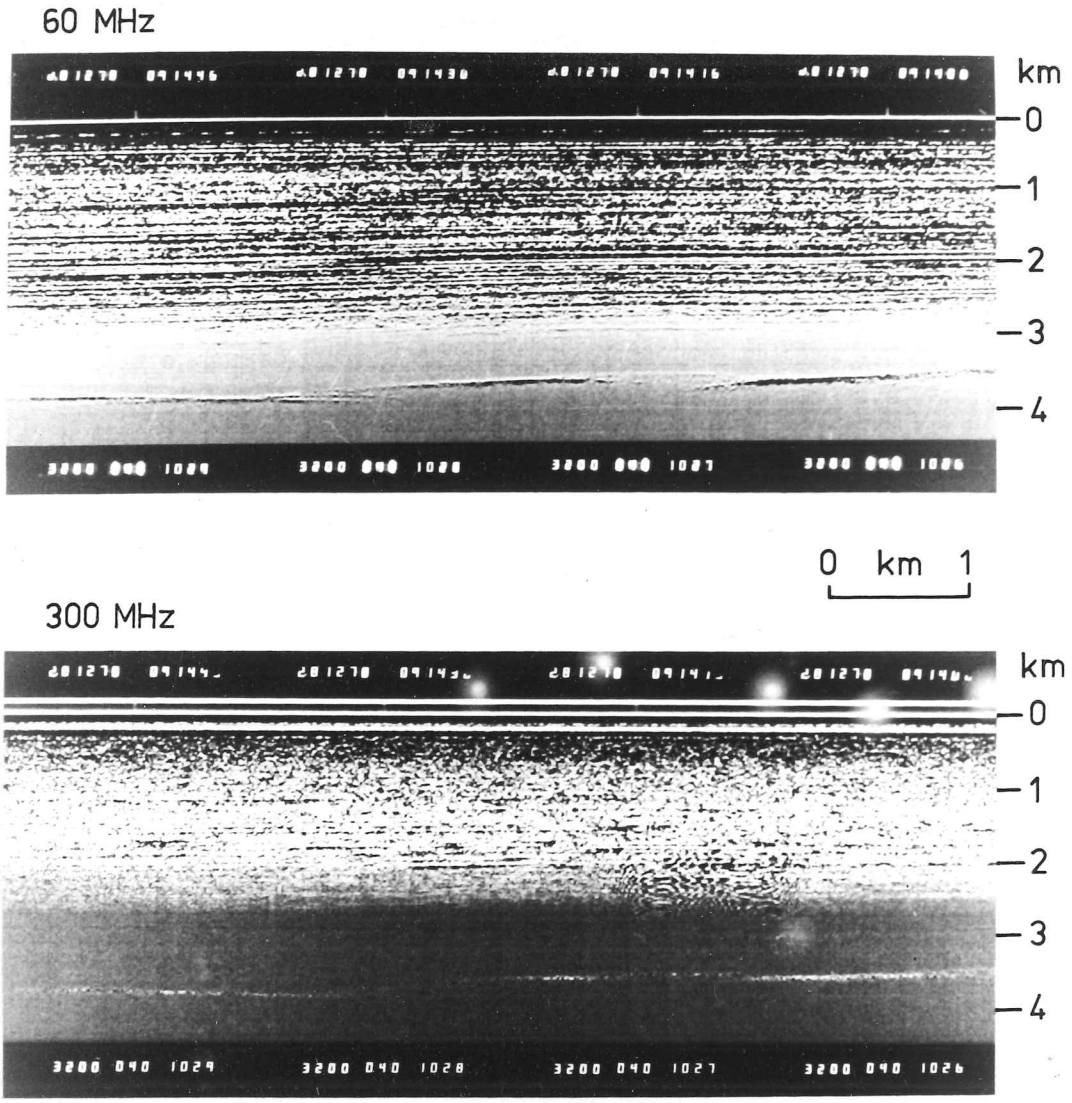

Fig. 2.3 Z-scope records from Dome C recorded simultaneously with the TUD 60 MHz and 300 MHz systems, 250 ns pulse.

ice sheet (which will subsequently be referred to as 'inclusions'), may produce a detectable short-range clutter echo (Evans & Smith 1969). As shown in section 4.4(b), changing frequency from 60 to 300 MHz should result in a 15 dB increase in the power scattered back from such inclusions, and this may be sufficient to obscure echoes from internal layers in the upper 500 m of the ice.

In order to investigate the possibility of increased back-scattered power from inclusions within the ice, a comparison of layer reflection coefficients observed with the two TUD systems has been attempted. Some results are shown in fig. 2.4 for South Pole and Dome C, but must be interpreted with caution as the power received by the 300 MHz system could not be reliably calibrated. This has therefore been done indirectly by measuring the received power whilst flying over the sea (assumed to have a reflection coefficient of -2 dB). The method of data reduction is described in Chapter 3. Estimated back-scattered power from inclusions at the two frequencies (section 4.4(b)) suggests that this is not likely to be detectable with the 60 MHz system, but may be a cause of power return from the near-surface layers with the 300 MHz equipment. If this is so then it would be an obvious explanation for the lack of layering structure seen with the 300 MHz system - although the power returned would be detectable the layers would be masked by short-range clutter from the inclusions within the firn. At both the sites where 300 MHz power measurements have been made the layering is very difficult to follow on the Z-scope records (figs. 2.3 and 2.5).

It has been suggested (Gudmandsen & Overgaard 1978) that if a number of thin layers combine to form a single reflecting zone (a 'multiple' reflector), the pulse shape may be wavelength dependent and eventually layer echoes will be observed at different depths for different radio frequencies. At Crête (Greenland) they and the author find that the depths of the layers are the same on the 60 and 300 MHz records to a depth of about 1000 m (the deepest detectable layer at 300 MHz), suggesting

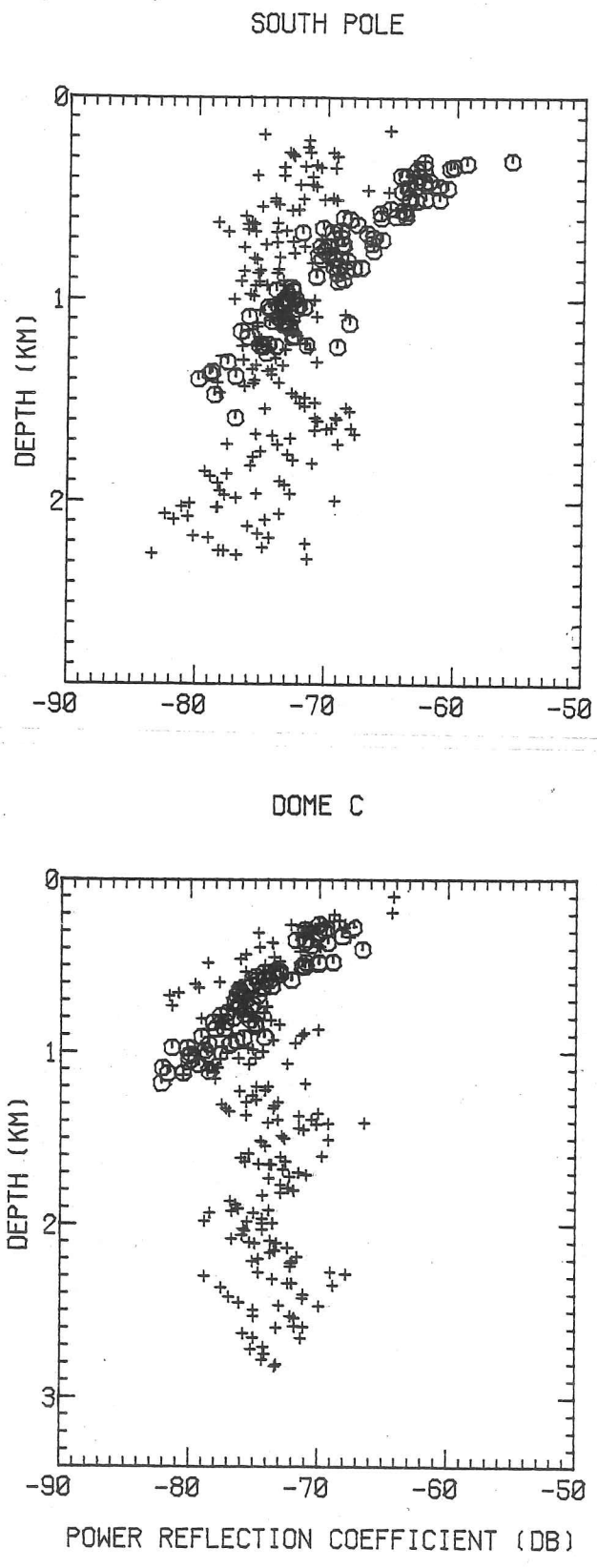

Fig. 2.4 Reflection coefficient vs depth profiles for internal echoes observed at South Pole and Dome C using 60 MHz (crosses) and 300 MHz (circles) equipment, 250 ns pulse length.

predominantly single reflectors. This is in agreement with other results from this site, which suggest mainly single reflectors to about 1000 m and combined reflectors below this depth using a pulse length of 250 ns or ~40 m in ice (see Chapter 5). In the Antarctic the depths of layer echoes, at sites where 300 MHz layering can be clearly seen, usually appear to be closely coincident at the two frequencies, although displacements of up to 40 m are sometimes seen (fig. 2.5). Such comparisons between layer positions with different frequency echo sounders are thus a possible way of distinguishing between 'single' and 'multiple' reflectors, and the observed slight shifts in layer position suggest that many layer echoes originate from 'multiple' reflecting zones. However the expected shifts may be small and will depend on the geometry of the component surfaces; a lack of change in layer position at only two different frequencies does not conclusively imply a single reflecting layer.

Comparison of measured layer reflection coefficients at more than one frequency is another potential method of distinguishing between reflections from single or multiple reflectors. For single isolated layers the reflection coefficient is a function of wavelength (eqn. [4.8]), whereas for multiple reflectors Clough (1977) has shown by numerical modelling that the total reflection coefficient is well approximated by that for a single interface with an averaged change in dielectric properties, and hence is not wavelength dependent (eqn. [4.5]). However it is difficult to reliably identify layer reflections on the 300 MHz records, and there is also a problem due to possibly significant power returns from inclusions within the ice at this higher frequency. Because of this uncertainty this method has not been attempted in the present study.

In summary, the differences in layering appearance observed with the two TUD systems may well be largely due to increased scattering in the firn layer due to density irregularities, probably a few centimetres in size. Although measurements of dielectric absorption made with the 60 MHz

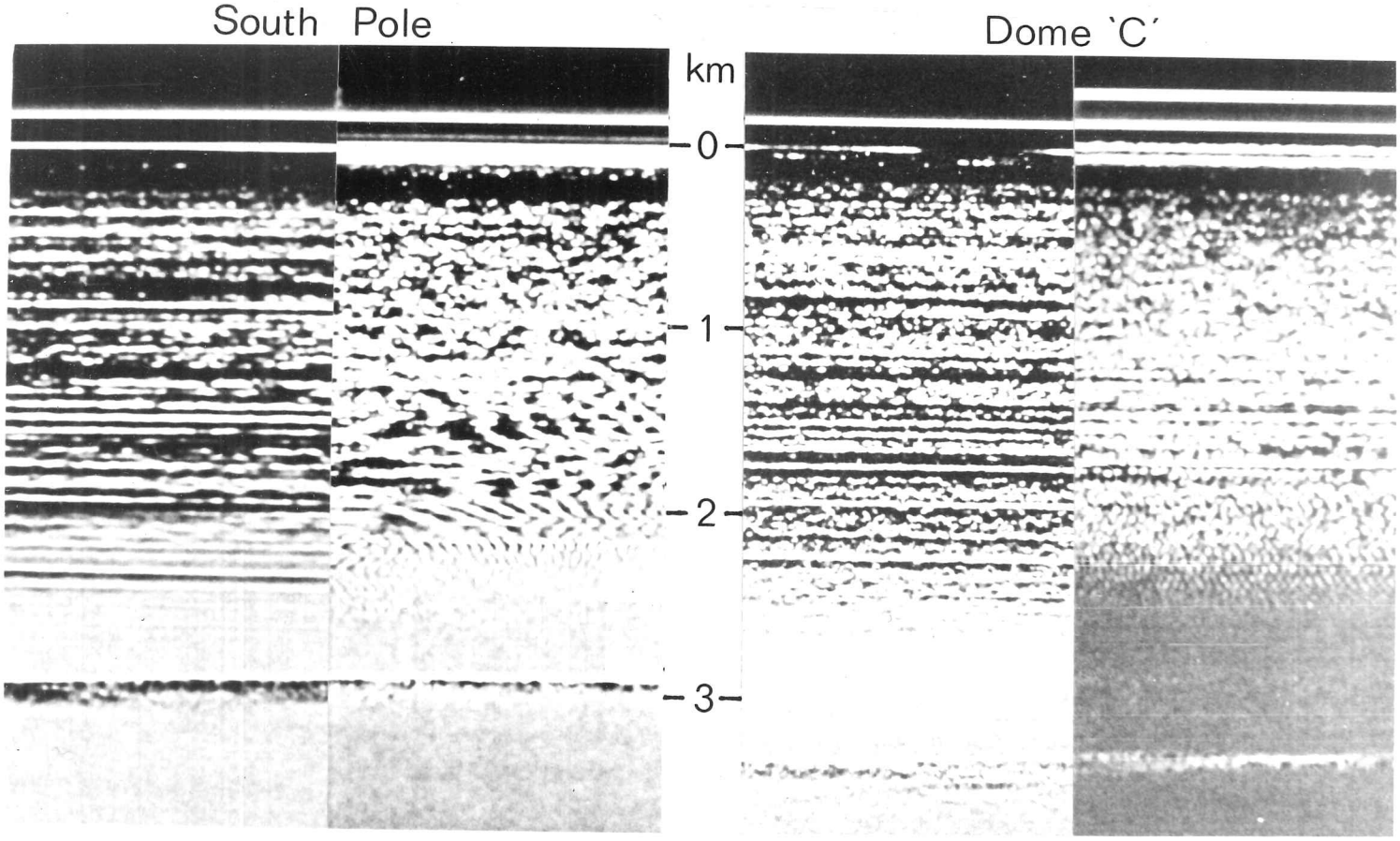

Fig. 2.5 60 MHz (left) and 300 MHz (right) Z-scope records from South Pole and Dome C, showing different appearance, and correlation between layers seen with the two systems.

equipment agree very well with laboratory measurements at 150 MHz (see Chapter 3), no comparison has been possible at 300 MHz, and so the possibility remains of higher dielectric attenuation than expected at this frequency. Differences in the positions of layers seen in the Antarctic at the two frequencies suggests that many echoes originate from 'multiple' reflecting zones, of less than half a pulse length in total thickness. Since internal layering is not reliably and unambiguously detectable with the 300 MHz system, the bulk of the rest of this work refers to the 60 MHz system.

2.3 Radio pulse length and resolution

Clearly it is desirable to know whether or not the reflecting surfaces are being adequately resolved by the echo sounder. Fig. 2.6 shows a Z-scope recording made at South Pole Station using 60 and 250 ns pulse lengths, and illustrates how the spacing between layers varies with pulse length. It is evident that in this case the 250 ns pulse is too long to resolve all the layers visible with a 60 ns pulse, which may itself be too long to resolve all the surfaces present.

For a pulsed radio-echo sounder with adequate receiver bandwidth, the range resolution depends on the duration of the transmitted pulse. In principle two reflecting surfaces cannot be resolved by the equipment if their relative separation is less than half the pulse length; in practice this is a simplification. The separation of power maxima will also depend on the rise time of the pulse and upon the reflection coefficients of the surfaces in question. This is clearly seen in fig. 2.7, which shows A-scope recordings obtained at the South Pole using 60, 250 and 1000 ns pulses, corresponding to ~10, 40 and 170 m in ice respectively; using the 1000 ns pulse the echo duration usually appears less than the nominal length of the transmitted pulse. This probably arises because of the differing reflectivities of neighbouring horizons distorting the shape of the

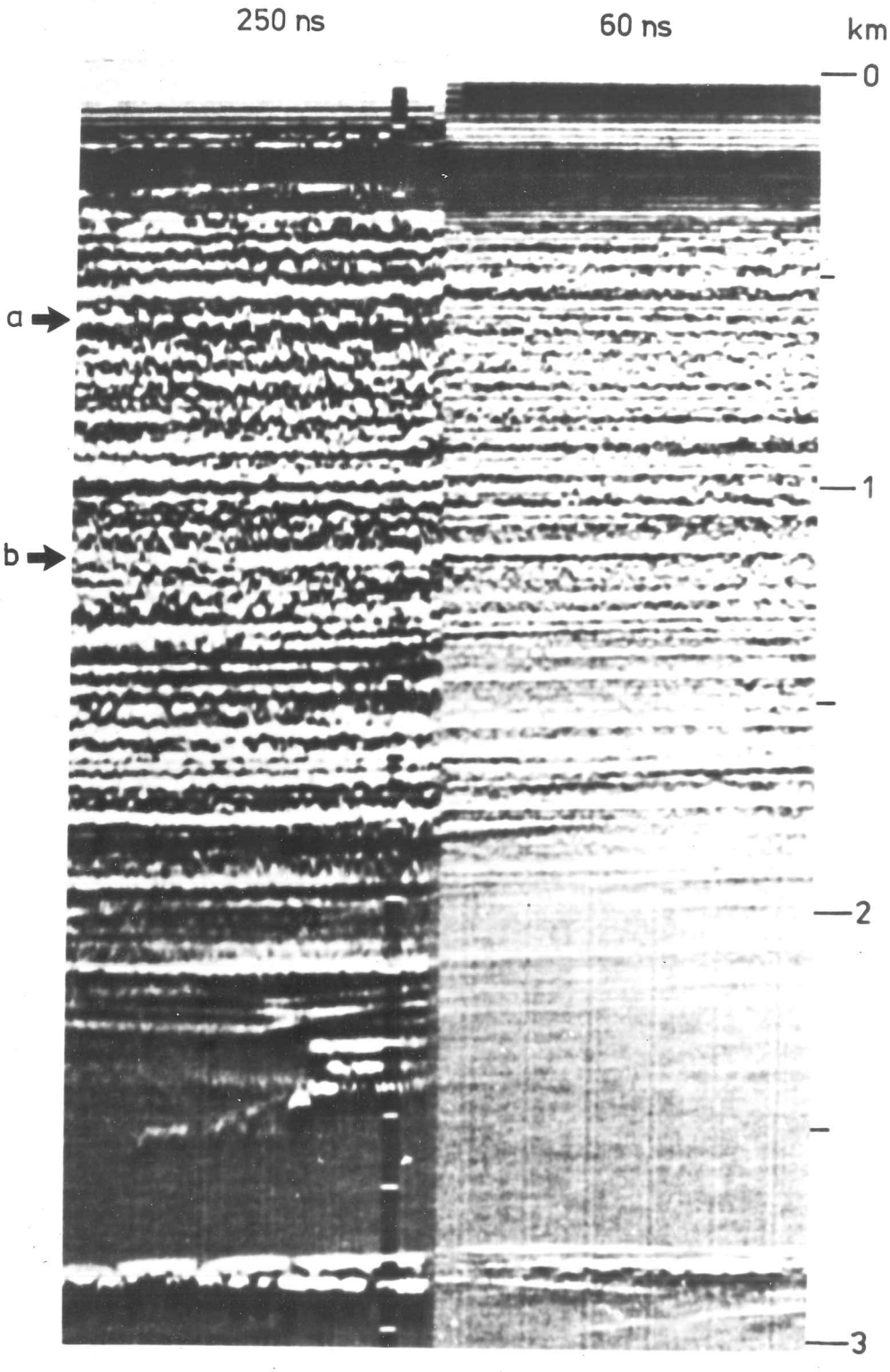

Fig. 2.6 60 MHz Z-scope recorded during take-off at South Pole using 250 ns and 60 ns pulse lengths:

(a) an example of an internal reflection which is resolved into two components using the shorter pulse length

(b) a reflection which remains unaffected by changing the pulse length.

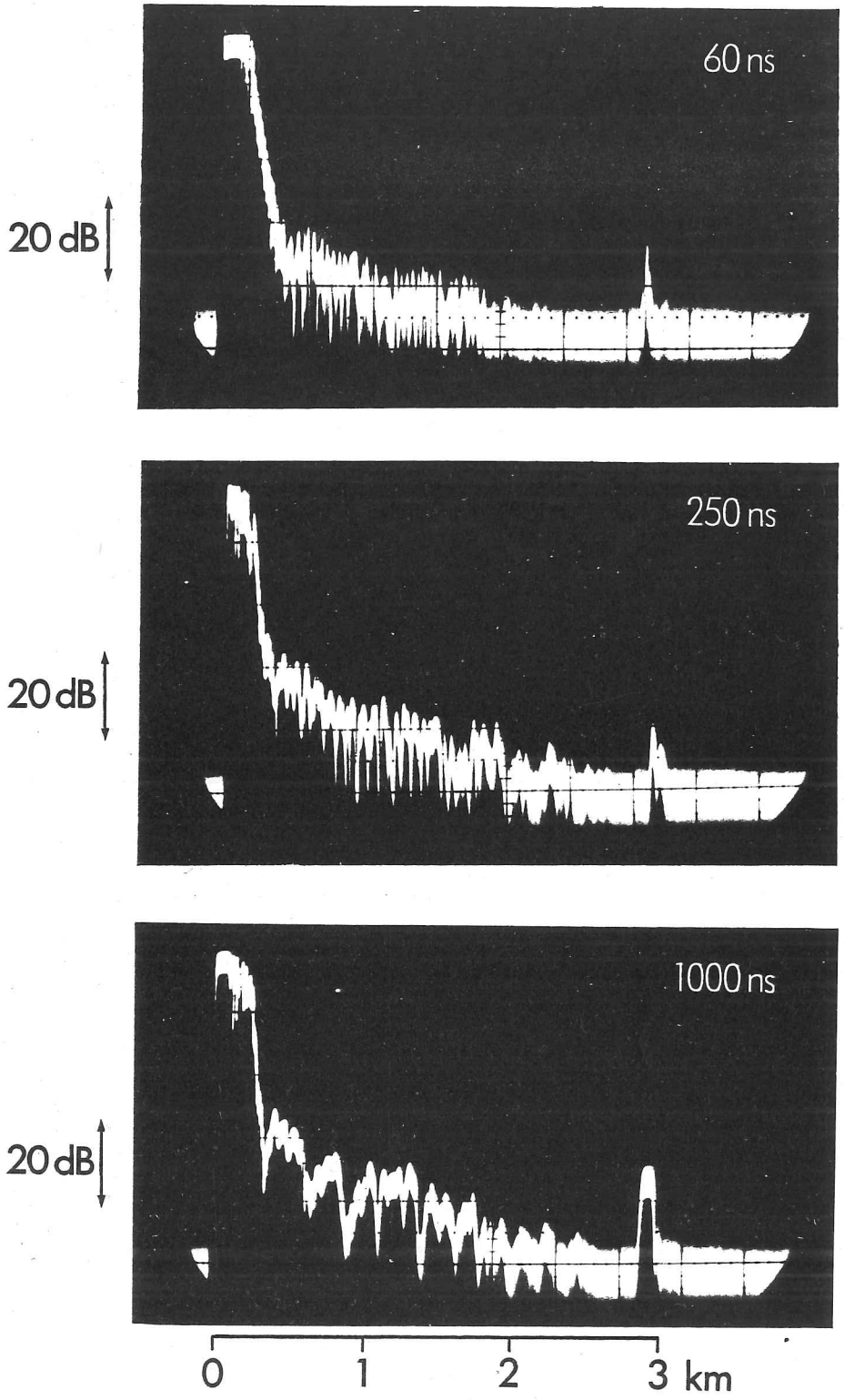

Fig. 2.7 60 MHz A-scope displays recorded using 60, 250 and 1000 ns pulse lengths, at the South Pole.

returned pulse, which may also contribute to the layering appearing broken-up on the Z-scope record.

Although the resolution cannot be calculated precisely, the rise time of the pulse will set a lower limit to it. The rise time is approximately constant for all pulse lengths available with the TUD sounder at about 30 ns, which implies a minimum resolution of about 5 m. In this case the second echo may appear merely as a shoulder on the first one, so the separation at which two surfaces may be unambiguously resolved may be much larger. This lower limit is however not attainable because the finite spot size of the recording oscilloscope prevents the resolution of two power maxima with a separation of less than the 'time diameter' of the spot. This limitation has previously been noted by Hargreaves (1977); using the 300 MHz TUD equipment operating at 60 and 250 ns, Hargreaves estimated the true reflector spacing to be of the order of 5-20 m at DYE-3, Greenland (~0.5 ma^{-1} accumulation), implying a temporal layer spacing of 10-40 yrs. His observations in east Antarctica, where the layers are expected to be more closely spaced than in Greenland because of generally lower accumulation rates, were apparently in contradiction with this; greater and not lesser layer spacings were observed. The probable cause of these confusing results is the inadequacy of the recording oscilloscopes to display changes in received power level which occur in a time axis distance of less than the the spot size of the oscilloscope. The spot size of 0.4 mm at the sweep rate normally employed (5 μs/cm) gives a spot time diameter of 200 ns, equivalent to ~34 m in ice, so it will be difficult to resolve two surfaces with a spacing of less than this. Measured layer spacings are presented in the following section.

2.4 Vertical separation and continuity of layer echoes

In this section measurements of layer separation (vertically) using several different pulse lengths and at a number of sites with different accumulation rates are presented. These show that generally layers in the Antarctic are uniformly spaced with a separation similar to the pulse length used. Together with observations on the horizontal continuity of individual layers, the relevance of this to the structure of the reflecting horizons is then discussed.

(a) distribution of layer spacings

A-scope recordings from various Antarctic sites and Crête, Greenland, have been analysed and the frequency distribution of inter-layer spacings obtained at each site. Measurements refer to layers below the near-surface region where the ice surface echo saturates the receiver, and above the region where absorption begins to prevent the detection of some layers. Data for Crête refer to the upper 2000 m only. Fig. 2.8 shows results from the South Pole using 60, 250 and 1000 ns pulse lengths; it can be seen that mean layer separations decrease as the pulse length is reduced. The cut-off in spacings below 20–40 m is thought to be due to the spot size limit of the oscilloscope, so we can only conclude that the true reflector spacing is less than this limit, corresponding to a temporal reflector spacing of <150 yrs. As the pulse length is increased to 250 and 1000 ns there is a greater proportion of echo spacings >40 m, indicating that here the resolution is beginning to be limited not by the oscilloscope, but by the pulse length. With a square pulse, two reflectors should only be unambiguously seen as separate power maxima if their separation is greater than the pulse length, but when their spacing exceeds half the pulse length then they should become detectable in the form of 'shoulders' on neighbouring returns.

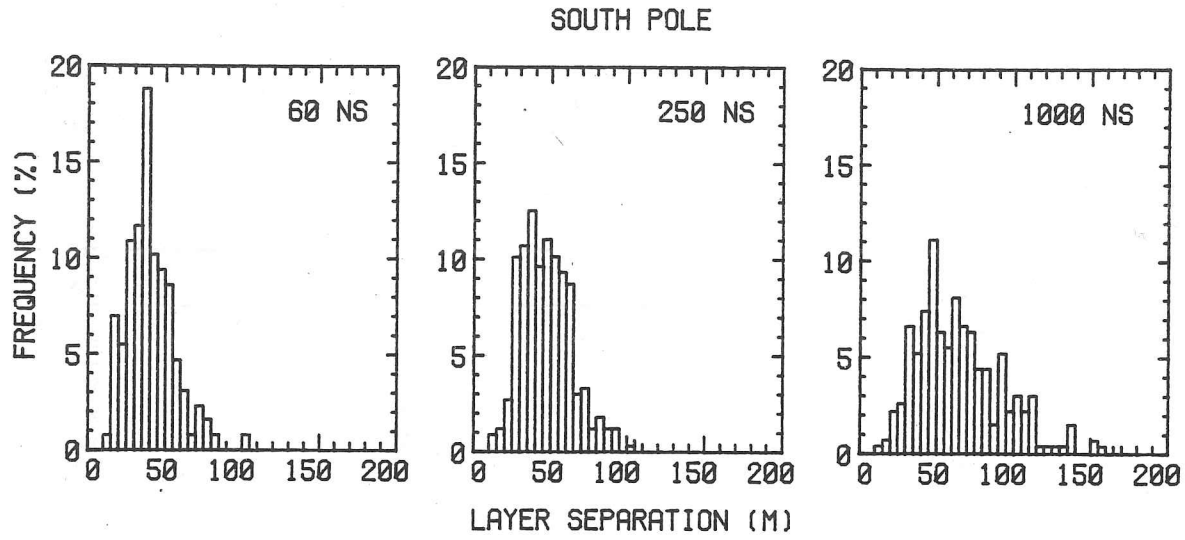

Fig.2.8 Distribution of spacings between 60 MHz A-scope layer echoes at South Pole with varying pulse lengths.

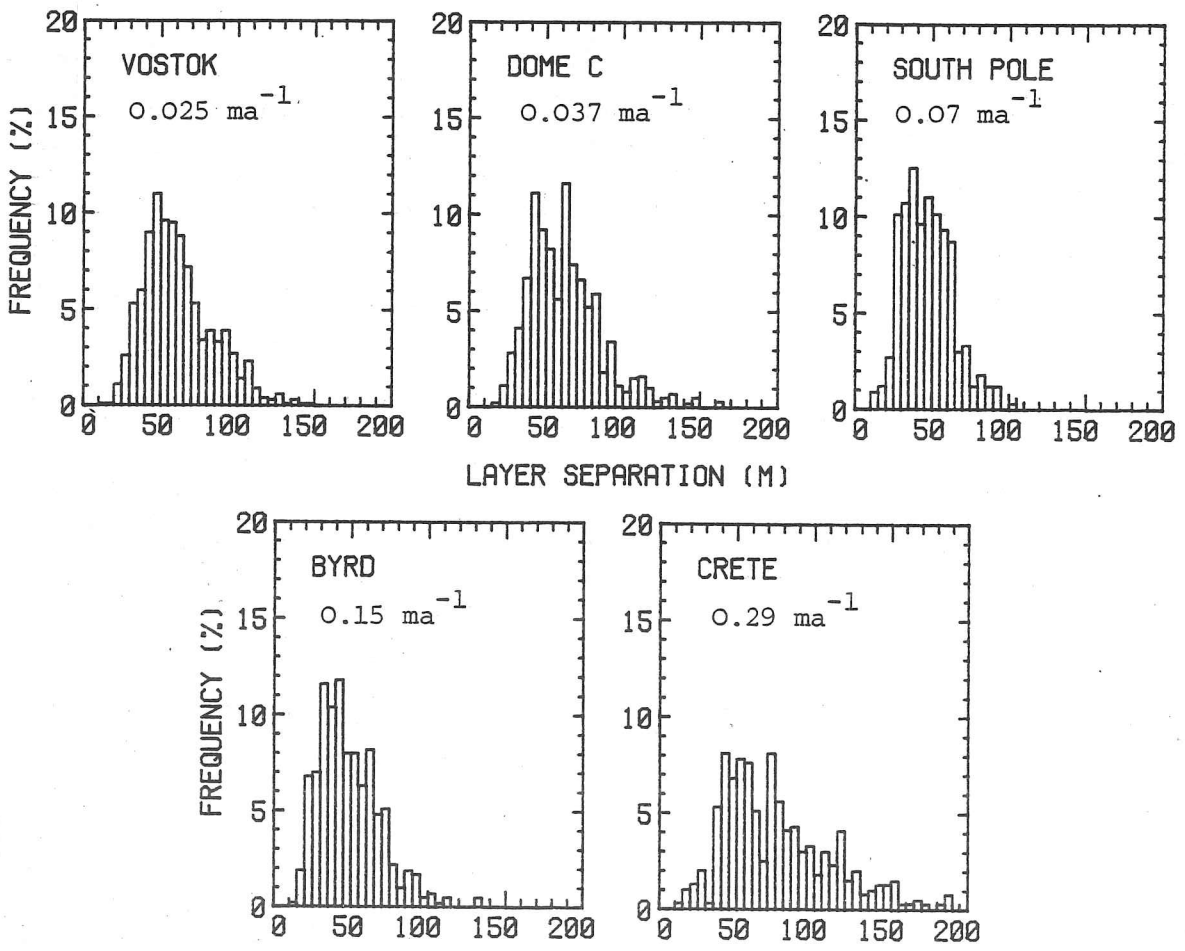

Fig. 2.9 Distribution of spacings at various sites arranged in order of increasing accumulation rates (approximate values given).

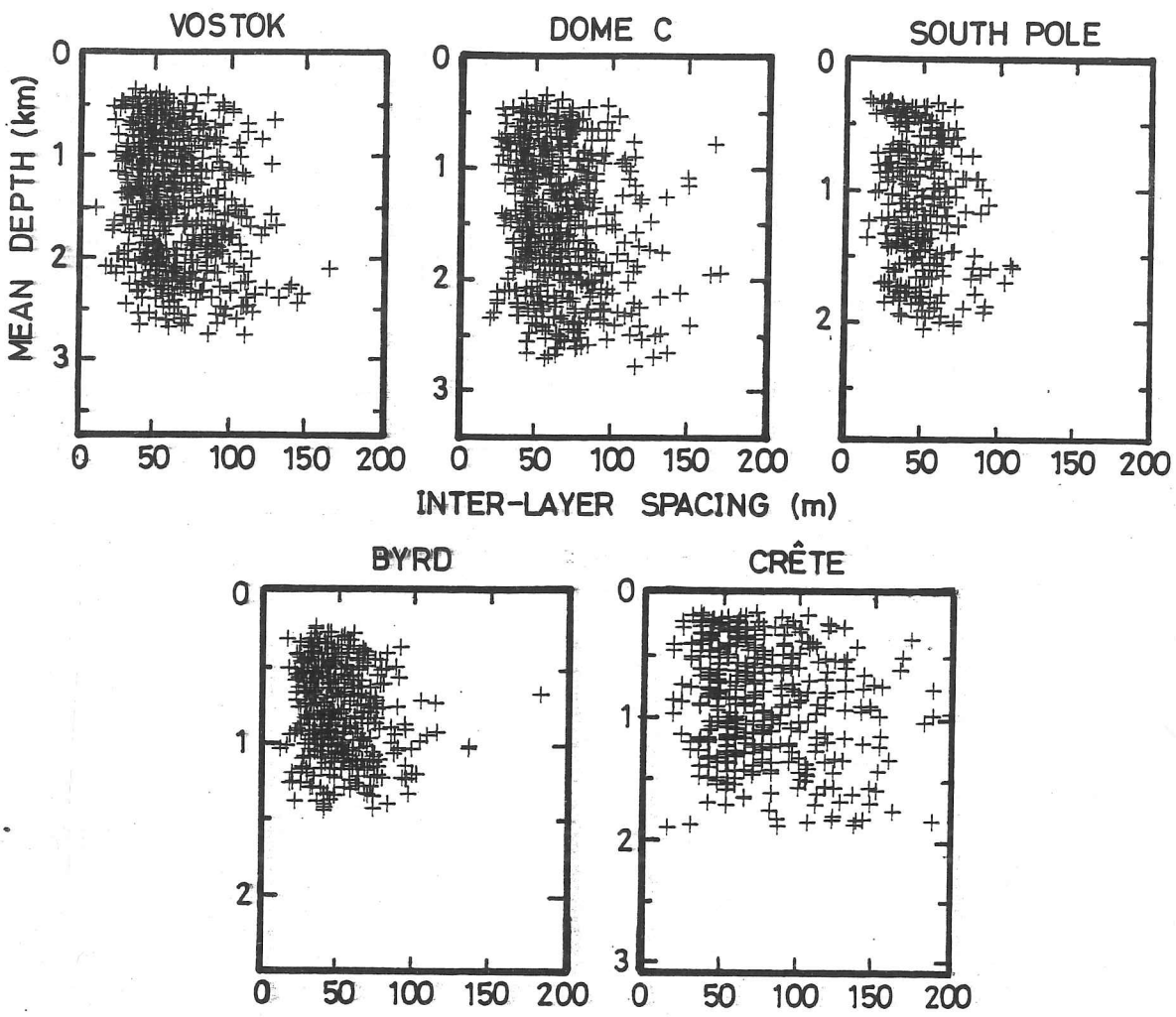

Fig. 2.10 Distribution of inter-layer spacings against mean depth at various sites.
60 MHz system, 250 ns pulse length.

TABLE 2.2 MEASURED LAYER ECHO SPACINGS

Site	Location	Accn. rate	Pulse length	Mean layer spacing	S.D.
		ma^{-1}	ns	m	m
F123/779	77°52'S, 99°08'E	0.024	250	68.0	21.8
Vostok	78°29'S, 106°48'E	0.024	"	61.6	23.2
Dome C	74°39'S, 124°10'E	0.038	"	62.5	24.3
South Pole	90°S	0.07	60	41.3	17.7
			250	47.3	17.2
			1000	65.0	28.6
F135/929	70°41'S, 133°50'E	0.14	250	59.7	21.5
Byrd	80°01'S, 119°30'W	0.15	"	49.1	21.3
F135/833	68°56'S, 136°45'E	0.22	"	61.3	20.6
F135/785	68°02'S, 138°07'E	0.27	"	56.6	20.6
Crete	71°07'N, 37°19'W	0.285	"	76.1	35.4

Values given are means of about 1500 measurements at each site, for separations between consecutive layer echoes throughout the ice thickness. Accumulation rates away from stations are approximate.

Recordings from sites with different accumulation rates, using a constant pulse length of 250 ns, show very similar spacing distributions (fig. 2.9), suggesting that in all cases the true reflector spacing is less than the spot size resolution limit. Only at Crête is there a significant proportion of inter-layer spacings greater than the ~40 m pulse length. This does not necessarily mean that the true layer spacing at this site is greater than the pulse length; due to the rapid fading of returns and the short exposure time of an A-scope photograph, some reflections may have temporarily faded below the detection threshold, so that the apparent spacing (of the remaining 'strong' echoes) may be several times the true reflector spacing.

As a further check we can examine the variation of echo spacings with depth at a particular site. Since the deeper ice layers are thinned by compression the true reflector separation must on average decrease with depth. By looking at the distribution of inter-layer spacings with depth at various sites (fig. 2.10), we find that at no site is there a significant change of layer separation with layer depth, indicating again that even near the surface the true reflector spacing cannot be resolved. Layer spacing statistics for these and other sites are summarised in Table 2.2.

It will be shown later (Chapter 5) that the deeper layer echoes in the Antarctic, and even shallow echoes in Greenland, are caused by layers of ice of elevated acidity relative to the surrounding ice. To illustrate further that increasing numbers of internal layers should be seen as the pulse length is reduced, the method developed in Chapter 4 has been used to estimate the reflection coefficient of each annual layer along the high-resolution ice core acidity profile measured at Crête (Hammer and others 1980; fig. 2.11(a)), and the total returned power has then been summed within windows of varying length representing varying pulse lengths (fig. 2.11(b), (c) and (d)). This shows that with shorter pulse lengths it should be possible to resolve a greater number of reflecting

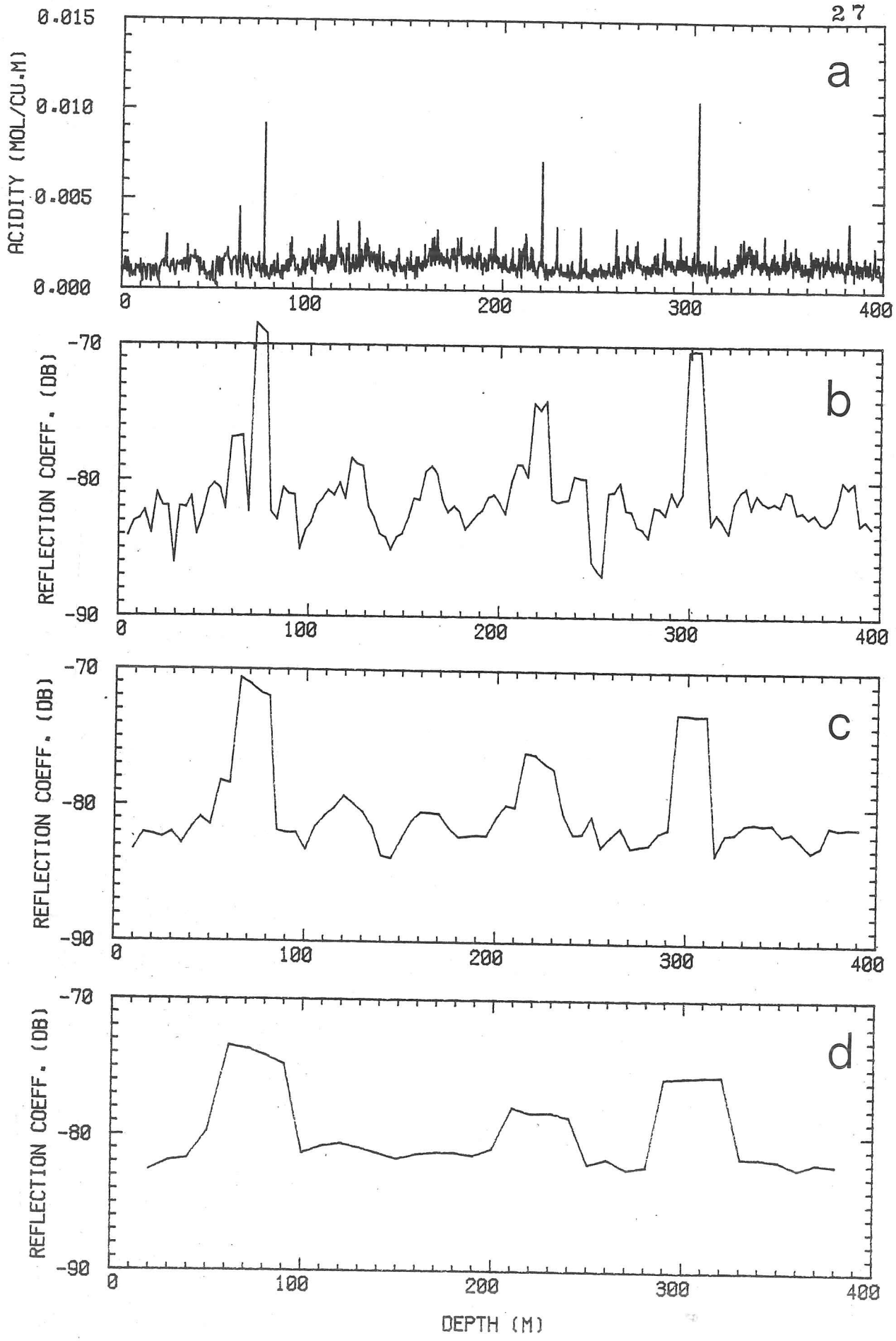

Fig. 2.11 (a) acidity profile measured along an ice core from Crete, Greenland, by Hammer and others (1980)

Simulated reflection coefficient vs depth profiles for pulse lengths of (b) 10 m, (c) 20 m, and (d) 40 m.

surfaces and hence obtain greater detail of the acidity variations. Measurements at Crête with a 250 ns pulse compare well with the predictions by this technique when a window length of 20-40 m is used (cf. fig. 5.1). Extension of this idea to the Antarctic where (assuming a similar temporal frequency of acidic reflecting horizons), reflecting layers are more closely spaced due to the generally lower accumulation rates, suggests that more and more layers will be resolved as the pulse length is reduced down to about 2 m or 10 ns (i.e. a single wavelength at 60 MHz). So for all pulse lengths >10 ns it is to be expected that mean layer echo spacings will be approximately equal to the pulse length, however the spot size limit of the recording oscilloscope will prevent the observation of any layer spacings less than about 34 m as mentioned above. With very long pulse lengths complications arise due to distortion of the pulse shape (fig. 2.7), which make it difficult to measure layer spacings reliably.

(b) continuity and structure of reflecting horizons

It is clear that at most sites, with the exception of near-surface layers at high-accumulation sites such as Crête, individual reflecting surfaces within the ice cannot be resolved by the present equipment. The observation has also been made that mean layer spacings are similar to the pulse length employed. It is important to take account of these findings when considering the continuity of the stratifications and the nature of the reflecting surfaces. The following hypothesis is proposed to account for the observations.

Reflections are received from groups of several thin horizons acting as composite reflecting zones. However, although some power is returned within each pulse length, the horizons with the largest changes in dielectric properties (e.g. the highest acidity layers) may govern the position of prominent layers (e.g. fig. 2.11); continuity of layer echoes is to be expected from continuity of deposition of these high acidity

horizons. Continuity of these horizons has been established by Hammer (1977), who observed the high acidity peak from the 1783 AD Laki eruption in ice cores from DYE-3, Crête and Hans Tavsen, Greenland. This is to be expected because of the atmospheric nature of their deposition.

As demonstrated for the acidity profile at Crête, the effective thickness of the reflective zones is governed by the pulse length used, so that all surfaces lying within the pulse length contribute to the observed reflection coefficient. The assumption is made that the spacings of the individual thin reflecting horizons is much less than the pulse length; detailed ice core acidity profiles and the temporal frequency of suitable volcanic eruptions at the present suggests that this is likely to always be the case, particularly in the Antarctic where accumulation rates are low.

The relatively short length of some layers may be explained in terms of varying layer separations. As the ice sheet thickness increases locally the separation of a given pair of echoes will increase until their separation is greater than the pulse length. When this happens it is possible for a new 'layer' to be observed between the two original layers, and this accounts for the uniformity of layer spacings at single sites.

Petrin (1975) has made a numerical simulation of PRC vs depth profiles for a stratified medium such as an ice sheet, and his results also show that power maxima corresponding to internal layers are found with spacings similar to the pulse length chosen, independent of the true reflector spacing when this is less than half the pulse length. An analogous situation is also observed in seismic profiling of ocean sediments. Measured reflection coefficients for layer echoes must refer to groups of surfaces, so it is valid to interpret these as representing the sum of the individual surfaces averaged over the length of the pulse.

Chapter 3

REFLECTIVITY AND ROUGHNESS OF INTERNAL SURFACES

3.1 The determination of power reflection coefficients

The power return and range of layer echoes can be determined from power maxima on A-scope recordings. Depths of layers are obtained from the time range, assuming a constant propagation velocity for radio waves in ice of 168 m μs^{-1} (Johari & Charette 1975; Robin 1975), and making a 10 m correction for the higher radio velocity in the firn layer (Robin and others 1969; see also Table 5.1).

The calibration of returned power in the field was simply made by connecting a series of attenuators between the transmitter and receiver and recording the strength of the received signal. The 60 MHz equipment was normally operated with a pulse duration of 250 ns, a 4 MHz receiver bandwidth and a nominal peak power output of 10 kW, in which mode the calculated system performance is 176 dB, but field measurements (Neal & Meldrum, personal communication) show that the real power output was ~7 kW, reducing the system performance to ~174 dB. This figure was used when estimating power reflection coefficients for internal layers by the procedure below. Although some measurements have been made with the 300 MHz system (Chapter 2) this has really only been done for trial purposes, and the results are not considered to be so reliable due to a less rigorous method of power calibration.

The reflectivity of an internal horizon, R, is only one of several factors determining the amount of power returned by it to the transceiver, $\langle P \rangle$, and in order to determine R it is necessary to estimate losses caused by geometrical spreading of the pulse and dielectric attenuation (D) in the overlying ice, and the gain from refraction of the pulse at the ice

surface:

$$\langle P \rangle = G - 20\log_{10}\left[\frac{\lambda_0}{8\pi(r_0+h/n)}\right] + R + D \qquad [3.1]$$

spreading + refraction term

where <P> is measured in dB relative to the transmitted power, and G is the mean square forward antenna gain. Geometrical and refraction contributions are obtained from the distances r_0 (terrain clearance) and h (layer depth), which are measured using the echo sounder. The (two-way) antenna gain for the TUD 60 MHz equipment (including losses in the antenna cables, power divider and T/R switch) has been measured as 21.4 dB (Skou & Sondergaard 1976). Dielectric absorption losses are calculated from temperature profiles and laboratory measurements of the radio wave attenuation in ice at various temperatures (Westphal 1963; Johari & Charette 1975). Temperature profiles were either estimated from a model, or obtained from measurements in boreholes (where available).

Various checks were made to determine the accuracy of this procedure. The principal errors arise in digitising the A-scope displays, and in the estimate of dielectric losses. The A-scope frames, from which the depth and power measurements were made, were enlarged and the positions of echo peaks measured using a DMAC digitising table, and punched onto paper tape for later computer processing. By repeatedly measuring the position of a layer echo peak the standard deviation in layer depth was determined to be 5.5 m, and in the returned power, 0.3 dB. The error in returned power is probably comparable to that introduced by non-linearity in the signal response curve, which was only calibrated at 10 dB intervals.

Dielectric losses were estimated using laboratory values of the dielectric absorption of ice as a function of temperature, in conjunction

with a temperature profile. The available attenuation measurements refer either to polar ice at a frequency other than 60 MHz (Westphal 1963) or to laboratory-grown ice (Johari & Charette 1975). As a check on the applicability of this data to polar ice at 60 MHz, the total absorption above a subglacial lake near Vostok Station was measured from RES data and compared with that calculated from laboratory values. This site was chosen because (a) the temperature profile can be reliably estimated from borehole temperature measurements at Vostok (Barkov 1974; Budd and others 1975), and (b) the PRC of the lake interface can be calculated from the permittivity difference with reliability. Ice shelves are not suitable for this purpose; Neal (1977) has shown that the basal reflectivity of the Ross Ice Shelf can vary greatly with location, and concludes that this is due to factors such as basal freezing and brine percolation.

From a number of measurements a mean value of 86.8±1.8 dB was obtained for the two-way dielectric absorption of the 4040 m-thick ice over the lake. This assumes the ice/water interface to have a reflection coefficient of -3.4 dB, calculated from the change in permittivity; this value could be altered slightly by factors such as debris in the basal ice, or dissolved salts in the water. However the slow fading of the radio echo suggests an extremely smooth interface, and temperature profile calculations support this as a basal melt rate of ~0.1 mma^{-1} is predicted. Dissolved impurities in the water could increase the PRC to about -1 dB, but not more, so the possible range of variation is quite limited. The observed value is in excellent agreement with that obtained from a calculated temperature profile and laboratory values of dielectric absorption as a function of temperature: Westphal's results (for polar ice at 150 MHz) indicate a total two-way attenuation of 87.1 dB, and Johari & Charette's values (for laboratory-grown ice at 60 MHz) give 86.4 dB. It is hence assumed that the procedure of estimating absorption losses from temperature profiles and attenuation coefficients gives results which are accurate enough, especially since at this site half of the absorption occurs in the lower 20% of the ice column, below the depth at which layers

are detected. Errors may still arise from inaccurate estimates of the temperature profile, but at the principal sites of interest (Byrd, Vostok and Dome C) this is largely avoided by using measured temperatures from boreholes.

Where measurements were not available, temperature profiles were estimated using the model by Budd (1969):

$$\Theta_z = \Theta_s - Z\left[\gamma_b \frac{1}{y}(\mathrm{erf}(y)-\mathrm{erf}(\xi y)) - \frac{V\alpha\lambda_e}{\dot{A}} 2(E(y)-E(\xi y))\right] \qquad [3.2]$$

where: $\dot{A}$ = accumulation rate

$\mathrm{erf}(x) = \int_0^x e^{-t^2}\,dt$

$E(x) = \int_0^x (e^{-z^2} \int_0^z e^{t^2}\,dt)\,dy$

J = mechanical equivalent of heat

K = thermal conductivity of ice = 2.3 $Wm^{-1}K^{-1}$

V = ice velocity

$y = \sqrt{\dot{A}Z/2\kappa}$ = dimensionless parameter

Z = ice thickness

α = surface slope

$\gamma_b = \gamma_g + \gamma_f$ = basal temperature gradient (geothermal + frictional)

$\gamma_f = \tau_b V/JK$

$\xi = z/Z$ = fractional ice thickness

κ = thermal diffusivity = 44 m^2a^{-1}

λ_e = surface temperature elevation gradient

Θ_s, Θ_z = temperature at surface, height z

τ_b = basal shear stress

This equation is based on a model which considers all frictional heating to be applied at the base of the ice sheet together with the geothermal heat flux, and takes into account the horizontal advection of cold ice

from upstream. Because of the absence of accurate glaciological input data at many of the sites, checks were again made to see what effect likely errors in input parameters had on the estimated absorption. The total absorption was found to be relatively insensitive to such changes, and the maximum error for a layer half-way down in the ice sheet was estimated to be no more than 3 dB, rising to 5 dB for the deepest layers.

Previous estimates of layer PRC have varied considerably; Table 2.1 lists all published values, and shows a range of -43 to -83 dB. This may be due to the use of different frequencies, pulse lengths and equipment, but the main differences probably arise from simplifications made in calculating PRCs. Frequently a constant ice temperature has been assumed, or a line fitted to many echo peaks on an A-scope display in order to obtain an average value for all layers at a particular location. In no case has allowance been made for the rapid fluctuation in returned power caused by the roughness of the reflecting surfaces; this may introduce an error of 5-10 dB into the PRC. However, these estimates were probably intended to give initial values for comparison with those based on hypotheses suggested for the origin of the layers, and so accuracy was not paramount. By improving the measurement procedure and making more careful estimates of other losses it has been possible to obtain more accurate results, which have led to more detailed studies of the probable origin of the echoes than was previously possible. Approximately 50,000 measurements at nearly twenty sites have been made during this study. Typical errors for measurements obtained from A-scope displays recorded with the Super 8 camera are estimated to be ±10 m in depth and ±2 dB in reflection coefficient.

3.2 The variation of reflection coefficient with layer depth

Profiles of layer reflection coefficient vs depth at various sites have been obtained from A-scope displays recorded in rapid bursts with a Super 8 cine camera in the manner described above. The values of layer depth and PRC obtained from each frame of the film were then plotted on one diagram (e.g. fig. 3.1(a)), giving a PRC vs depth profile for that site. By using many A-scope displays recorded over a horizontal distance of only a few hundred metres, the individual layer echoes may be clearly seen as groups of measurements at constant depth; the spread of values for each layer covers a range of ~5 dB, largely due to the variation in returned signal strength caused by the layer roughness on a scale comparable with the radio wavelength. By taking an average of 100-200 measurements for each layer echo this fluctuation may be smoothed out - but layer reflectivity also varies on larger scales, and an estimate for a layer obtained from a single camera burst is probably only representative of that layer for a distance of a few kilometres.

Fig. 3.1 shows the correlation between A-scope peaks and Z-scope layers; note the lack of correlation between measured echo strength and echo brightness on the Z-scope film. Because the Z-film is differentiated the layer brightness is related to the rate of increase of returned power, and not to the power itself. The sites for which PRC vs depth profiles have been produced are shown on fig. 3.2. Profiles for principal Antarctic stations (Vostok, Dome C, South Pole and Byrd) are shown in fig. 3.3; profiles from other sites appear in figs. 6.6 and 6.10. In all these diagrams the top of the box represents the ice surface, and the base the bedrock.

From such profiles two regions in the ice sheet may be distinguished; an upper zone (typically 400-600 m thick) shows a rapid and continuous decrease in PRC with depth, which is consistent both in character and magnitude with that expected for reflections caused by fluctuations in ice

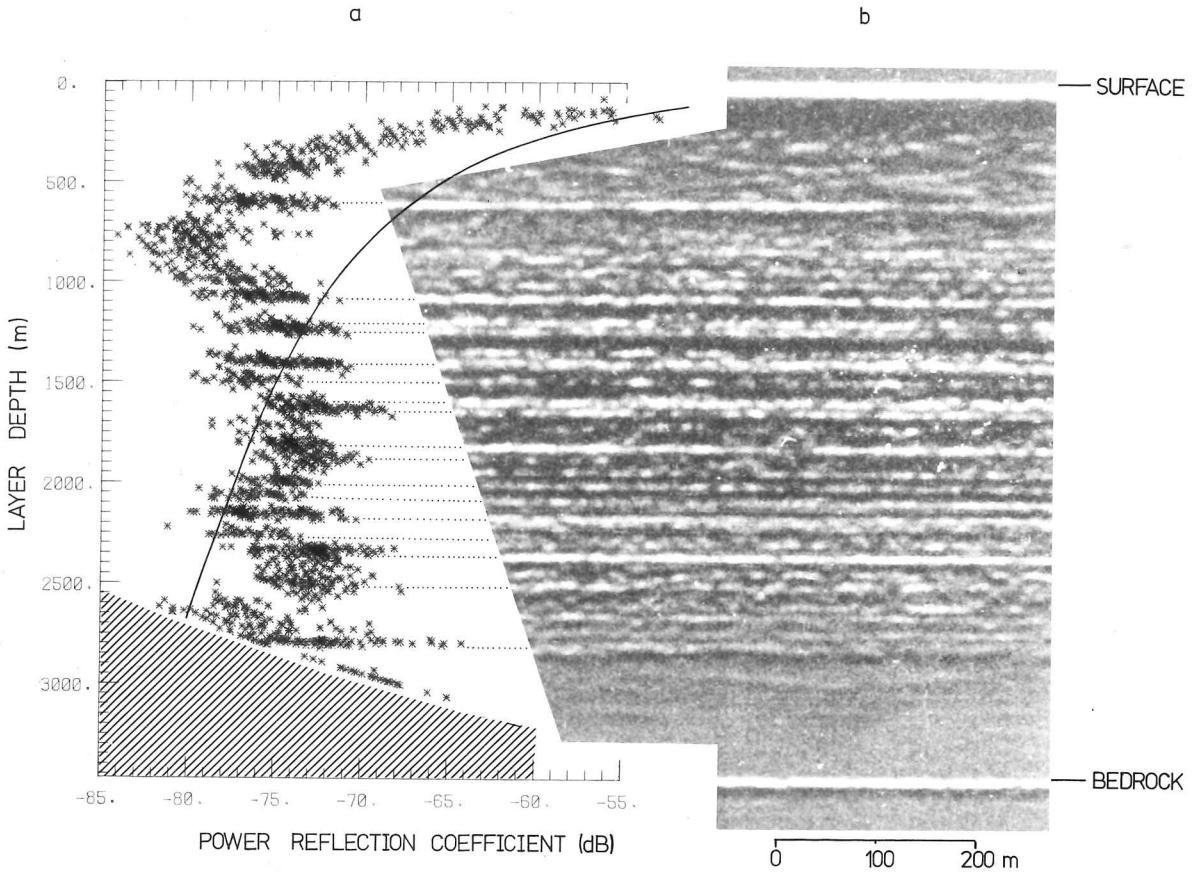

Fig. 3.1 (a) Reflection coefficient vs depth profile (at site F136/608, ∿100 km NW of Dome C) from many power measurements obtained with the TUD 60 MHz radar, using a 250 ns pulse length, 4 MHz receiver bandwidth and 10 kW peak power. Solid line shows maximum likely PRC expected from density fluctuations (for a simple clear ice/bubbly polar ice interface), and shaded area is that beyond the detection limit.

(b) corresponding section of Z-scope film. Dotted lines connect groups of PRC measuremenst with layers.

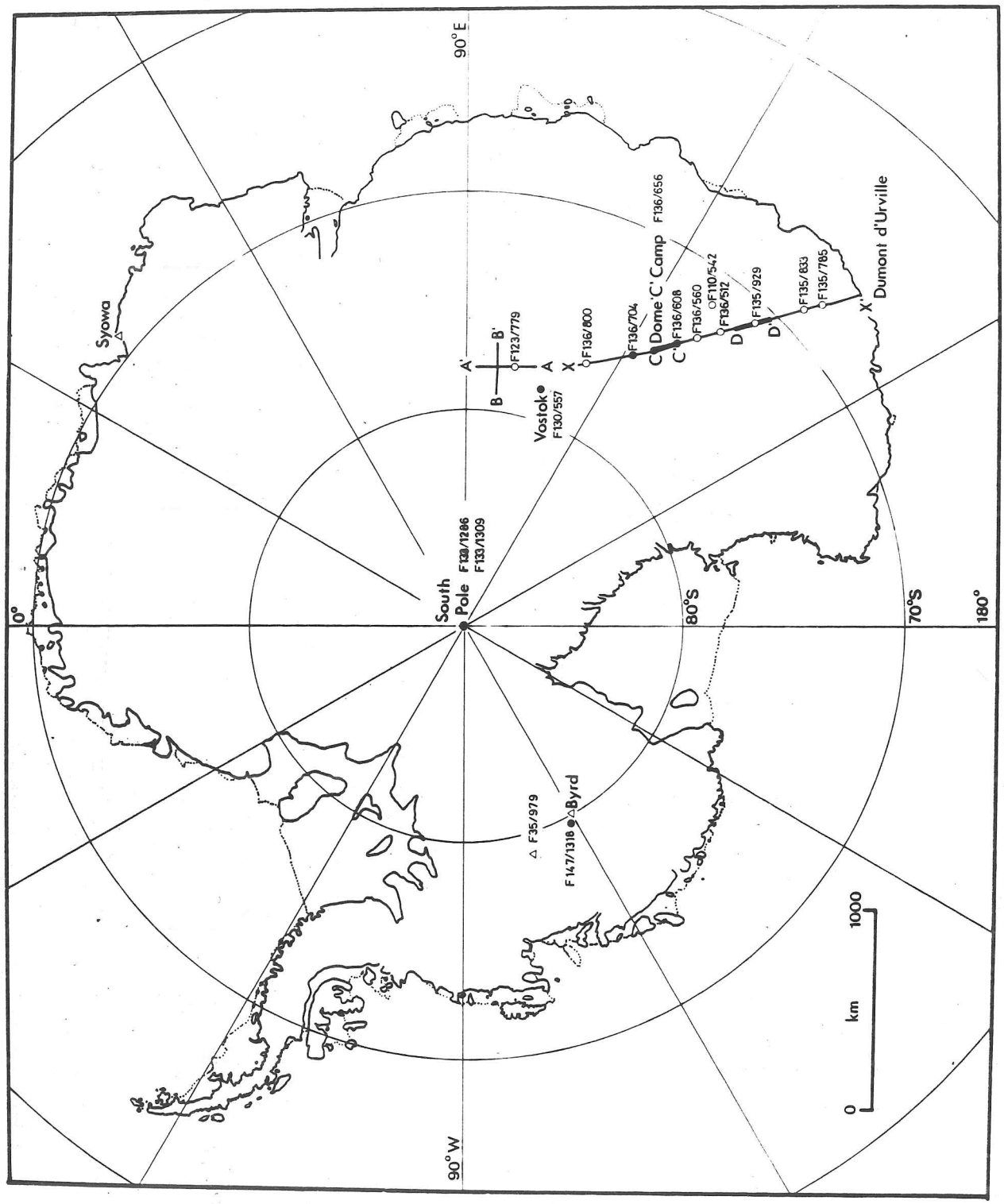

Fig. 3.2 Location map for power measurement sites:

Open circles:	measurements at ∿2 m intervals
Solid circles:	" ∿2 km "
Thin lines:	principal sections with power measurement sites on them
Heavy lines:	sections with measurements every 2 km
Triangles:	other locations where measurements made

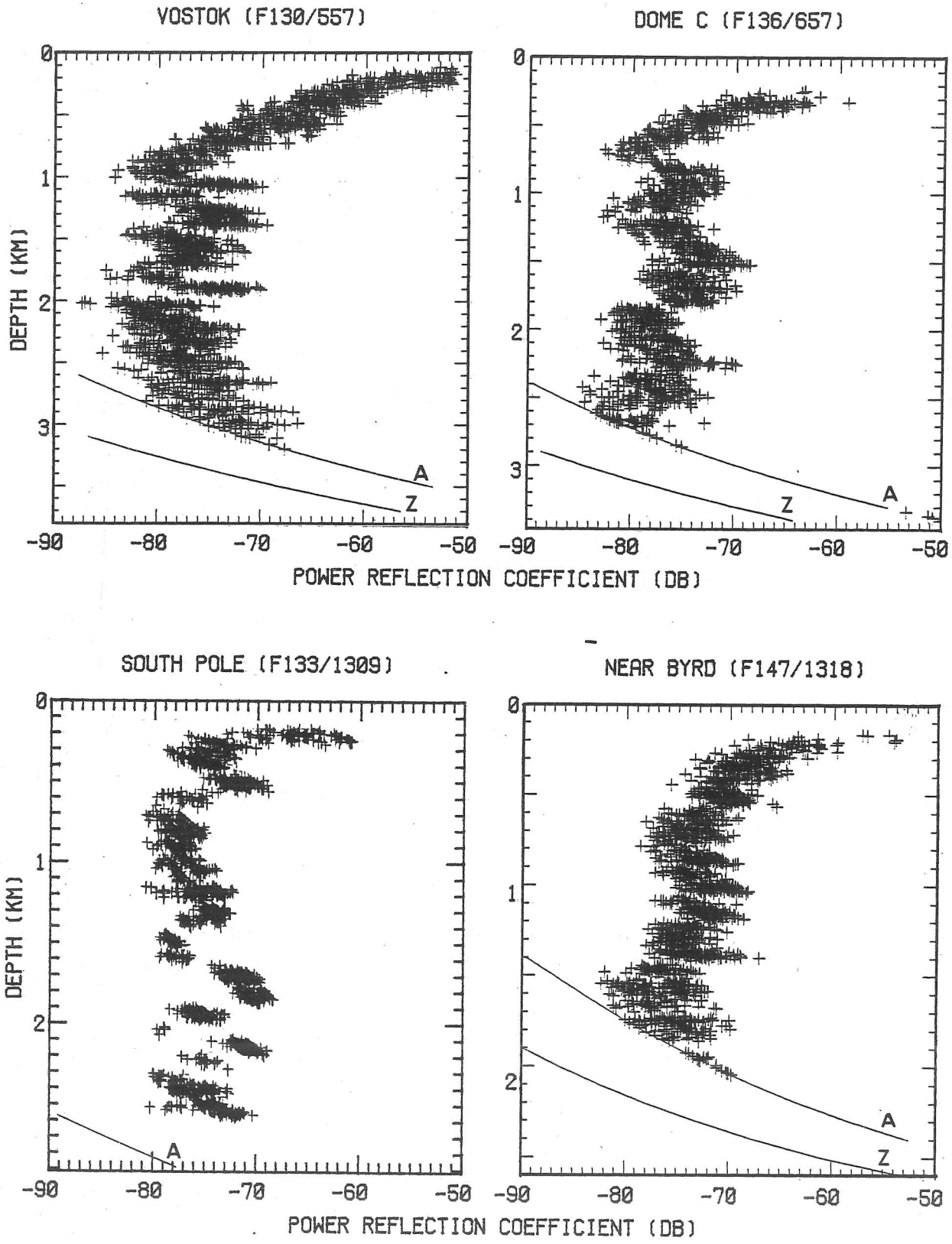

Fig. 3.3 Reflection coefficient vs depth profiles for layers observed at principal Antarctic stations, from calibrated 60 MHz radar A-scope displays recorded at 2 m intervals. Lines represent A- and Z-scope detection limits.

density (see next chapter). Comparison of profiles obtained at different aircraft terrain clearances, and calculations of the amount of power expected to be returned from wide-angle surface scatter (section 4.4(a)), show that surface scatter could not be responsible for artificially shaping the PRC vs depth curve, and normally would not even be detectable below 100 m depth. Note also the lesser horizontal continuity of layers in the upper region, both on the Z-scope (fig. 3.1(b)) and in the lack of clear groups of values on the PRC vs depth profile; this probably arises because of the localised nature of the density fluctuations thought to be responsible for the reflections in this zone.

A second zone contains echoes whose PRCs do not follow any regular trend with depth. In this region the layers seem to be roughly regularly spaced, with PRCs in the range -80 to -70 dB. As will be seen later this is what might be expected on the hypothesis that the echoes arise from layers of ice containing very low levels of acidic impurities of volcanic origin, causing the ice to have an elevated loss tangent.

The lower limit of the second zone is determined either by the attainment of the system detection limit (which is principally governed by the attenuation in the ice), e.g. at Byrd, or by a basal layer-free zone being reached, e.g. at South Pole, where the basal layer-free zone is ~250 m thick (see fig. 6.3). This zone has a variable thickness (~50-1000 m) which appears to depend upon the bedrock relief and ice velocity. Its probable cause and occurrence are discussed in Chapter 6.

3.3 Large scale horizontal variations in layer reflectivity

The recording interval of available A-scope data is not well suited to the analysis of large scale variations in layer reflectivity. The duration of each Super 8 recording burst is only about 1 km, and so it is necessary to turn to the single A-scope frames recorded every CBD (~2 km spacing).

This recording interval enables reflectivity variations on a scale >10 km to be investigated, with the important proviso that the measurement at each point is reliable. As seen in the previous section, layer reflection coefficients fluctuate rapidly over a range of about 5 dB, so using the available recordings we expect to be able to resolve variations in reflection coefficient only if they are >5 dB in amplitude and >10 km in wavelength.

On the hypothesis that the reflecting surfaces are depositional in nature, it is reasonable to suppose that the distribution of material will depend on weather systems and other atmospheric factors. The concentration of marine impurities in snow, for instance, is observed to fall off with increasing distance from the coast (e.g. Boutron & Lorius 1977). Aerosols introduced to the Antarctic from the lower stratosphere may, on the other hand, be deposited primarily on the higher interior of the continent. The long route and journey time (1-3 yrs) for aerosols to be deposited in polar snow (Appendix 1) may mean that regional variations in the rate of deposition are largely smoothed out by the effects of mixing in the atmosphere and changing weather patterns. However, it remains possible that variations in layer reflectivity will occur over very large distances as a result of such atmospheric processes. Secondly, since the reflection coefficient of a layer depends upon its thickness (eqn. [4.8]), we expect that the reflectivity of individual layers will be affected by fluctuations in the rate of accumulation.

Results from the 1968-69 Japanese Antarctic Research Expedition (JARE) Traverse from Syowa Station to the South Pole have shown that the rate of accumulation does not just decrease regularly from the coast to the interior, but that pronounced fluctuations occur on scales of 20-60 km (Endo & Fujiwara 1973). The cause has been shown to be preferential deposition of snow in shallow depressions in the ice surface, tens of metres deep and up to several tens of kilometres across. Such depressions have been widely observed in the Antarctic and Greenland by both

conventional optical levelling techniques (Robinson 1964; Budd & Carter 1971; Mälzer 1964) and by satellite radar altimetry (Brooks and others 1978), and are clearly visible on satellite images (e.g. in Rose 1978). Not all such surface undulations are wind-drift accumulation waves; Budd & Carter (1971) have shown that stationary waves with wavelengths ~2-6 times the ice thickness can be generated by flow over bedrock undulations; however varying local accumulation rates might be expected over all such features whatever their primary cause.

The magnitude of the fluctuations in accumulation rate associated with these depressions is quite large; on the slope between Syowa and Plateau Stations the Japanese observed that the accumulation rate regularly varied between 0.02 to 0.12 ma^{-1} in an area with a mean accumulation rate of ~0.07 ma^{-1}. On the high plateau region variations were much smaller, the range being only about 0.01 ma^{-1} in the region of Plateau Station (~0.04 ma^{-1} accumulation).

Annual layers deposited in such areas should show regular variations in thickness associated with these changes in accumulation rate. Applying eqn. [4.8] to the JARE data we may estimate that these thickness variations would cause the PRC of a single annual layer containing acidic impurities to vary over a 10-15 dB range on the slope region, and over approximately 5 dB on the inland plateau. Such reflectivity variations, if they applied to the zone of layers thought to be responsible for each internal reflection seen, may be detectable with the available measurements and equipment.

The hypothesis that near-surface internal echoes are caused by density fluctuations (section 4.3(a)) does not suggest how reflection coefficients might vary over long distances, because the causes of the fluctuations are not themselves well understood. Inspection of Z-scope records shows that the horizontal continuity of layers in the near-surface region (i.e. those thought to be due to density fluctuations) is much less

than in the deeper ice, where volcanic acid layers are thought to be the dominant cause of reflections. This has thwarted attempts to study large scale reflectivity variations of near-surface layers, but itself suggests that the density fluctuation mechanism operates primarily over areas of only a few square kilometres.

Two 150 km-long sections from the Dome C to Dumont d'Urville track (see fig. 6.9) have been analysed to look for possible long wavelength reflectivity variations. The first section lies in the inland plateau region, and the second on the katabatic slope area; the positions of the sections are shown on the location map (fig. 3.2). Several long horizons were traced on the Z-scope record along each section (the same as those shown on fig. 6.9, with one addition), and layer PRCs were then measured from A-scope records at CBD intervals. The results are shown on fig. 3.4, (a) plateau section and (b) slope section.

In the plateau region the PRC measurements show small random fluctuations which do not exceed in amplitude or wavelength the estimated minimum values for reliable detection of a true variation. These fluctuations therefore probably arise from the inherent uncertainty of single measurements. In the slope region the layers studied show (a) larger short-scale fluctuations in PRC, and (b) large-scale changes in PRC of 10-15 dB amplitude. The short-scale fluctuations probably reflect the greater range of layer thicknesses possible because of the greater accumulation rate. The large changes in layer reflectivity over 50-100 km may be the result of long wavelength accumulation variations; since each radio-echo layer is believed to originate from a number of closely spaced reflecting surfaces, we may expect to see only the combined effect of the layer thickness variations. This may account for the lack of variations on a scale less than 50 km. The distance for which layers may be followed unambiguously on the Z-scope records prevents further studies of individual layers over longer distances.

than in the deeper ice, where volcanic acid layers are thought to be the dominant cause of reflections. This has thwarted attempts to study large scale reflectivity variations of near-surface layers, but itself suggests that the density fluctuation mechanism operates primarily over areas of only a few square kilometres.

Two 150 km-long sections from the Dome C to Dumont d'Urville track (see fig. 6.9) have been analysed to look for possible long wavelength reflectivity variations. The first section lies in the inland plateau region, and the second on the katabatic slope area; the positions of the sections are shown on the location map (fig. 3.2). Several long horizons were traced on the Z-scope record along each section (the same as those shown on fig. 6.9, with one addition), and layer PRCs were then measured from A-scope records at CBD intervals. The results are shown on fig. 3.4, (a) plateau section and (b) slope section.

In the plateau region the PRC measurements show small random fluctuations which do not exceed in amplitude or wavelength the estimated minimum values for reliable detection of a true variation. These fluctuations therefore probably arise from the inherent uncertainty of single measurements. In the slope region the layers studied show (a) larger short-scale fluctuations in PRC, and (b) large-scale changes in PRC of 10-15 dB amplitude. The short-scale fluctuations probably reflect the greater range of layer thicknesses possible because of the greater accumulation rate. The large changes in layer reflectivity over 50-100 km may be the result of long wavelength accumulation variations; since each radio-echo layer is believed to originate from a number of closely spaced reflecting surfaces, we may expect to see only the combined effect of the layer thickness variations. This may account for the lack of variations on a scale less than 50 km. The distance for which layers may be followed unambiguously on the Z-scope records prevents further studies of individual layers over longer distances.

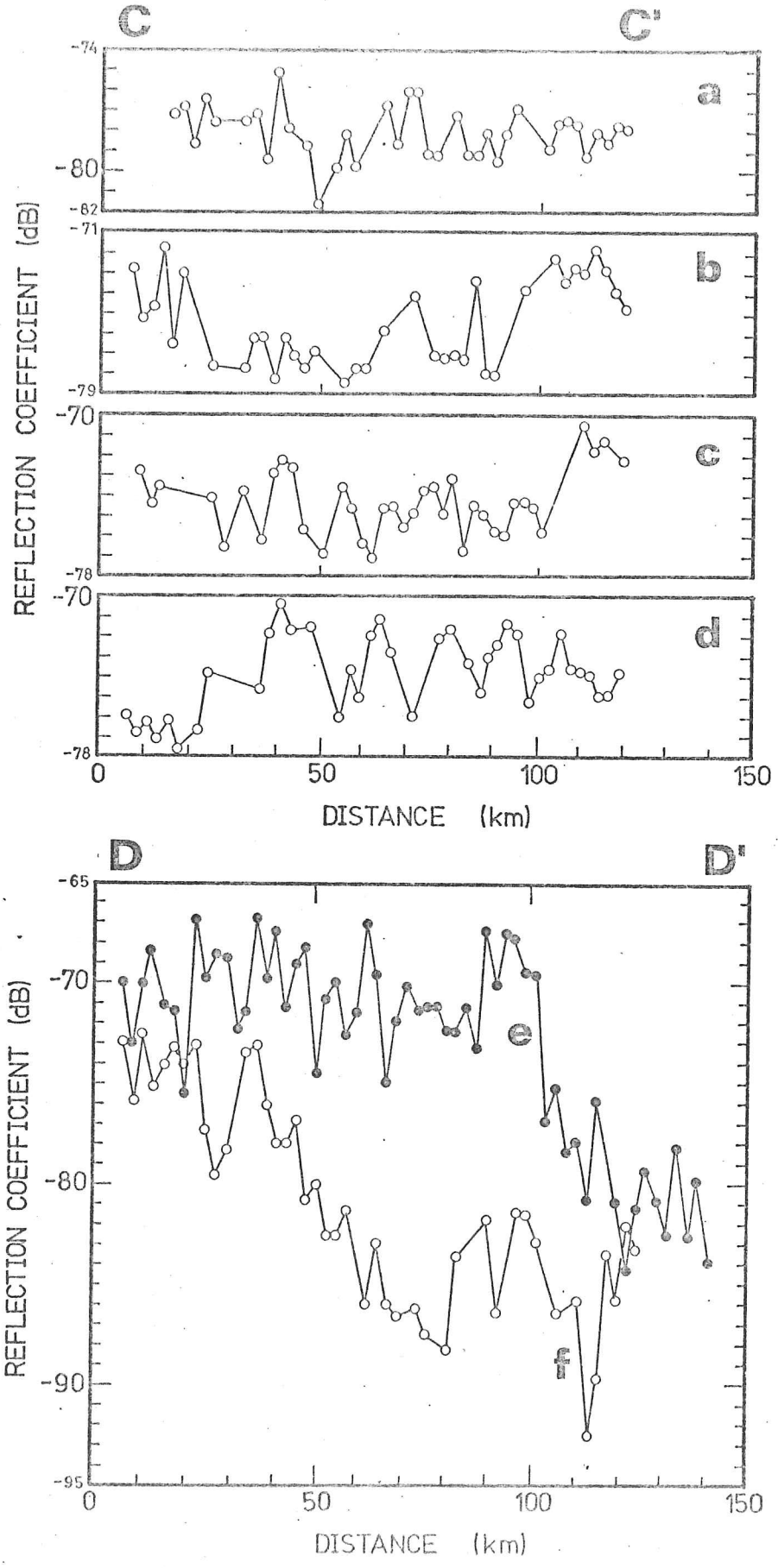

Fig. 3.4 PRCs from single measurements at ∿2 km intervals along CC' (plateau area) and DD' (slope). Layer depths and estimated ages:

(a) 755-930 m, ∿27 kaBP, (b) 1220-1410 m, ∿48 kaBP,
(c) 1630-1820 m, ∿68 kaBP, (d) 2130-2390 m, ∿86 kaBP,
(e) 550-900 m, ∿7 kaBP, (f) 1150-1600 m, ∿15 kaBP.

3.4 Fading in the returned signal

The power returned by the internal horizons fluctuates rapidly (fades) as the aircraft moves above the ice surface. This may either be caused by roughness of the reflecting surface on a scale comparable to the radio wavelength (for this purpose 'roughness' may refer either to a physical surface or to a surface of dielectric discontinuity within the ice), or by the existence of a rough surface (such as the ice sheet surface) lying between the reflector and the echo sounder (this possibility is discussed later). The fading is noticeable on expanded Z-scope recordings by the speckled appearance of some of the layers, but is seen more clearly when watching the A-scope display in real time. Measurement of these fluctuations in power level may be made either by oscilloscope cine photography or by the echo strength measurement (ESM) device, which produces a continuous record of the peak power returned within a specified range window against time (Neal 1976). Both these methods were used during the 1974-75 and 1977-78 Antarctic field seasons, but the ESM device was normally used to measure the fading of the bedrock echo, and few examples of the variation in power returned from layer echoes have been recorded with it. Fig. 3.5 shows an example of an ESM recording of the return from a layer echo, together with recordings of other types of reflecting surface.

Two approaches have been used in radio-echo sounding to determine the roughness of a reflecting surface. Harrison (1972) related the power variance (V_p) and the autocorrelation function (ρ_p) of the power returned from a surface to the roughness parameters of that surface; Oswald (1975) described a method in which the observed echo pulse shape was compared with theoretical shapes for pulses returned from surfaces of specified roughness. Neal (1977) has developed both approaches, and has given a more general solution for the power variance and autocorrelation function of the returned power than Harrison. The use of echo pulse shapes is impracticable for this study, as special recording techniques are

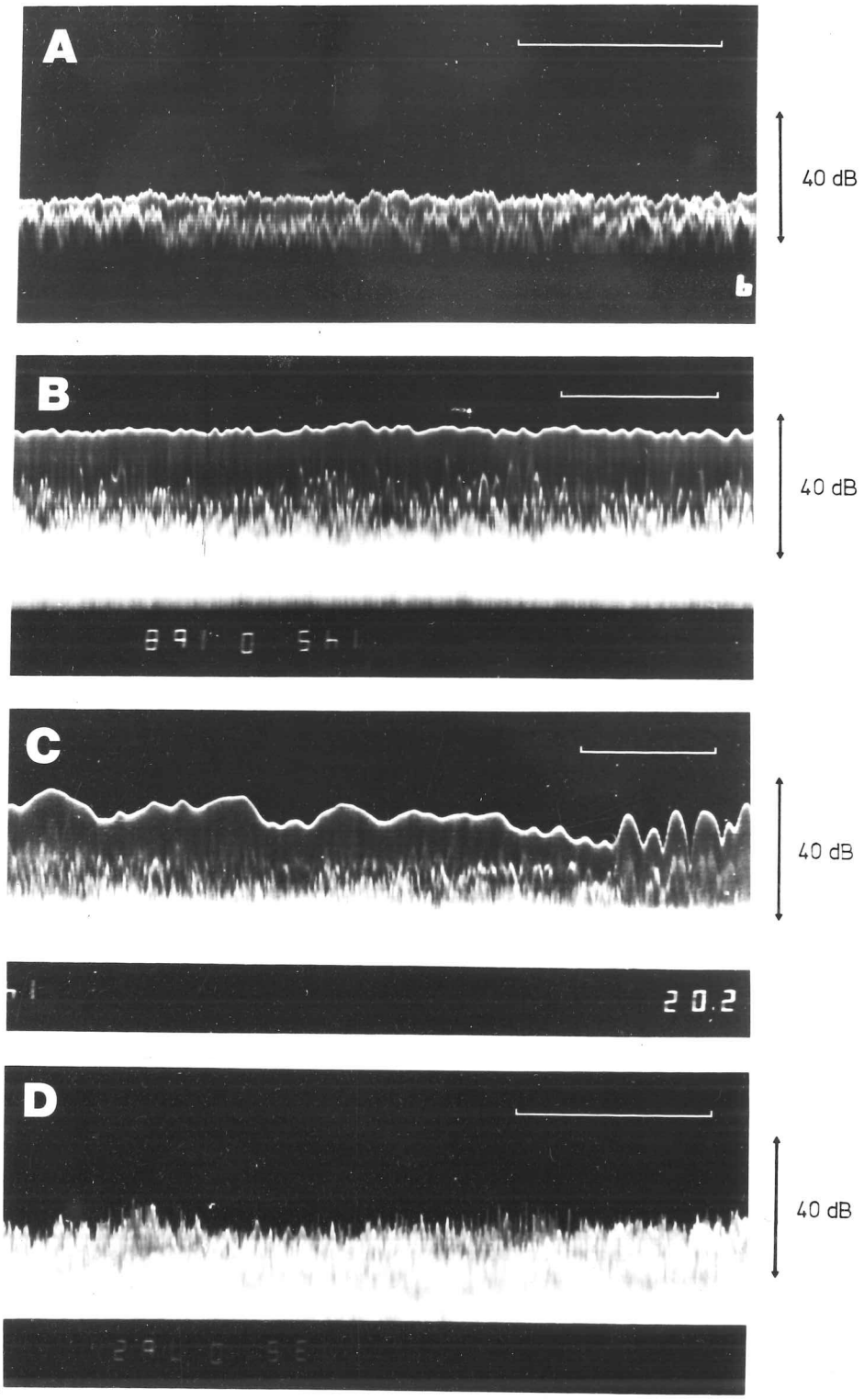

Fig. 3.5 60 MHz ESM records showing power profiles for various reflecting surfaces:

(a) internal layer (79°13'S 108°00'W), unknown depth, terrain clearance (TCL) = 340 m

(b) ice shelf surface (79°44'S 179°45'W), TCL = 8000 m

(c) smooth ice shelf bottom (83°14'S 175°17'W), ice thickness = 550 m, terrain clearance = 8200 m

(d) bedrock (67°37'S 138°36'E), ice thickness = 1790 m, terrain clearance = 790 m.

Horizontal scale bars = 500 m.

necessary in order to resolve the pulse shape adequately, and there has been no opportunity for this. However the existing records do give a qualitative impression; layer echoes are sharp and symmetrical without a trailing edge, and are similar to those observed for smooth ice/water interfaces. Echoes returned from bedrock are often asymmetrical with long trailing edges, indicative of a diffuse reflector which returns power at larger angles to the vertical.

In this work the method developed by Neal (1977), based on the measurement of the variance and autocorrelation function of the returned power, will be used to derive the parameters ϕ_o (RMS phase shift imposed by the layer roughness on the returned signal), β_o (RMS slope of the layer), and σ (RMS vertical deviation from the mean horizontal plane). These parameters may be derived from measurements of V_p and ρ_p of the peak power returned from a surface, so long as certain conditions are met: the returned signal should not be limited by either the antenna beamwidth nor the pulse length, and the returned power must be sampled at a rate greater than the Nyquist sampling frequency.

Neal's approach uses an approximate form of the Kirchhoff formula to deduce an expression for the power returned to the transceiver. This is then used to compute the variance and autocorrelation function of the returned power. The Kirchhoff approximation is only valid providing:

(a) local radii of curvature of the reflecting surface exceed $\lambda\sigma/\pi$
(b) shadowing and multiple scattering are negligible
(c) polarisation effects are small
(d) range of surface is much greater than the radio wavelength

all of which are considered reasonable in the present situation. It is also assumed that the Fresnel reflection coefficients are independent of the local angle of incidence, which is true whilst the angle of incidence is less than about 80° (i.e. in all practical situations), and that at the

point under consideration the area of illumination is not limited by the antenna beamwidth. With the 60 MHz system this should not occur for pulse lengths less than about 300 ns.

The normalised forms of the power variance and autocorrelation function are defined by eqns. [3.3] and [3.4]:

$$V_p = \frac{\langle P^2 \rangle}{\langle P \rangle^2} - 1 \qquad [3.3]$$

$$\rho_p(\xi,\eta) = \frac{\langle P(x,y)\ P(x+\xi,y+\eta)\rangle - \langle P(x,y)\rangle^2}{\langle P(x,y)\ P(x,y)\rangle - \langle P(x,y)\rangle^2} \qquad [3.4]$$

Neal derived analytical solutions for V_p for specified limiting conditions (Table 3.1).

The solutions contain the dimensionless parameters A and R:

$$A = \frac{\lambda^2 r}{4\pi^2 L^2 p} \qquad R = \frac{\lambda r}{\pi L^2} \qquad [3.5]$$

Parameter A may be used to mathematically define long and short pulses: for a long pulse A<1, and for a short pulse A>1. For a long pulse both V_p and ρ_p are strongly dependent on surface roughness (via ϕ_o), which can therefore be evaluated, but for a short pulse the dependence is very weak, tending to the limits $V_p \to 0$, $\rho_p \to 1$. The limiting pulse length that will provide information about the surface roughness is approximately:

$$p = \frac{\lambda^2 r \Delta}{4\pi^2 L^2} \qquad \Delta = \begin{cases} 1 \text{ for } \phi_o < 1 \\ \phi_o^2 \text{ otherwise} \end{cases} \qquad [3.6]$$

Strictly speaking, this applies to phase-modulating surfaces illuminated

TABLE 3.1 RELATIONSHIPS BETWEEN POWER VARIANCE (V_p), SURFACE CORRELATION LENGTH (L) AND ROUGHNESS STATISTICS FOR SPECIFIED LIMITING CONDITIONS.

LIMITING CONDITIONS	STATISTICAL EXPRESSION
$\phi_o^2 << 1,\ A << 1$	$V_p = 2\phi_o^2\ (1-2A-1/(1+R^2))$
$\phi_o^2 >> 1,\ A\phi_o^2 << 1,\ R >> 1$	$V_p = 1 - \exp(-2\phi_o^2)$
$\phi_o^2 << 1,\ A >> 1$	$V_p = A\phi_o^2/(1-2\phi_o^2)$
$\phi_o^2 >> 1,\ A\phi_o^2 >> 1$	$V_p = \dfrac{1 + \sum_{m=1}^{\infty} \phi_o^2/m!\,(1+Am)}{\left(1 + \sum_{m=1}^{\infty} \phi_o^2/m!\,(1+2Am)\right)^2} - 1$ where $V_p \to 0$ as $A \to \infty$

and: $A = \dfrac{\lambda^2 r}{4\pi^2 L^2 p}$, $R = \dfrac{\lambda r}{\pi L^2}$

by an isotropic antenna, but the requirement for a perfectly isotropic antenna is unnecessarily severe and it is only necessary that the limit $p < r\theta_w^2$ be satisfied, where θ_w is the half beamwidth at the -8 dB (e^{-1}) point (15° for the 60 MHz sounder). Neal also showed that the average horizontal spacing between power maxima in the case of pulse limiting is given by:

$$\Lambda = \frac{\lambda}{\sqrt{3}}\sqrt{\frac{r}{p}} \qquad [3.7]$$

so for observed mean spacings greater than Λ it may be assumed that pulse limiting is not occurring.

From closely spaced observations of the peak power returned from a reflecting surface it is therefore possible to check whether pulse limiting is occurring, and if it is not, to calculate the variance and the autocorrelation length of the received signal. From Neal's work ϕ_o may then be calculated, and hence the roughness parameters β_o and σ :

$$\beta_o = \frac{\sqrt{2}\,\sigma}{L} \qquad \sigma = \frac{\lambda\phi_o}{4\pi n} \qquad [3.8]$$

Before attempting to determine layer roughnesses by the above method we should consider the possible affect of the ice sheet surface and firn layer in modulating the returns from deeper layers. In order to do this fully it would be necessary to measure the power returned from the ice sheet surface at all points where the internal layering is investigated. However this has not been possible since the sensitivity required in order to detect the weak bedrock echoes caused the surface return to saturate the receiver, making an estimate of the variation in power return from the surface impossible. Over the Ross Ice Shelf the situation is different - there are areas of very strong, slowly-fading basal returns which, combined with ice almost an order of magnitude thinner than that found inland, allowed the simultaneous measurement of variations in the power

received from the ice shelf surface and base by Neal (1977). Since the surface roughness of the ice shelf is thought to be similar to that of the inland ice, his conclusions about the effect of the ice surface on the deeper reflections are relevant here. Neal deduced that:

$$V_{p_{bottom}} \simeq 0.1\ \phi^2_{o_{top}} + 2\phi^2_{o_{bottom}} \qquad [3.9]$$

Typically, ϕ_o=0.15 rads for the ice shelf surface, 0.125 rads for the ice shelf base in smooth-bottomed areas and 0.425 rads in rough-bottomed areas. Using a value of ϕ_o=0.06 rads for an internal layer (see Table 3.2), it is seen that the effect of the ice sheet surface in modulating the power returned by internal echoes is not important. Although not used in this study, a simple way of checking whether or not the ice surface is modulating the internal echoes would be to calculate correlation coefficients for the power returned by successive layers. This method cannot be used for the ESM data where only one layer can be studied at a time.

3.5 Derived roughness characteristics for internal layers

It was initially hoped to use the Super 8 A-scope recordings to study the fading in power returned from internal layers. Unfortunately this has proved impracticable due to difficulty in measuring the received power consistently between frames, and in following the same layer from frame to frame. To illustrate these problems fig. 3.6 shows measurements of returned power at ~2 m intervals along the flight track (from Super 8 film recorded at site F136/608, near Dome C), for three layer echoes and bedrock. The bedrock echo is well above the local noise level and easily identifiable, and the returned power appears to contain only relatively small errors. However the power measurements for internal layers show a great deal of variation, much more than on ESM records of layering and impressions from watching the A-scope display in the field. Fig. 3.7 shows the power

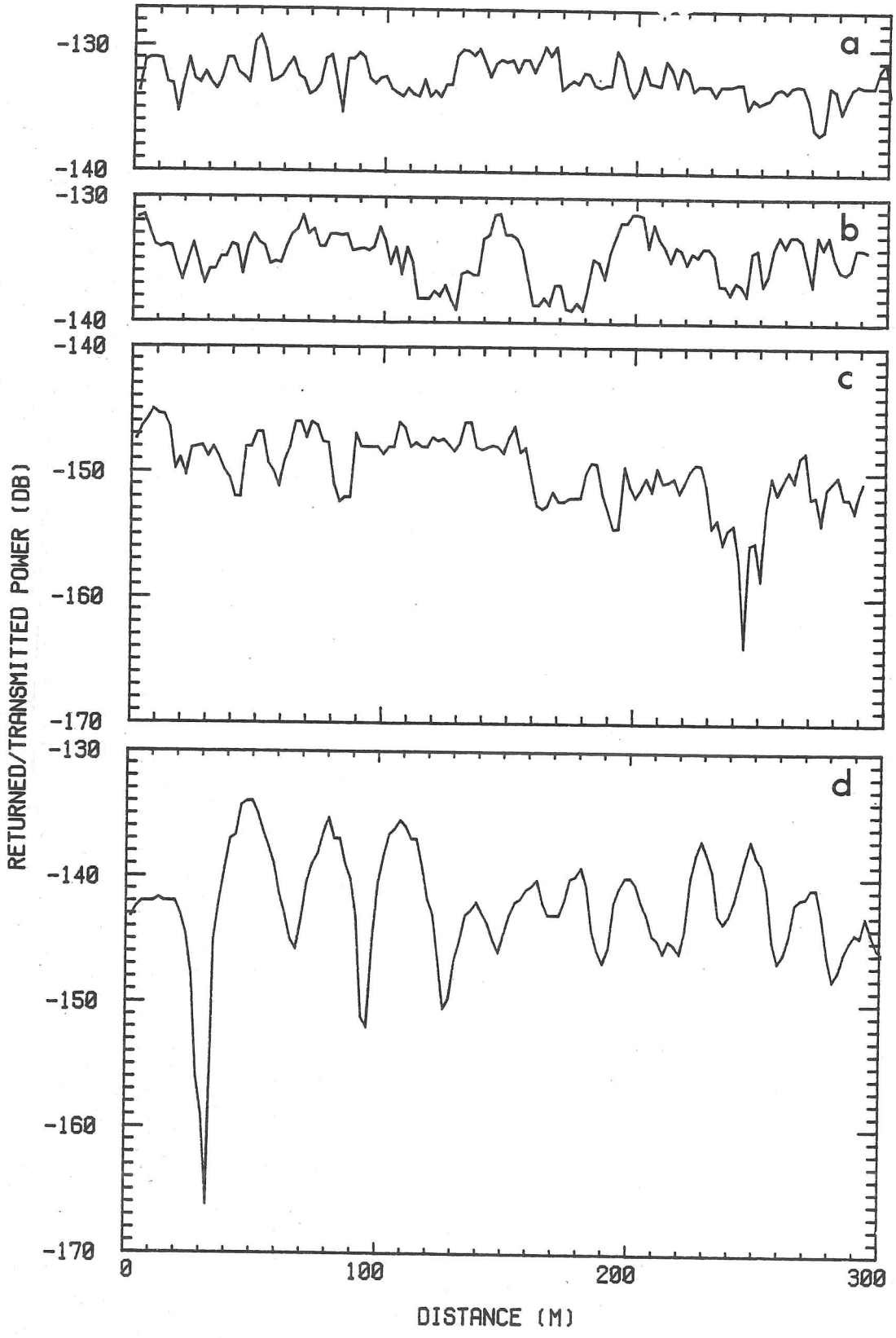

Fig. 3.6 Returned/transmitted power vs distance along track for three internal layers and bedrock, from Super 8 A-scopes recorded at ∿2 m intervals (at site F136/608):
(a) layer at 1280 m, (b) layer at 1450 m, (c) layer at 2200 m, (d) bedrock at 3500 m depth.

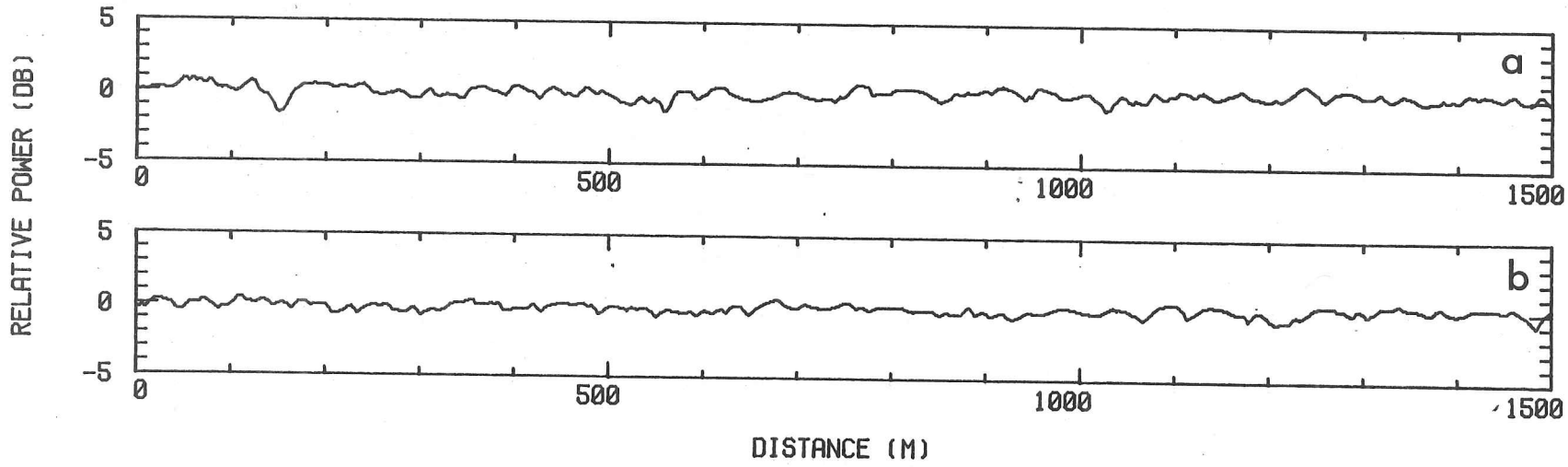

Fig. 3.7 Relative returned power against distance for two internal layers, from ESM recordings at site F35/979:
(a) layer depth ∿ 1000 m, (b) layer depth ∿ 1340 m.
Ice thickness = 2225 m, terrain clearance = 360 m.

returned from two layers at a site in West Antarctica, as measured from an ESM record. It is clear that these measurements contain much less scatter than those obtained from Super 8 records.

It is concluded that it is not practicable to obtain sufficiently consistent power measurements for studies of the fading of internal layer echoes from the Super 8 film, and that this is probably due to not following the same layers between frames, and to small errors in power calibration between successive frames. The use of ESM records removes these sources of error, and the present analysis will therefore be restricted to the ESM data.

Power distributions for the two layers in fig. 3.7 are shown in fig. 3.8. It is seen that there is a good match with the theoretical distribution for a surface with $\phi_0 = 0.06$ rads (eqn. [5.7], Neal (1977)). The autocorrelation functions for the power returned by these layers are shown in fig. 3.9, and the derived roughness parameters given in Table 3.2, together with those for other surfaces*. These results reveal the internal layers to be very smooth indeed.

The measured phase shift ϕ_0 for the internal layers may be compared with an estimate for that of a surface deposited on the ice sheet and subsequently buried in the ice. ϕ_0 is related to the surface relief by eqn. [3.8]. As the surface snow undergoes densification to form ice the RMS vertical deviation from the mean horizontal plane, σ, will decrease, and compression in deep ice will result in a further reduction of the relief. Assuming an initial snow density of 400 kgm^{-3} and a final ice density of 920 kgm^{-3} we have $\phi_0(\text{ice}) = 0.43\ \phi_0(\text{surface})$. For a layer half-way down in

---

* Note that although the Super 8 data is unsatisfactory for studying layering, measurements such as those in fig. 3.6(d) have been used to obtain estimates of the small scale roughness of the ice sheet bed at two East Antarctic sites where the signal is well above the local noise level.

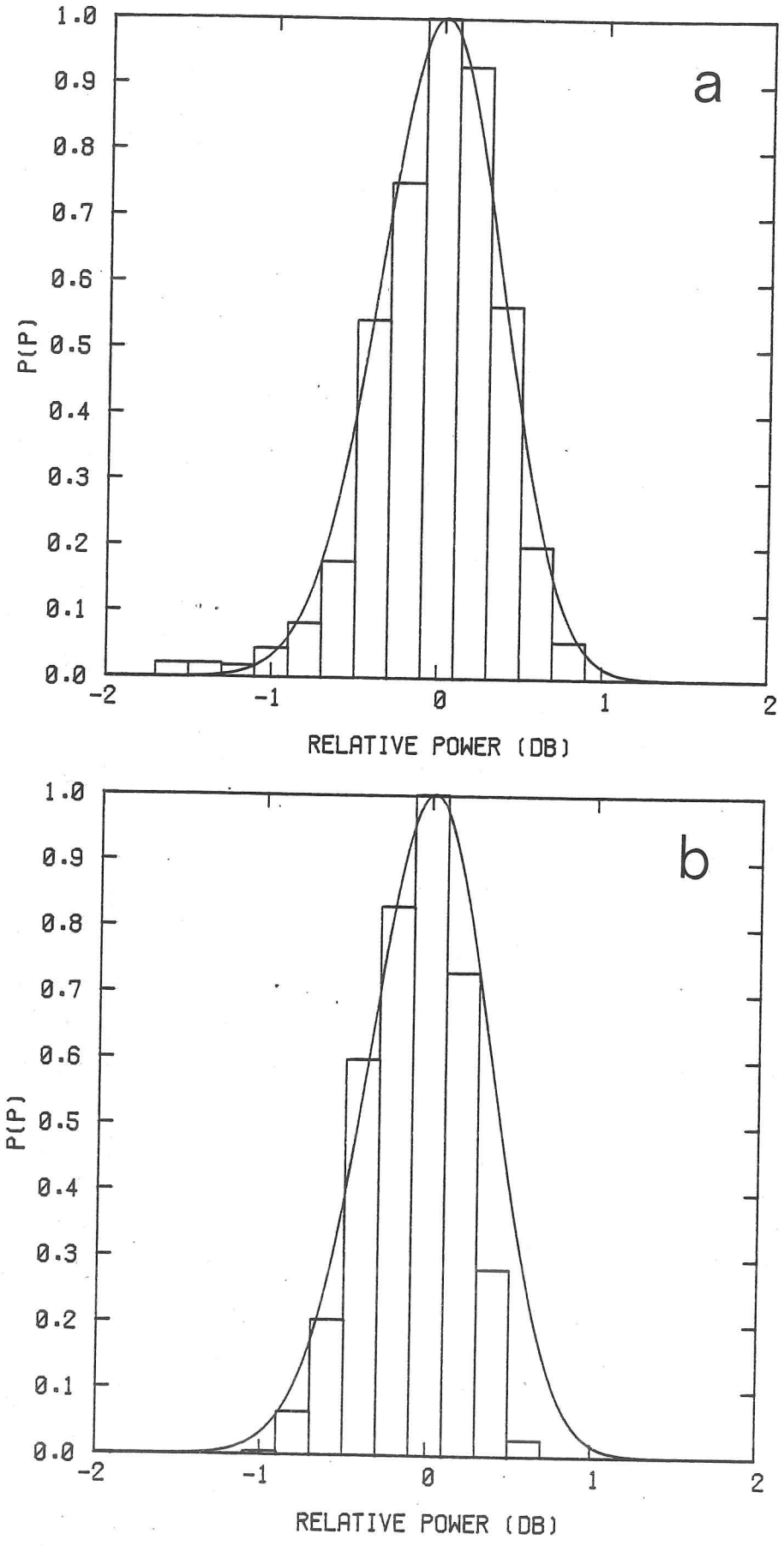

Fig. 3.8 Normalised distribution of power returned from two internal layers at (a) 1000 m, (b) 1340 m depth, at site F35/979. Curves represent theoretical distributions for surfaces characterised by ϕ_0 = 0.06 rads.

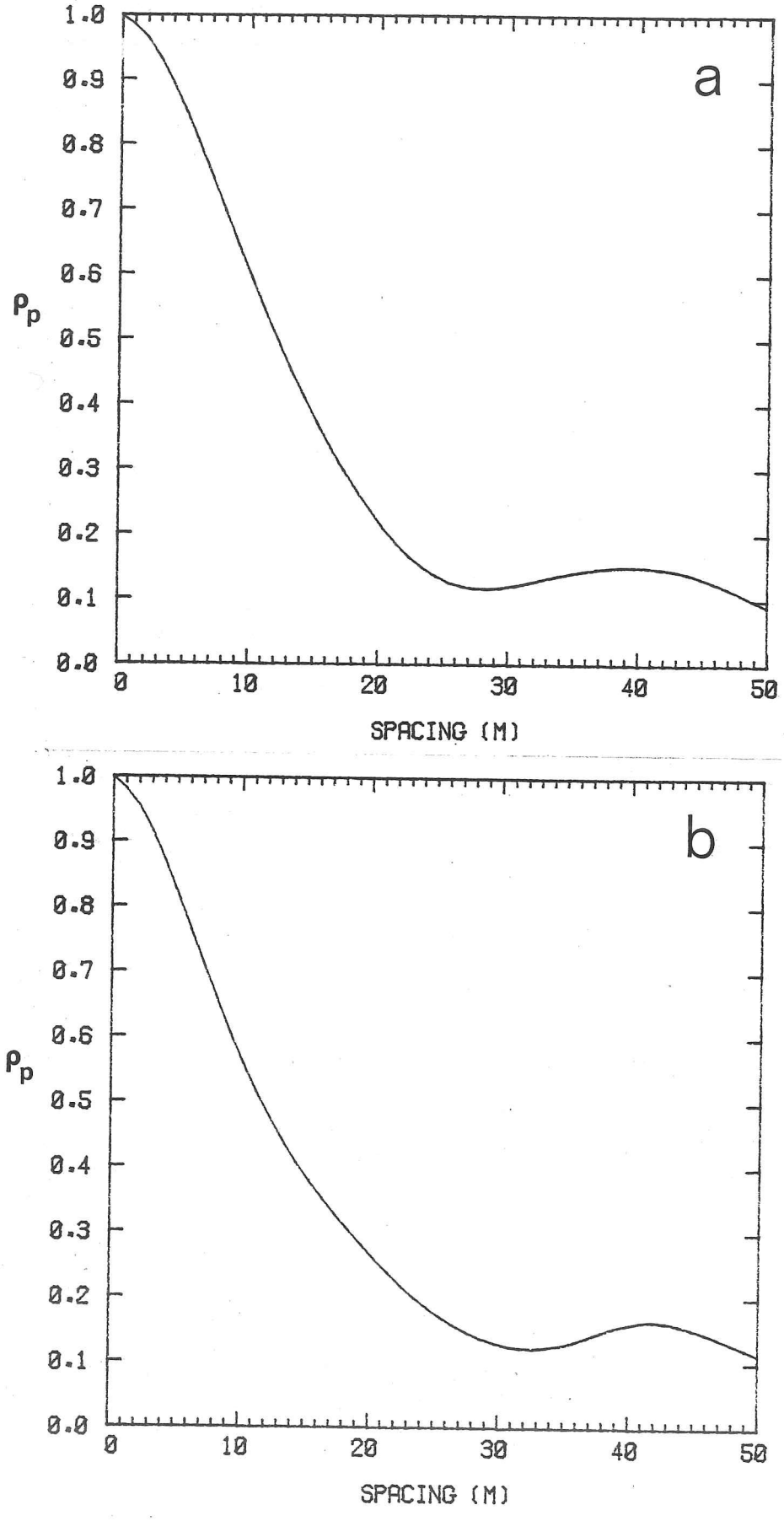

Fig. 3.9 Autocorrelation functions of the power returned from two internal layers at (a) 1000 m, (b) 1340 m depth, at site F35/979 (79°08'S 107°15'W).

TABLE 3.2 STATISTICS FOR VARIOUS REFLECTING SURFACES

Interface	Position	Terrain clearance (m)	Ice thickness (m)	Number of measurements	V_p	β_o (rads)	ϕ_o (rads)	L (m)
air/sea *	77°14'S 177°54'E	1100	-	497	0.24	0.5	0.0039	41.0
air/snow*	77°25'S 171°38'E	970	-	805	0.058	0.19	0.0036	16.5
-	84°24'S 163°43'W	750	-	567	0.067	0.21	0.0055	12.0
ice/water*	77°25'S 171°38'S	970	220	805	0.027	0.14	0.0016	27.5
-	84°24'S 163°43'W	750	750	567	0.37	0.49	0.012	12.5
ice/bedrock	73°50'S 126°23'E	800	3500	143	0.82	0.80	0.022	11.0
-	71°27'S 127°26'E	380	2510	116	0.62	0.84	0.036	7.0
internal layer	79°08'S 107°15'W	360	1000	686	0.007	0.06	0.0012	16.0
-	79°08'S 107°15'W	360	1340	771	0.004	0.05	0.0010	16.5

* from Neal (1977)

the ice (as in fig. 3.7), ϕ_o will be further reduced by a factor of two. Finally the change in radio wavelength must be accounted for, giving ϕ_o (ice)=0.215n ϕ_o(surface)=0.38 ϕ_o(surface), where n is the refractive index of ice.

Using ϕ_o=0.15 rads for the air/snow interface of the Ross Ice Shelf (Table 3.2) therefore gives an estimate of ϕ_o=0.06 rads for a reflecting surface of depositional origin. The good agreement of this estimate with the observed values for internal layers supports the hypothesis that the deeper layers are due to atmospherically deposited impurities. It should be pointed out, however, that this comparison may be an over-simplification, since it is likely that several surfaces contribute to each layer echo seen when using a pulse length of several tens of metres; this cannot be allowed for by the present theory.

3.6 Summary

Measurements of the reflection coefficients of internal layers have revealed three distinct zones within the ice column. Near the surface (generally <500 m depth) reflection coefficients decrease rapidly with depth, and here echoes are thought to arise from fluctuations in ice density. Below this region PRCs show no pronounced overall trend, and echoes are believed to arise from layers of acidic impurities within the ice sheet (see Chapters 4 and 5). Near to the bedrock layering disappears, and this is thought to be due to complex deformation over long periods (see Chapter 6).

Variations in reflection coefficient on a scale of tens of kilometres are observed which may be due to local fluctuations in accumulation rate at the time of deposition of the reflecting layers. Short-period fading is also observed, which enables the roughness of the surfaces to be described statistically. Interpretation of these roughness estimates suggests that the internal layers are depositional in origin.

Chapter 4

MECHANISMS FOR INTERNAL REFLECTIONS

4.1 Power reflected from internal layers

Internal reflections arise from dielectric discontinuities within the ice mass. Such discontinuities in dielectric properties have a number of possible physical causes, and to decide which are plausible it is necessary to know how a change in a specific physical property of the ice affects its dielectric properties. Firstly, the relationship between reflection coefficient and changes in the dielectric properties of the ice will be summarised. This treatment follows that of earlier authors, e.g. Paren (1981).

The PRC of a smooth interface between polar ice (medium 1) and polar ice with a small change in some property (medium 2), illuminated at near normal incidence is:

$$R = \left| \frac{Y_1^* - Y_2^*}{Y_1^* + Y_2^*} \right|^2 \qquad [4.1]$$

where Y_1^*, Y_2^* are the complex intrinsic admittances of the two media. For media of similar characteristics $Y_1^* = Y_2^* + \Delta Y^* = Y^* + \Delta Y^*$, and to a first-order approximation:

$$R = \left| \frac{\Delta Y^*}{2Y^*} \right|^2 \qquad [4.2]$$

which may be written:

$$R = \left| \tfrac{1}{2} \Delta(\ln Y^*) \right|^2 \qquad [4.3]$$

Y^*, normalised to the free space admittance, is equal to the square root of the complex relative permittivity ε^*, where $\varepsilon^* = re^{-i\delta}$, so:

$$\ln Y^* = \tfrac{1}{2} \ln \varepsilon = \tfrac{1}{2} \left[\ln \varepsilon' - \ln \cos\delta - i\delta \right]$$

where the real part of ε^*, the relative permittivity ε', is $r\cos\delta$. A change in admittance may arise from either a variation $\Delta\varepsilon$ in ε' or $\Delta\delta$ in δ.

$$\frac{\Delta Y^*}{Y^*} = \frac{d(\ln Y^*)}{d\varepsilon'} . \Delta\varepsilon' + \frac{d(\ln Y^*)}{d\delta} . \Delta\delta$$

$$= \tfrac{1}{2} \left[\frac{\Delta\varepsilon'}{\varepsilon'} + (\tan\delta - i) . \Delta\delta \right] \qquad [4.4]$$

From [4.2] and [4.4]:

$$R = \frac{1}{16} \left[\left(\frac{\Delta\varepsilon'}{\varepsilon'} + \tan\delta . \Delta\delta \right)^2 + (\Delta\delta)^2 \right] \qquad [4.5]$$

This is the general form of the relation between R and changes in the relative permittivity, ε', and phase angle, δ. For changes in one variable only this simplifies to:

- for permittivity changes only

$$R = \frac{1}{16}\left[\frac{\Delta\varepsilon'}{\varepsilon'}\right]^2 \qquad [4.6]$$

- for loss tangent changes only

$$R = \frac{1}{16}\left[(1 + \tan^2\delta).(\Delta\delta)^2\right]$$

but $\Delta(\tan\delta) = \sec^2\delta.\Delta\delta$, and for small δ, $\cos\delta \simeq 1$:

$$R = \frac{1}{16}\left[\Delta(\tan\delta)\right]^2 \qquad [4.7]$$

The power reflection coefficient, R', for a single thin layer of ice of altered properties may be related to that expected for a single interface by:

$$R' = 4\sin^2\left[\frac{2\pi\ell}{\lambda}\right].\ R \qquad [4.8]$$

providing $\ell < \frac{1}{4}\lambda$, where ℓ is the thickness of the layer and λ the radio wavelength in ice.

The simplest case of multiple layering occurs when N thin layers are randomly spaced (in such a way that all phase delays are equally likely), in a zone whose total thickness is less than half the pulse length, for which case:

$$R_{zone} = NR' \qquad [4.9]$$

Thin layers of ice with small permittivity contrasts may hence be more

readily detected by the echo sounder if they occur in groups than if they occur in isolation. To give a reflection coefficient of -70 dB from a single layer 0.01 m thick would require $\Delta\varepsilon'/\varepsilon'=0.03$, whereas for a zone half a pulse length thick composed of many 0.01 m thick layers $\Delta\varepsilon'/\varepsilon'=0.0002$ may be sufficient, when using a 60 MHz sounder and a 250 ns pulse length. Some more complex cases of multiple layering have been treated by Harrison (1973) and Clough (1977).

In the following sections, relations between dielectric properties and changes in various physical properties of the ice are considered, and hence the feasibility of changes in such properties causing layer echoes assessed.

4.2 Previously suggested causes for reflections

(a) density fluctuations

Robin and others (1969) suggested variations in ice density as the possible cause of an intermittent layer echo that was observed during an over-snow traverse from Tuto-Camp Century in 1964. In that area it was reasonable to postulate that a clear ice layer, surrounded by bubbly polar ice of lower density, might be formed by a rare climatic warming, which soaked the surface snow layer. This is not a reasonable explanation in most parts of the Antarctic, where surface melting never occurs; however ice cores and pits dug at such locations reveal the presence of thin ice layers a few millimetres thick, ice wedges a centimetre or more in thickness, wind crusts and depth hoar layers, which must be formed by other mechanisms.

Robin and others calculated the reflection coefficient of such a single layer of clear ice of thickness ℓ as:

$$R = \left[\frac{\pi \ell \Delta\rho}{\lambda\rho}\right]^2 \qquad [4.10]$$

and estimated $\Delta\rho$ to be:

$$\Delta\rho\{gcm^{-3}\} = \frac{0.1}{P\{atm\}} \qquad [4.11]$$

where P is the overburden pressure. Paren & Robin (1975) used this to estimate the reflection coefficient resulting from a density change across a single boundary. The values obtained are comparable with those observed for internal layer echoes down to ~1000 m depth, below which the power reflected from such density variations becomes very small. Clough (1977) and Ackley & Keliher (1979) have found a correlation between the depths of density fluctuations and those of radio-echo layers at Byrd Station and Cape Folger (East Antarctica), respectively. This mechanism is discussed further in section 4.3.

(b) dust & ash bands

Layers of foreign material such as dust or volcanic ash included in the ice have been suggested (Robin and others 1969; Harrison 1972). In the deep core drilled at Byrd Station twenty-five distinct tephra layers and roughly 2000 dust bands (grain size generally <5 μm) have been observed (Gow & Williamson 1971), most of the ash layers being 0.5 mm thick or less. The concentration of particulate material in the bands is typically 0.04 kgm^{-3}. Similar bands of volcanic dust and ash have been observed in the Dome C core (Kyle and others, unpublished).

The electrical properties of dirt-laden ice have not been studied experimentally, but the permittivity may be estimated from Looyenga's mixing formula (Glen & Paren 1975). The permittivity, ε_m, of a mixture of two dielectrics of permittivity ε_1, ε_2 with a volume fraction v of material 2 is:

$$\varepsilon_m = \left[v(\varepsilon_2^{1/3} - \varepsilon_1^{1/3}) + \varepsilon_1^{1/3} \right]^3 \qquad [4.12]$$

Rocks possess permittivities of between 5 and 10, and loss tangents of <0.03. The upper limit to reflection coefficients for dust layers may thus be obtained from values of $\varepsilon_2=10(1-0.03i)$ for rock and $\varepsilon_1=3.2(1-0.007i)$ for ice. It is found that the permittivity of 'dusty' ice containing 0.04 kgm^{-3} of rock is only $2x10^{-5}$ higher than that of clean ice, giving R=-116 dB for a dusty/clean ice boundary. Even the maximum layer thickness of 0.06 m and maximum concentration of 1 kgm^{-3} reported by Gow & Williamson for the Byrd core yields only -86 dB, and particle concentrations were generally very much lower than this.

Both Clough (1977), using a SPRI Mk II echo sounder modified to operate at 50 MHz, and the author, using the TUD 60 MHz and 300 MHz equipment, have compared the depths of layer echoes observed at Byrd with the positions of dust and ash bands reported in the Byrd core, but no correlation has been found.

It is clear that dust and ash layers in the ice are barely capable of giving detectable radio reflections, and cannot be responsible for the multitude of strong reflections that have been observed at Byrd and elsewhere. This is in agreement with the conclusions of Robin and others (1969).

(c) ice crystal orientation

Harrison (1972) suggested that since ice is structurally anisotropic its RF permittivity might also be expected to be anisotropic, and hence that layers of ice containing crystals alternately in preferred and random orientations might give detectable reflections. The occasional existence of such layers has been confirmed by ice core analysis, for example Gow & Williamson (1976) report a band in the Byrd core at 911 m depth which seems to show a greater vertical c-axis orientation and smaller crystal sizes than the surrounding ice, and Russell-Head & Budd (1979) have made similar observations on a core from Law Dome, East Antarctica.

Experiments performed on the Greenland ice sheet by Hargreaves (1977) and observations by Steed (personal communication) have shown that signals reflected from internal layers are weakly elliptically polarised, suggesting that the ice mass is birefringent. Hargreaves estimated a minimum value for the anisotropy of the permittivity of polar ice of 0.028%, almost two orders of magnitude less than that detectable by laboratory experiments, and estimated that boundaries due to changes in crystal orientation might cause reflections of up to -80 dB. However other effects which reflection at this type of boundary should produce were not observed in polarisation measurements. A detailed study of crystal fabrics has been made on a 324 m core from Cape Folger (Ackley & Keliher 1979), from which it was concluded that observed variations in ice crystal orientation did not coincide with the two observed layer echoes in the area, and were insufficient to account for reflection strengths >-85 dB. Layer echoes are therefore unlikely to be caused by this mechanism.

(d) loss tangent variations

Factors considered so far all operate via changes in the real part of the permittivity. The alternative mechanism is a change in loss tangent, which is essentially determined by intrinsic and impurity defects within

the crystal lattice.

Paren & Robin (1975) proposed two possible causes for changes in loss tangent; varying (soluble) impurity concentrations, and a possible difference between the loss tangents of polar ice and 'laboratory' or refrozen ice (Glen & Paren 1975; Fitzgerald & Paren 1975), perhaps due to different conditions under which freezing occurred. The difference in electrical properties between these two types of ice is not well understood; polar ice generally has a much higher conductivity than laboratory ice, even when impurity concentrations are identical. If polar ice is melted and refrozen in the laboratory it is found to behave similarly to 'laboratory' or temperate glacier ice, but this melting and refreezing is not likely to happen on the Antarctic ice sheet. Reynolds & Paren (1980) have suggested recrystallisation as the mechanism responsible for the anomalous behaviour of polar ice. However there is no evidence to suggest that layers of 'pure' ice exist within the polar ice, and this difference in electrical properties is therefore not considered further here.

Fluctuations in the concentration of atmospherically-borne contaminants have been suggested as a possible cause of a changed loss tangent, but there is little experimental evidence for large variations in the concentrations of specific impurities, except for material of volcanic origin (Boutron & Lorius 1979; Busenberg & Langway 1979). Paren & Robin concluded that varying but low levels of impurity in polar ice could cause significant variations in loss tangent, especially if the impurity levels fluctuate around or below a 'solubility limit' (Paren & Walker 1971).

Conductivity profiles along Greenland ice cores (Hammer 1977; Hammer and others 1980) have shown that layers of ice containing relatively high concentrations of acidic impurities of volcanic origin do exist in ice sheets. The conductivity of such ice layers can be many times that of the surrounding ice. Gudmandsen & Overgaard (1978) showed that the depths at

which layer reflections were observed at Crête closely matched those of conductivity peaks. Layers of acidic ice therefore appear to be a likely cause of layer echoes.

(e) bubble geometry

Evidence from the Cape Folger core (Ackley & Keliher 1979) indicates that at depth included air bubbles can become substantially distorted from their initial roughly spherical shapes. Such anisotropy alters the dielectric properties of the ice and may cause detectable reflections.

In the Cape Folger core two zones containing bubbles greatly elongated in the direction of ice flow were found in association with density changes, and these zones also coincided in depth with two layer echoes. Ackley & Keliher have derived theoretical expressions for the permittivity of the ice in terms of the eccentricity and orientation of included air bubbles (or other macroscopic impurities), and application of these expressions to the observed variations in bubble geometry suggests maximum reflection coefficients of -80 to -90 dB. However these reflection strengths are some 20 dB weaker than those expected from the associated density changes, indicating that changes in bubble elongation and orientation constitute only a secondary effect.

4.3 Proposed models for internal reflecting surfaces

(a) density fluctuations

In this section the power returned by layers of clear ice surrounded by bubbly polar ice will be estimated as a function of depth. The expression for $\Delta\rho$ (eqn. [4.11]) will be compared with measured ice core densities, and observations of density fluctuations from ice core stratigraphy studies discussed. The resulting model for power reflected

from clear ice layers will be compared with measured PRC vs depth profiles.

Bubbly polar ice may be considered as clear ice containing air bubbles which become isolated from the surface and from one another below the firn layer (when ice densities exceed about 820 kgm^{-3}), and which are then compressed by the weight of the overlying ice. This gives a relation between density contrast $\Delta\rho$ and overburden pressure, P:

$$\Delta\rho = \frac{0.11\rho_I P_o}{0.89P + 0.11P_o} \qquad [4.13]$$

where P_o is atmospheric pressure at the ice surface and ρ_I the density of clear ice at P_o. Approximating this yields the relation [4.11] previously obtained by Robin and others (1969).

The reflection coefficient from a simple clear ice/bubbly polar ice boundary may be taken as the likely upper limit on reflections from density fluctuations in ice sheets. Assuming [4.11], the resulting maximum reflection coefficient may be obtained from [4.6] and an empirical relationship between ice density and permittivity, $\sqrt{\varepsilon'}=n=1+0.00085\rho$ (Robin and others 1969), to give R_{max} at depth h (metres) as:

$$R_{max}=0.717/h^2 \qquad [4.14]$$

The accuracy of eqn. [4.11] has been checked by comparing the observed density profile at Byrd with the profile that would result if the ice were entirely bubble-free (fig. 4.1). Since the published density profile (Gow 1970) was measured at in situ temperatures but atmospheric pressure, the compressibility of the ice may be ignored and the clear ice density profile will be solely a function of temperature (Eisenberg & Kauzmann

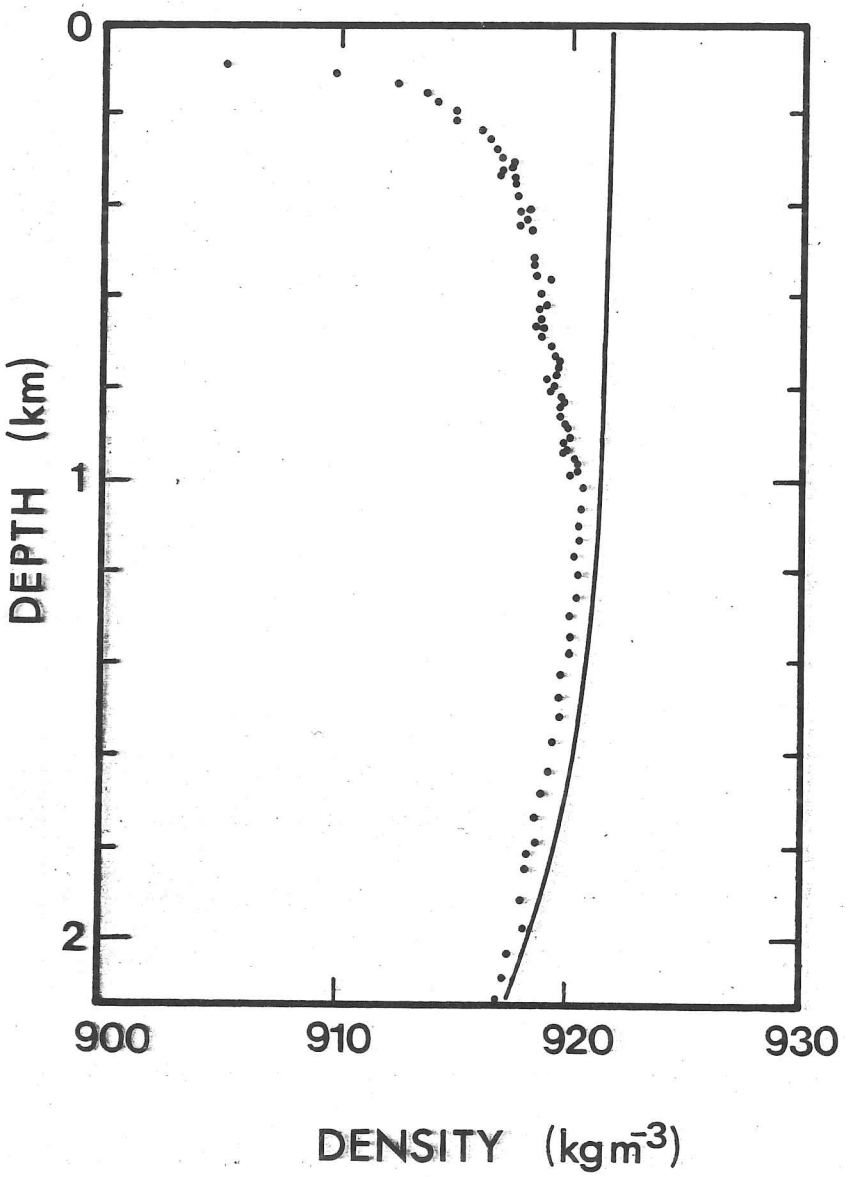

Fig. 4.1 Observed ice core densities vs depth at Byrd Station (dots, after Gow 1970), and calculated density profile for clear ice from laboratory measurements (solid line). Both sets of data are corrected to in situ temperatures but atmospheric pressure.

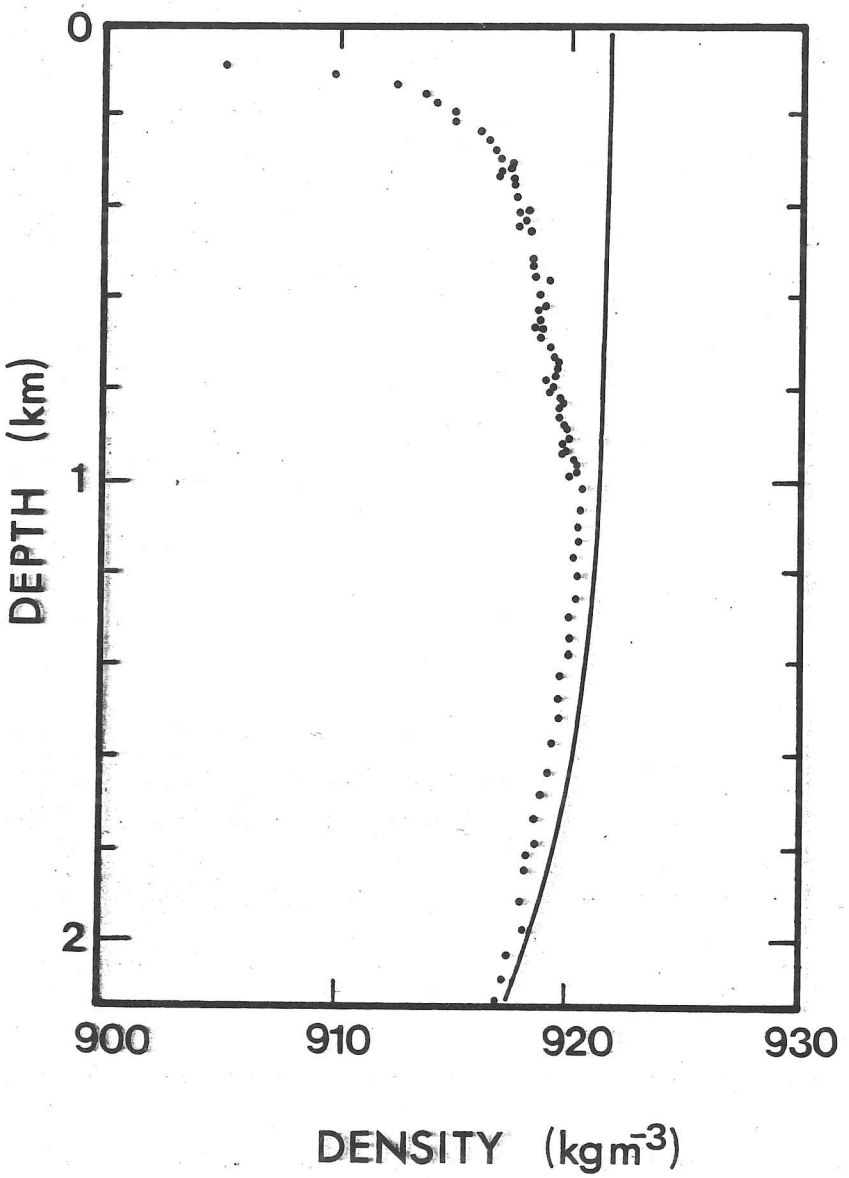

Fig. 4.1 Observed ice core densities vs depth at Byrd Station (dots, after Gow 1970), and calculated density profile for clear ice from laboratory measurements (solid line). Both sets of data are corrected to in situ temperatures but atmospheric pressure.

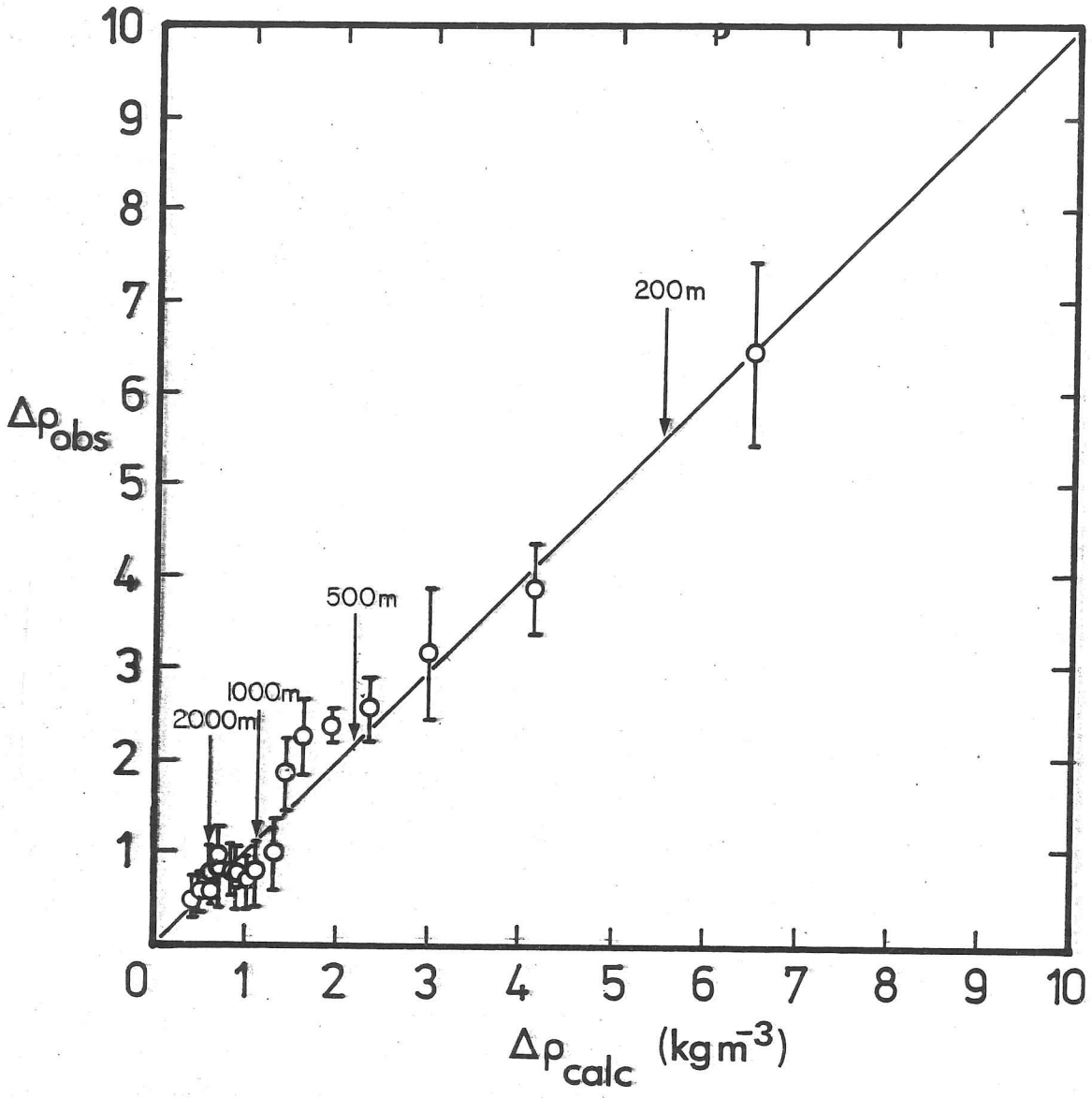

Fig. 4.2 Comparison of density contrasts obtained from the difference between the observed density profile and the estimated density profile for clear ice at Byrd Station ($\Delta\rho_{obs}$), and from eqn. 4.11 ($\Delta\rho_{calc}$). Arrows indicate ice depths.

1969). The difference between the observed profile and the estimated clear ice profile gives the maximum density contrast at any depth. Fig. 4.2 shows a good agreement between these 'observed' density differences and values calculated from [4.11], using a constant ice density of 920 kgm^{-3} to convert overburden pressures to depths.

Studies of ice core stratigraphy and density variations have been reported for deep ice cores from Byrd Station (Patenaude and others 1959; Gow 1970; Clough 1977), Site 2, Greenland (Langway 1970) and Cape Folger (Ackley & Keliher 1979). At Site 2, for which the most detailed information is available along a 411 m core, thin (1-2 mm thick) clear ice layers were found to be 'common' below 70 m depth, and thicker (3-5 mm thick) layers were also present. Other features 'indicative of melt', probably the remains of depth hoar or firn strata, were also found with thicknesses of 5-20 mm. At Byrd the thickest ice layers ranged up to 10 mm thick, but were always associated with dirt layers ~0.5 mm thick. Apart from these dirt-associated melt layers, no other obvious signs of melt were detected in the core. In a core drilled at Old Byrd Station in 1957, many thin ice layers about 4 mm thick were noted both singly and in closely spaced groups at regular intervals (Patenaude and others 1959).

Physically realistic density variations are therefore likely to be due to clear ice layers a few millimetres thick, and to groups of such layers. Eqn. [4.9] shows that the grouping together of thin layers can greatly enhance the total reflection coefficient, however the difference in reflectivity between a single thin layer and a group of such layers will be independent of depth, so it is the shape of the estimated PRC vs depth curve which is important, rather than absolute magnitudes. Fig. 4.3 shows a measured PRC vs depth profile near Byrd, and predicted curves (using eqns. [4.14] and [4.8]) for a simple clear ice/bubbly polar ice interface and for single layers 0.01 and 0.1 m thick.

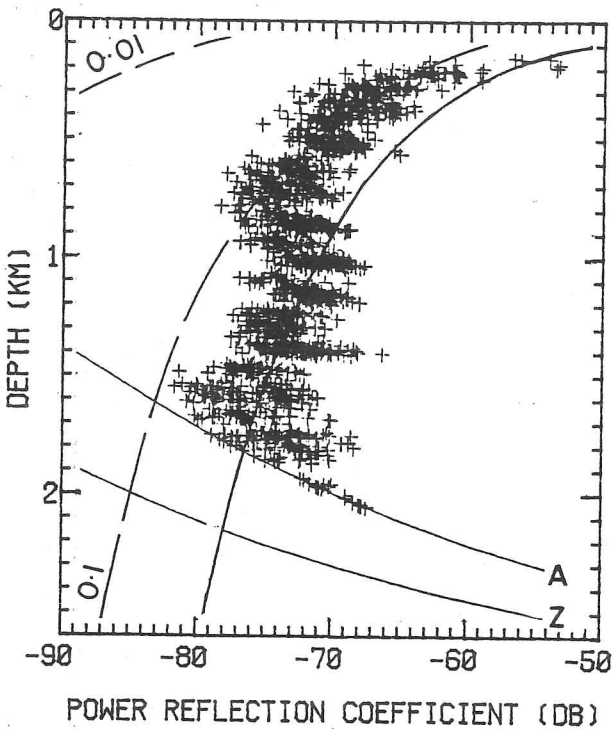

Fig. 4.3 PRC vs depth profile near Byrd (site F147/1318), and predicted PRCs for s simple clear/polar ice boundary (thick solid line), and 0.1 and 0.01 m thick clear ice layers (dashed lines). Detection limits for A- and Z-scope records are shown.

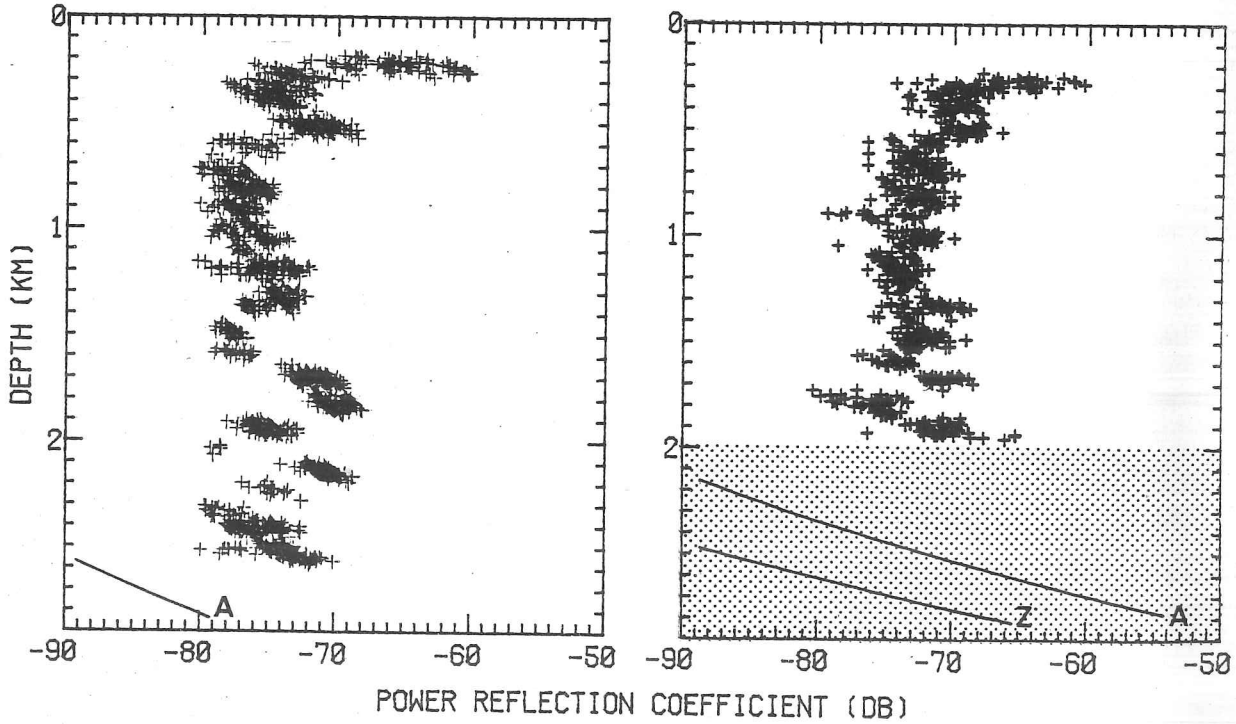

Fig. 4.8 PRC vs depth profiles obtained (a) on the ground, (b) at 200 m terrain clearance, at the South Pole, demonstrating the lack of significant wide-angle scatter. Layer echoes in shaded area were obscured by station echoes.

The important conclusion from this comparison is that the shape of the observed fall-off of PRC with depth from the surface to ~500 m closely matches that predicted by the above simple model. The absolute magnitude of reflection coefficients predicted by this model are not so significant; any observed reflection coefficient could be explained in terms of either a single ice layer or a group of thinner layers. There is also evidence that the depths of measured density variations correspond with those of radio-echo layers at Byrd and Cape Folger (Clough 1977; Ackley & Keliher 1979).

It is concluded that small density fluctuations are observed to exist in the upper 500-1000 m of polar ice sheets, and that they are of sufficient magnitude to give radio-echoes of a similar strength to those observed, particularly if they occur in closely spaced groups. The agreement between the observed decrease in PRC with depth and that predicted by the above model is good evidence for the operation of this reflection mechanism, and also shows that reflections from density fluctuations become too weak to be detected by RES below about 400-600 m at most Antarctic sites.

(b) variations in soluble impurity concentrations

Layers of ice containing enhanced concentrations of dissolved impurities can give rise to radio reflections via the associated change in loss tangent. Hammer (1977) has shown the existence of layers of ice containing high H^+ concentrations (due to acids of volcanic origin) in the Greenland ice sheet. The small effect on high frequency conductivity of other possible ions (such as marine Na^+, Ca^{2+}, etc.), suggested both by theoretical considerations and by the lack of any effect of increased Na, K, Mg, Ca and SO_4^{2-} concentrations between 1300-1800 m depth in the Byrd core (Cragin and others 1977) on the d.c. conductivity of the ice (Gow 1970), effectively rules out the possibility of radio-echoes from layers of ice containing high concentrations of these species. Furthermore,

widespread high-conductivity layers of such impurities have not been observed (Boutron & Lorius 1979; Busenberg & Langway 1979).

The following method of relating the H^+ concentration in layers of acidic ice surrounded by ice with lower (background) acid concentrations, to the resulting reflection coefficient is suggested. As this method will be used later to estimate ice acidities from measured PRCs, it will be demonstrated with this in mind, i.e. showing how a measured PRC may be converted into an equivalent acidity estimate.

Ice loss tangent, $\tan\delta$, may be simply related to the high frequency (h.f.) conductivity, σ_∞, by:

$$\tan\delta = \frac{\sigma_\infty}{2\pi f \varepsilon_o \varepsilon'} \qquad [4.15]$$

where ε_o is the permittivity of free space, ε' the permittivity of the ice, and f the ice sounding frequency. Using this and eqns. [4.7] and [4.8] we can express a measured reflection coefficient in terms of the necessary change in h.f. conductivity and reflector thickness to account for the reflection. By estimating the layer thickness from the known duration of high acidity layers (Hammer 1977), the change in h.f. conductivity is calculated and added to the known 'background' h.f. conductivity to obtain σ_∞ (layer). To convert this into an acidity we now represent acidic polar ice by laboratory-grown ice doped with hydrofluoric acid (HF), and estimate the equivalent HF concentrations that would be required in order to obtain the same h.f. conductivities for the layer and for the background ice, using the laboratory measurements of Camplin and others (1978) at the appropriate ice temperature.

Fig. 4.4 shows the experimental relationships between σ_∞ and HF concentration, c, in the temperature and concentration range of interest. For numerical calculations the data have been approximated by linear equations of the form $\sigma_\infty = Ac+B$, and the coefficients A and B given in Table 4.1 for various temperatures and concentration ranges. This analogy with HF-doped ice is necessary because there are no experimental measurements available of h.f. conductivity or loss tangent for polar ice doped with volcanic impurities, and HF-doped laboratory ice is considered to be the nearest approximation available. From the two 'equivalent HF concentrations' for the acidic ice layer and the background ice, we obtain the change in equivalent HF concentration necessary to account for the observed reflection coefficient. The final estimate of the layer acidity is obtained by adding this elevated equivalent HF concentration to the known background acidity of polar ice, which has been measured as $(1.1\pm0.1)\times10^{-3}$ molm^{-3} at Crête (Hammer and others 1980) and $(1-2)\times10^{-3}$ molm^{-3} at Dome C (Legrand 1980). Fig. 4.5 demonstrates this method schematically.

The laboratory studies show that the h.f. conductivity of HF-doped ice is temperature dependent, so acidities estimated by this procedure will also be, although in fact the effect is small because the conductivity of the background ice also changes with temperature. Fig. 4.6 shows the estimated temperature dependence of reflection coefficient for various elevated acidities. It is seen that above -30°C there is little variation with temperature, but that at lower temperatures R drops by ~0.3 dB/degree. This is probably not easily detectable in practice as these lower temperatures are only found in the near-surface layers, where layer reflections are thought to be mainly due to density variations. Fig. 4.7 shows the estimated reflection coefficient for a simple acidic ice/background polar ice interface as a function of acidity difference at various temperatures.

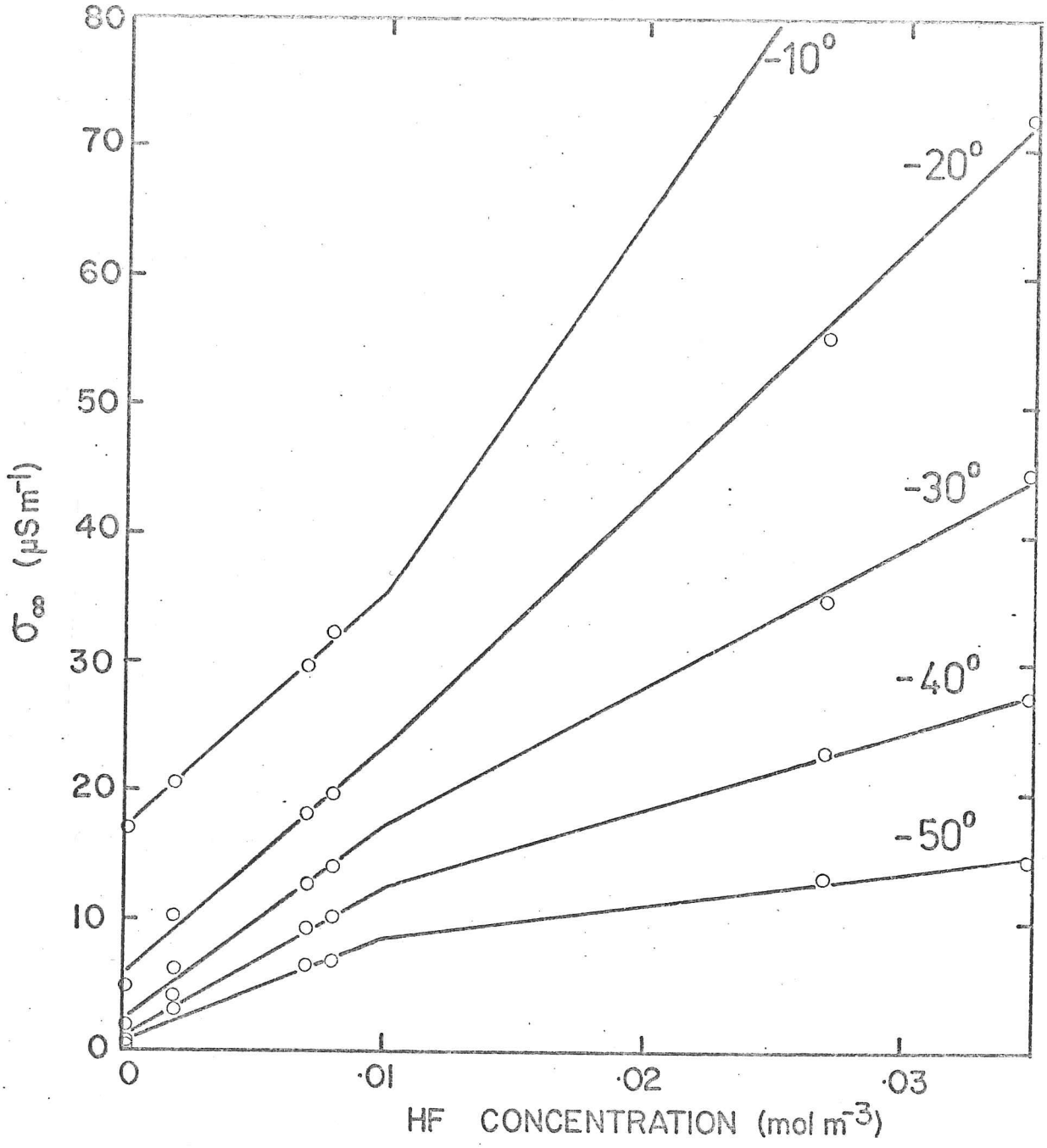

Fig. 4.4 Measured high frequency conductivity of HF-doped laboratory ice (circles), and linear relations used to approximate them (data from Camplin and others 1978).

TABLE 4.1 LINEAR APPROXIMATIONS FOR HIGH FREQUENCY CONDUCTIVITY OF HF-DOPED ICE.

High frequency conductivity in Sm^{-1} is given by $\sigma_\infty = Ac+B$ for ice containing c $molm^{-3}$ of HF at temperature T, where:

T	c < 0.01		0.01 < c < 0.035	
^oC	A ($x10^{-3}$)	B ($x10^{-6}$)	A ($x10^{-3}$)	B ($x10^{-6}$)
-10	1.85	17.0	2.95	6.0
-20	1.75	6.0	1.95	4.0
-30	1.55	2.0	1.09	6.5
-40	1.15	1.0	0.58	7.0
-50	0.75	1.0	0.25	6.0

Fig. 4.5 Schematic representation of method of relating acidity changes to reflection coefficients.

MEASURE REFLECTION COEFFICIENT, R

ESTIMATE LAYER THICKNESS, ℓ

single or multiple reflector?

CALCULATE $\Delta(\tan\delta)$ and $\Delta\sigma_\infty$

$$R_s=[\tfrac{1}{4}\Delta(\tan\delta)]^2$$

$$R=4\sin^2(2\pi\ell/\lambda).R_s$$

$$\Delta\sigma_\infty=2\pi f\varepsilon_o\varepsilon'.\Delta(\tan\delta)$$

σ_∞(layer)=σ_∞(background)+$\Delta\sigma_\infty$

TREAT ACIDIC ICE AS HF-DOPED ICE, OBTAIN c_{HF}(layer), c_{HF}(background) FROM LAB. DATA, HENCE Δc_{HF}

ESTIMATED LAYER ACIDITY = BACKGROUND ACIDITY + Δc_{HF}

COMPARE RESULTS WITH ICE CORE DATA

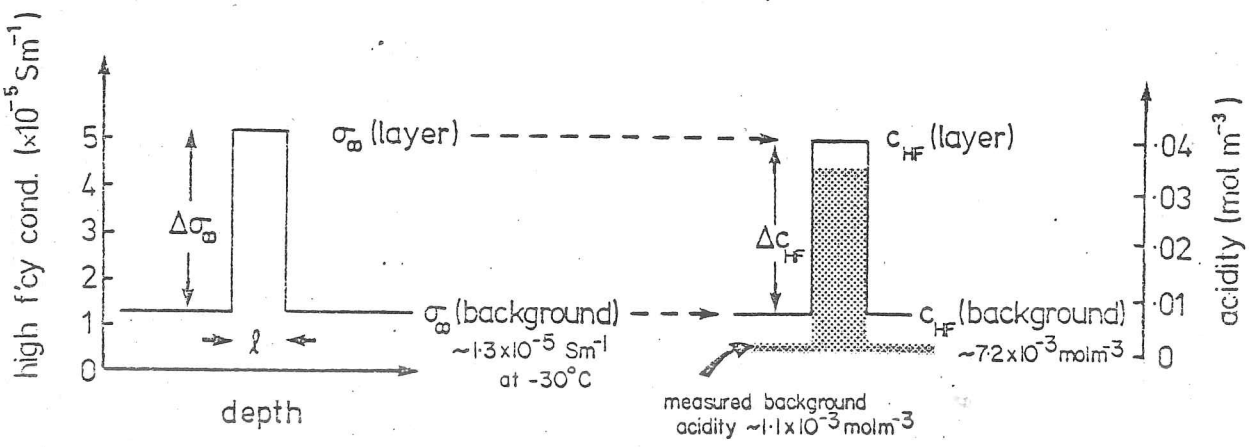

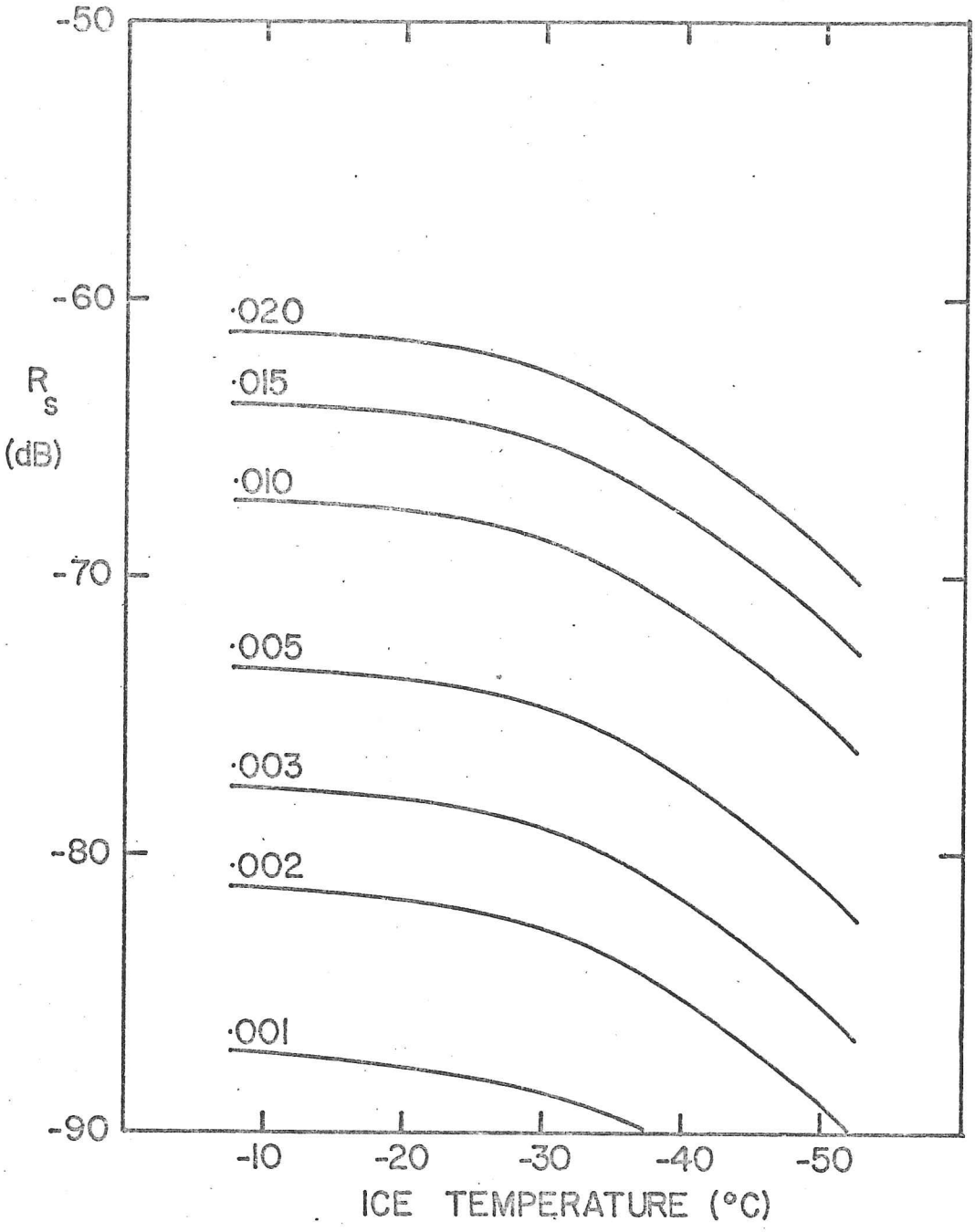

Fig. 4.6 Estimated variation of reflection coefficient with temperature for simple interface and various acidity differences (in mol m^{-3}) between acidic ice and background polar ice.

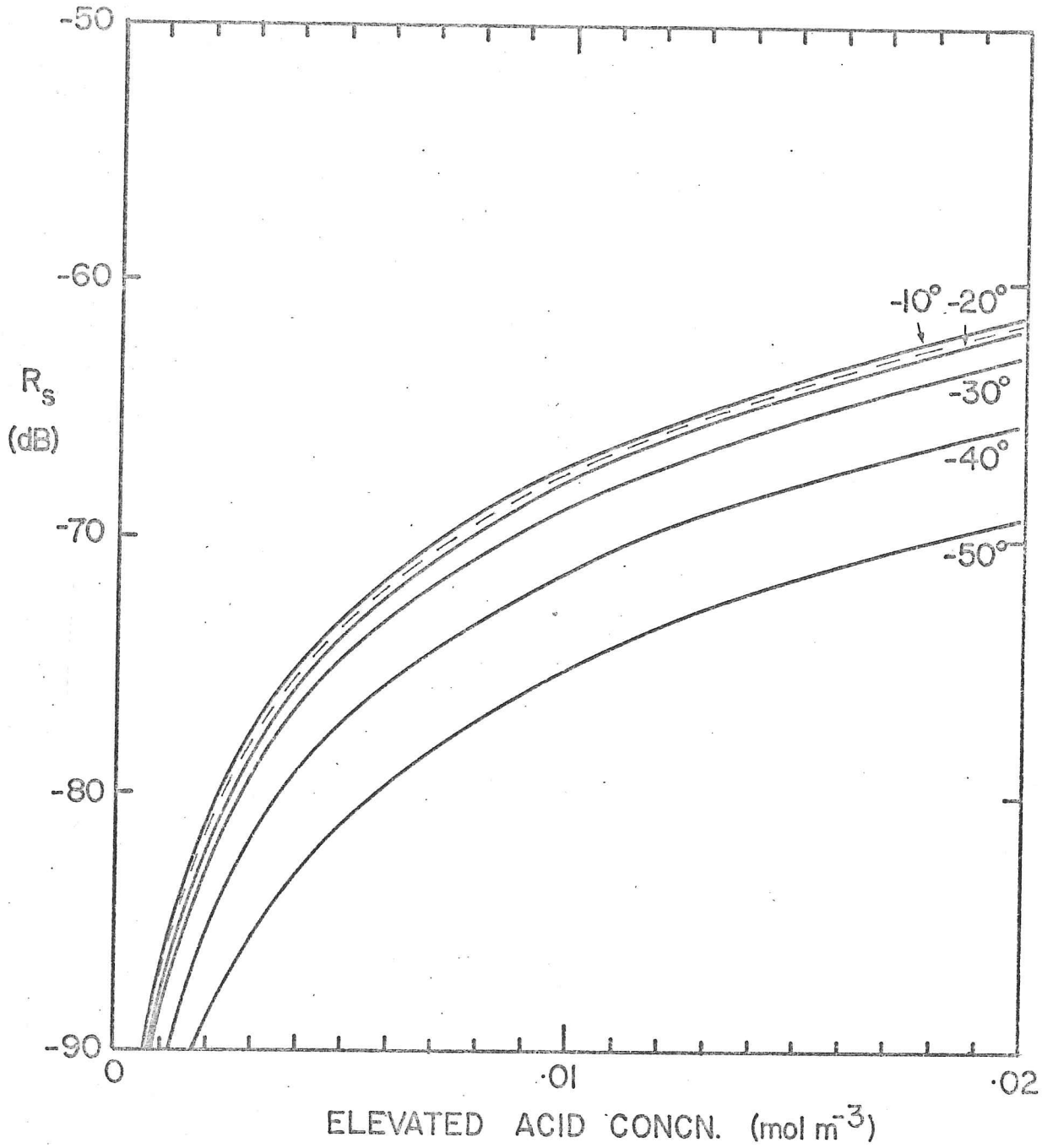

Fig. 4.7 Estimated variation of reflection coefficient, for interface between acidic ice and background polar ice, with elevated acidity. Solid lines, by analogy with HF-doped ice; dashed line, theoretical method.

A theoretical argument is presented below which gives very similar results to the above empirical procedure, and which provides an explanation for the approximate proportionality between reflection coefficient and the square of the acid concentration change, which is implied by the results above (fig. 4.7).

At RES frequencies the h.f. conductivity of ice has two components, due to the ionisation defect concentration, $\sigma_{\pm}$, and the Bjerrum defect concentration, σ_{DL} (eqn. [2.125], Hobbs 1974):

$$\sigma_{\infty} = \sigma_{\pm} + \sigma_{DL} \qquad [4.16]$$

Dissolved impurities at the concentrations considered here are unlikely to significantly alter σ_{DL} (Hobbs 1974), but will have a large effect on $\sigma_{\pm}$ (Paren 1973), so $\Delta\sigma_{\infty} = \Delta\sigma_{\pm}$. The ionic component is well approximated by (Jaccard 1959):

$$\sigma_{\pm} = J_{\pm}^2 \sigma_o \qquad [4.17]$$

where σ_o is the static conductivity of the ice and $J_{\pm}$ is the effective charge on the ion. σ_o for doped ice is expected to depend on the mobility (μ_+) and additional concentration (Δc) of ions in the doped ice, relative to the surrounding ice (Camplin and others 1978; cf. eqn. [2.33], Hobbs 1974):

$$\Delta\sigma_o = \frac{\Delta c N_A e \mu_+}{J_{\pm}} \qquad [4.18]$$

This leads to a relation between the elevated H^+ concentration Δc and the resultant change in loss tangent, $\Delta(\tan\delta)$:

$$\Delta(\tan\delta) \simeq \frac{J_{\pm}\Delta c N_A e \mu_+}{2\pi f \varepsilon_0 \varepsilon''} = 0.17\Delta c \quad \{\mathrm{molm}^{-3}\} \qquad [4.19]$$

There is some uncertainty in $\mu(H^+)$; accepted values at the melting point lie in the range $(5\text{-}50)\times10^{-8}$ $m^2V^{-1}s^{-1}$ (Onsager 1973), but more recent work gives $(2.7\pm0.1)\times10^{-8}$ $m^2V^{-1}s^{-1}$ (Camplin and others 1978, from the h.f. behaviour of HF doped ice). It has been suggested that perturbation of the equilibrium between H_3O^+ and negatively-charged L defects, as a result of excessive fields applied during previous (low frequency) experiments, may have resulted in over-estimates in the past. Kunst & Warman (1980) have also observed a doubling in virtual proton mobility between -5° and -30°C, so μ_+ is probably the most poorly known parameter. The value given by Camplin and others is used here, together with their estimate of 0.702 for $J_{\pm}$.

The relationship estimated from eqns. [4.19] and [4.7], between the acidity contrast across a simple acidic ice/background polar ice boundary and the resulting reflection coefficient, is shown in fig. 4.7. Clearly the results are almost identical with those from the empirical model at an ice temperature of ~-15°C. From eqns. [4.7] and [4.15] it is clear that the reflection coefficient is proportional to the square of the change in h.f. conductivity. Because the laboratory measurements of h.f. conductivity and HF concentration show an approximately linear relationship at these very low concentrations, the reflection coefficients calculated by the empirical method are approximately proportional to the square of the concentration difference, as is deduced theoretically (eqn. [4.19]).

As an independent test of the estimates, Overgaard (personal communication) has measured the loss tangent of a high acidity layer found in the Crête core and dated at AD 1783 (attributed by Hammer (1977) to volcanic impurities from the eruption of Laki (Iceland) in that year), and of four samples of the surrounding ice. This layer exhibited one of the

largest changes in acid concentration observed in the 404 m Crête core. Overgaard found a peak value of 4×10^{-3} for $\tan \delta$ and values of $2\text{-}4 \times 10^{-4}$ for the surrounding ice at -14°C, giving a value of -60 to -61 dB for the reflection coefficient of a single interface. This compares well with estimates of -61.1 dB (by comparison with HF-doped ice) and -61.2 dB (from the theoretical argument), taking the peak acidity as 0.021 $molm^{-3}$ (Hammer 1980). The agreement between these independent estimates of reflection coefficient from acid concentrations is taken as an indication of the validity of the methods described here.

The method of analogy with HF-doped ice for estimating acidities from reflection coefficients is preferred here, because of its basis on experimental data and its inclusion of temperature effects. In the following chapter it will be used to compare acidity estimates from RES with values measured along ice cores; again the close agreement found supports the validity of the method.

4.4 Other causes of power return

In this last section power returns other than from internal reflecting surfaces are considered, in order to check that reflections from layers are not confused by reflections from other sources, principally wide-angle scattering from the ice sheet surface and back-scatter from inclusions within the firn.

(a) scattering from the ice surface

It is reasonable to suggest that the sharp fall-off of PRC with depth, observed in the upper region of profiles such as fig. 3.1(a), is due to wide-angle surface scatter and is not connected with the internal structure of the ice. Direct measurement of the energy returned by surface scattering is impossible because signals are returned at the same time as

those from within the ice sheet.

A simple way of finding what effect surface scatter shows is to compare PRC vs depth profiles obtained at the same site but at different terrain clearances. Fig. 4.8 shows two profiles recorded at the South Pole, the first at ground level whilst taxiing, and the second at a terrain clearance of ~200 m. If surface scatter is normally detectable then it should be absent from the first profile. It is readily seen that the two profiles are very similar, so in this instance surface scattering is not detectable, presumably being weaker than the reflections from the internal layers. Terrain clearances for other sites where PRC vs depth profiles were obtained were generally greater than 200 m, but comparison of these profiles indicates that there does not appear to be any link between terrain clearance and the fall-off of PRC with depth. The only cases where scattering is apparent on the Z-scope record are at high altitudes (~1000 m) over heavily crevassed terrain, as found around the margins of ice streams for example (Rose 1978).

In addition we can estimate the expected power scattered back from the surface, making use of measured surface roughness parameters (Table 3.2). The power returned from a specularly reflecting surface characterised by an RMS slope β_o, when viewed at an angle Θ to the normal is (eqn. [7.78], Harrison 1972; Beckmann & Spizzichino 1963):

$$\frac{P_\Theta}{P_t} = \frac{A G^{\frac{1}{2}} D \sqrt{\frac{1}{2}\pi}}{16\pi r^3} \cdot \frac{\cot^2\beta_o}{\cot^4\Theta} \cdot \exp\left(\frac{-\tan^2\Theta}{\tan^2\beta_o}\right) \qquad [4.20]$$

Application of this equation together with the known antenna characteristics of the 60 MHz equipment (Skou & Sondergaard 1976) shows that detectable amounts of power will not be received until either $\beta_o > 0.5$ rads or the terrain clearance exceeds ~4000 m, much greater than that at which any PRC vs depth profiles presented here were obtained. The

measurements by Neal (1977) indicate that on the surface of the Ross Ice Shelf $\beta_o < 0.01$ rads, so surface scatter is not expected to be a problem under normal conditions.

(b) back-scattering from firn inclusions

The near-surface layers of polar ice sheets contain a large number of small inhomogeneities such as ice lenses, cracks, and air bubbles (~10% air by volume, according to Gow (1970)). Large scale inhomogeneities within the ice are difficult to allow for quantitatively, but Evans & Smith (1969) have shown that Rayleigh scattering from small (relative to the radio wavelength), randomly distributed inclusions may give rise to a readily detectable short-range clutter echo, although the resulting loss to the forward wave is insignificant.

The power returned from a shell of thickness half a pulse length (p) at range r by ice containing inclusions of mean radius b and with a concentration of m m^{-3} is (Smith 1971):

$$\frac{P_r}{P_t} = \frac{64\pi^3 G^2 p}{3 O r^2 \lambda^2} \cdot \left[\frac{\varepsilon_2 (\varepsilon_1 - \varepsilon_2)}{\varepsilon_1 + 2\varepsilon_2} \right]^2 \cdot mb^6 \qquad [4.21]$$

Typical air bubble radii and concentrations in the firn at Byrd Station have been reported as 0.2-0.5 mm, and ~10^8 m^{-3}, respectively (Gow 1970). Fig. 4.9 shows an observed 60 MHz power vs depth profile near Byrd, together with estimates of power returned by scatter from the surface and from air bubbles within the firn. This shows that scatter from bubbles is not likely to be detectable with the 60 MHz equipment. Comparison of these estimates for air bubble scattering with 300 MHz measurements, such as in fig. 2.4, shows that at depths <500 m the observed power return decays in a similar way with range as the estimated back-scattered power, but is about 10 dB weaker. Bearing in mind the poor calibration of the received power

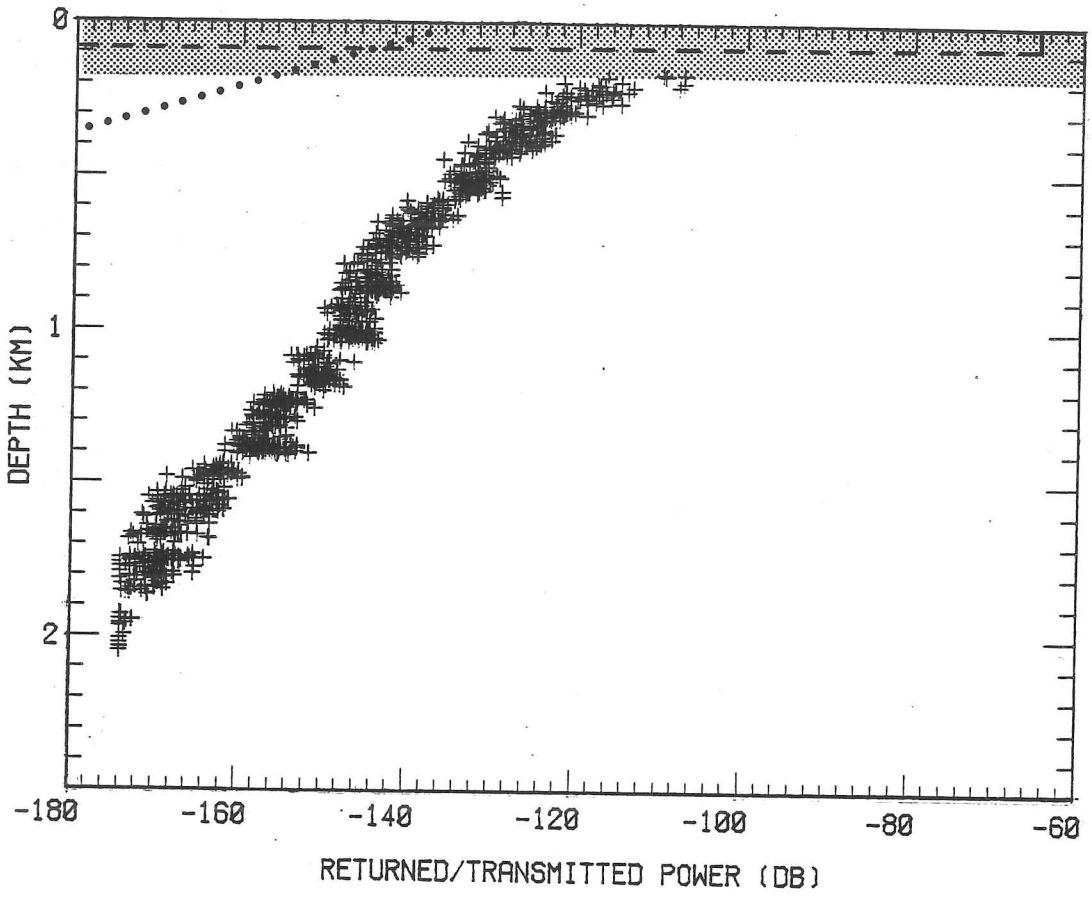

Fig. 4.9 Observed received/transmitted power vs depth near Byrd (site F147/1318), with estimated returns from wide angle surface scatter (dashed line) and scatter from air bubbles within the firn (dotted line). Shading represents the approximate depth to which the receiver is saturated by the strong surface echo. 60 MHz, 250 ns pulse.

for the 300 MHz system, it is possible that back-scattering from within the firn is important in this case.

No measurements of the concentration or size distribution of larger inclusions such as ice lenses have been published, and it is difficult to estimate what they might be. However since the back-scattered power is strongly dependent on radio wavelength any such back-scattering should return ~15 dB more power at 300 MHz than at 60 MHz. Comparison of 60 and 300 MHz power measurements (fig. 2.4) suggests that in the upper few hundred metres some contribution from back-scattering at 300 MHz may be detectable. PRC vs depth profiles recorded near to the coast, where ice temperatures are higher and ice lenses may be expected to be more common, do not appear to show increased power levels near the surface however, (e.g. site F135/785, fig. 6.10). The only situation where such back-scattering from ice lenses seems to be unambiguously observed is in southern Greenland, where the summer surface temperatures may rise above melting point. In this region heavy scattering from within the ice has been reported by Gudmandsen (1976), where it prevents the detection of internal layer echoes.

Chapter 5

ACIDITY LEVELS IN ICE SHEETS FROM RADIO ECHO SOUNDING

5.1 Introduction

The previous chapter has demonstrated how measured layer reflection coefficients may be used to estimate the acidity changes responsible for the observed reflections. This method is applied here to obtain acidity profiles. Other factors which may influence the estimates are discussed, and since it has been demonstrated that high acidity layers are primarily caused by volcanic activity (Hammer 1977), a volcanological interpretation of the results is given.

5.2 Acidity measurements at Crête and Camp Century

In order to make a comparison between acidity levels estimated by radio-echo sounding and those from ice core analyses, the first site chosen is Crête, for which a very detailed acidity profile is available along a 404 m core (Hammer and others 1980). At Camp Century there is another profile available, although it is not so reliable due to the poor quality of the core. Work is currently in progress on a third acidity profile at DYE-3 which will extend to bedrock at 2037 m (Sullivan 1981; M.M. Herron, personal communication).

The RES data used are single A-scope displays recorded during the 1974 season of the Danish-American Greenland RES Programme, using the 60 MHz TUD system and a 250 ns pulse length, kindly supplied by S. Overgaard of the Technical University of Denmark. Although variations in PRC due to fading are expected between A-scope frames, the similarity of the profiles at the two sites near Crête suggests that this is not pronounced here.

Unfortunately rapid recording of A-scope displays by cine photography has never been attempted during airborne echo sounding in Greenland, and so power measurements can only be made every CBD, i.e. at ~2 km intervals. The depth ranges of the RES profiles are calculated from the time range as before, and the usual 10 m correction for higher radio velocities in the firn layer applied. Since the value of 10 m was originally estimated on the basis of density profiles from South Pole, Maudheim and Site 2 (Robin and others 1969), the depth correction was recalculated using density profiles from seven Greenland sites (Herron & Langway 1980). These values are given in Table 5.1 and show a mean of 8.0±0.8 m, so the accepted value of 10 m has continued to be used. Note that at Crête the shallowest internal layer occurred at 75 m depth (where the ice density is ~840 kgm^{-3}), i.e. below the level at which most of the higher velocities occur. Depth estimates at Crête in the upper 500 m are believed to be accurate to ±5 m.

Because the ice core acidity profile suggested that many of the high acidity layers occurred at intervals greater than the pulse length, the complete record of received power vs depth has been used (fig. 5.1), rather than just power maxima (as in the Antarctic where pulse length always limits resolution), and reflection coefficients estimated as in section 3.1. An estimated temperature profile with a surface temperature of -30°C and a basal temperature of -10°C has been used to estimate dielectric absorption, in conjunction with Westphal's values of the attenuation coefficients.

Acidity estimates were then made as described previously, assuming a background acidity of 0.0011 $molm^{-3}$, as measured on the ice core (Hammer and others 1980), and a reflector thickness equivalent to one year's accumulation of ice (0.285 m), since the ice core profile shows that this is the duration of most acidity peaks. In fig. 5.2 these estimates are compared with the ice core acidity profile. The RES profiles appear smoothed because of the long pulse length used (~40 m here), but it is

TABLE 5.1 DEPTH CORRECTIONS FOR HIGHER RADIO VELOCITY IN FIRN LAYER AT GREENLAND SITES

Site	70 m density kgm^{-3}	Depth correction m
North Central	841	8.8
Crête	838	8.2
Site 2	846	7.9
Milcent	846	7.6
DYE-3	816	8.3
South Dome	816	8.5
DYE-2	856	6.5

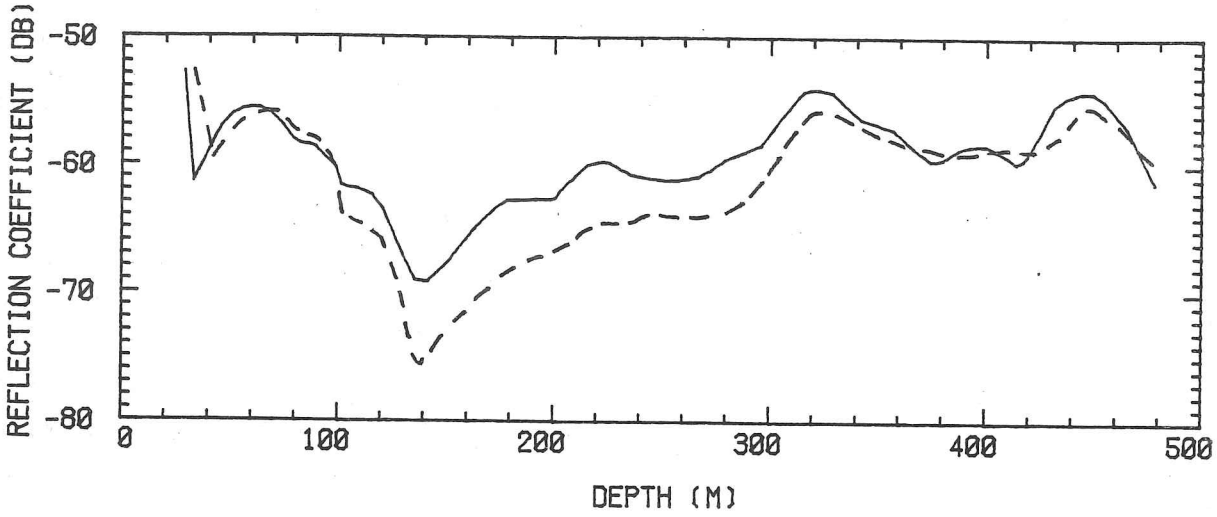

Fig. 5.1 Reflection coefficient vs depth measured at two sites near Crête (solid line, ∿10 km N; dashed line, ∿15 km S). 60 MHz, 250 ns pulse, terrain clearance = 500 m.

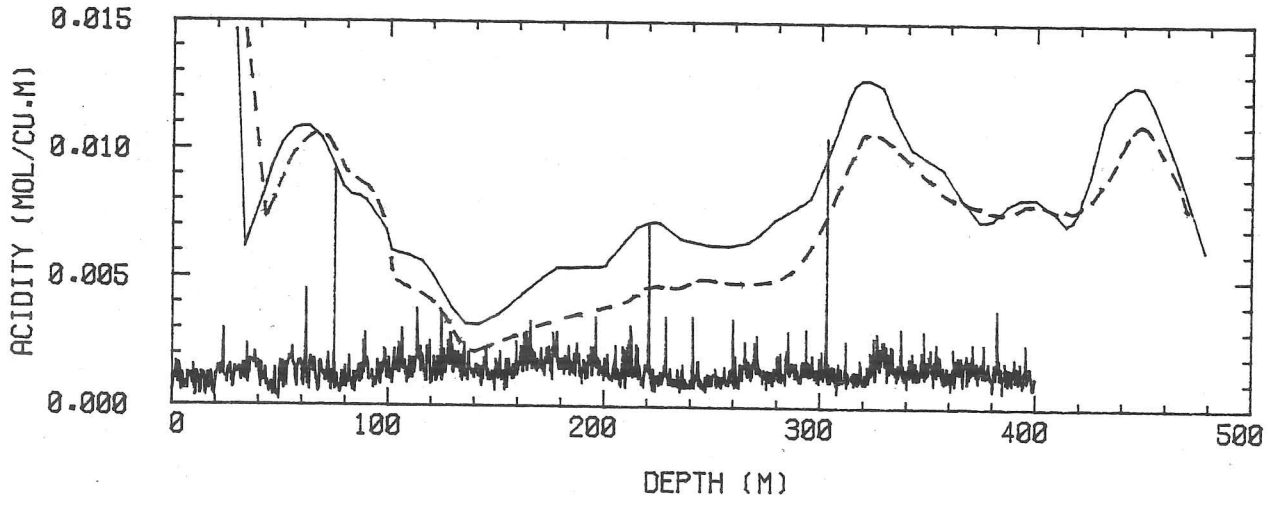

Fig. 5.2 Comparison of mean annual acidities derived from RES at two sites near Crête (solid and dashed lines) and from ice core measurements on a 404 m core (from Hammer and others 1980).

clear that each of the three highest acidity layers measured on the core correspond to peaks on the RES profiles, and that the magnitudes of the peak values are also very similar.

Although it is not possible to obtain any further detail from the RES profile, it is possible to simulate the reflection coefficient vs depth profile seen using the ice core profile, as shown in fig. 2.11. However this is a rather crude method of demonstrating the smoothing effect of long pulse lengths; by taking the mean of one high acidity peak and many background values, the predicted reflection coefficient is much lower than is observed. The observed reflection coefficients match well those predicted from the magnitude of the peak acidity change alone, however (fig. 5.2).

Because the background acidity measured at Crête is much lower than that of HF-doped ice with the same conductivity (0.0011 and 0.0072 $molm^{-3}$, respectively), it is not necessarily to be expected that the acidities estimated from RES will be equal to the ice core values, but that they will be related in some way. The similarity of the profiles indicates, however, that at Crête the absolute acidity may be satisfactorily estimated by the direct analogy with HF-doped ice used here.

It is interesting to note that one of the first observed internal layer echoes, near Camp Century in 1964 (Robin and others 1969), was dated at AD 957±100 yrs. This is very close to the date of the highest acidity layer detected in the 404 m Crête core, and correlated with the eruption of Eldgja (Iceland) in AD 934±2 yrs. It therefore seems likely that this layer echo did not arise as first thought from a density variation caused by 'a few days of warm weather', but from the high acidity layer due to this eruption. A profile of melt feature abundance along a 901 m core from DYE-3 shows a minimum at this time (Herron and others 1981), suggesting that a particularly prominent melt feature is unlikely to be a cause for this particular reflection.

The comparison with measured acidity levels may be extended by comparing the complete RES-derived acidity vs age profile for Crête with the ice core acidity record at Camp Century, which goes back to ~10 kaBP (no suitable RES power measurements are presently available from Camp Century). However we cannot assume that reflections from depths greater than a few hundred metres at Crête come from isolated thin reflectors. Since the spacing of high acidity layers (i.e. those several times the background acidity) in the upper 400 m is only slightly greater than the pulse length, it is clear that by about half-way through the ice sheet we are likely to encounter more than one reflecting surface in the spatial pulse length. This is in fact noticeable on Z-scope records when changing the pulse length from 250 to 60 ns (i.e. ~40 to 10 m in ice); what appear as single layers at 250 ns can be resolved into two or three layers at the shorter pulse length at depths of ~500 m and below (Gudmandsen & Overgaard 1978). Also, the mean spacing between layers does not generally decrease with depth, as would be expected on average for isolated reflectors because of the thinning of annual layers with depth. Furthermore, if acidities are estimated on the assumption that the reflectors have a thickness equivalent to one year's accumulation (i.e. thinning with depth), the derived values become unreasonably large at depths >1000 m. When several reflecting surfaces occur in the space of a pulse length and their separations and thicknesses are not known, an accurate estimate of the total reflection coefficient is not possible.

However Clough (1977) has shown by numerical modelling that for closely spaced reflecting layers with randomly varying layer spacing and thickness, the total reflection coefficient is well approximated by that for a single interface with an averaged change in dielectric properties. For a layer of given reflection coefficient, the corresponding change in high frequency conductivity (and hence the derived acidity) is only weakly dependent on the assumed layer thickness when this is greater than about 0.2 m (at the present radio wavelength of 2.8 m), until interference effects dominate the returned power. It is also very similar to that

obtained for a simple interface (fig. 5.3). A layer thickness equivalent to one year's accumulation of ice at the surface is therefore assumed here for the entire ice column, and allows continuity with acidity estimates near the surface.

Mean annual acidities measured on the Camp Century core (Hammer and others 1980) are compared with estimates from Crête in figs. 5.4(a) and (b), which also serve to demonstrate the effect of temperature variations down the ice column on acidity estimates. Fig. 5.4(a) shows estimated acidity assuming a constant ice temperature of -30°C, and fig. 5.4(b) for a profile with a surface temperature of -30°C rising to -10°C at the base. Layer depths at Crête have been dated using the non-uniform vertical strain rate model of Dansgaard & Johnsen (1969), estimating their parameter h (the height above bedrock where the vertical strain rate becomes non-constant) from the data given by Reeh and others (1978); measured depths at Crête are also shown on the diagram. For clarity the RES acidity profile from only one site near Crête has been shown.

Most of the strong acidity signals from the Camp Century core are found to correspond with peaks on the RES record, but below a depth of about 1000 m the radio-echo peaks appear to become displaced by up to 50 m (approximately one pulse length) downwards from the ice core acidity peaks. This may be due to a systematic error in dating between the two sites, or to a genuine effect caused by the nature of the reflectors. At ~9-10 kaBP seven high acidity layers occur within a distance of ~80 m and do not appear to correlate with a radio-echo layer; it is suggested that interference effects may be responsible for this anomaly. Note that there is no ice core acidity data for 1.5-2.0 kaBP, where the RES results indicate a high acidity layer at about 1600±150 yrs BP.

The RES record prior to 10 kaBP shows very low acid levels between 14-23 kaBP (corresponding to the widespread gap in layering reported by Gudmandsen (1975)) and some poorly resolved peaks extending to ~30 kaBP,

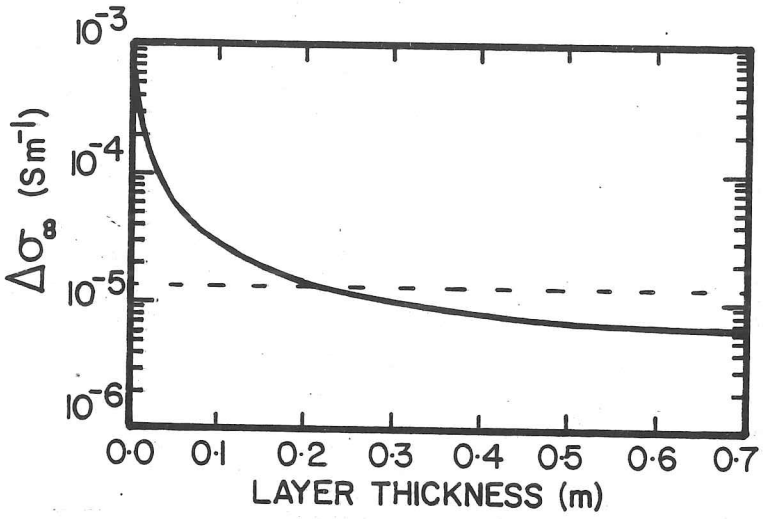

Fig. 5.3 Necessary change in high frequency conductivity ($\Delta\sigma_\infty$) to produce a reflection coefficient of -70 dB for layers of acidic ice of varying thickness up to ¼λ (0.7 m), and for a simple interface (dashed line).

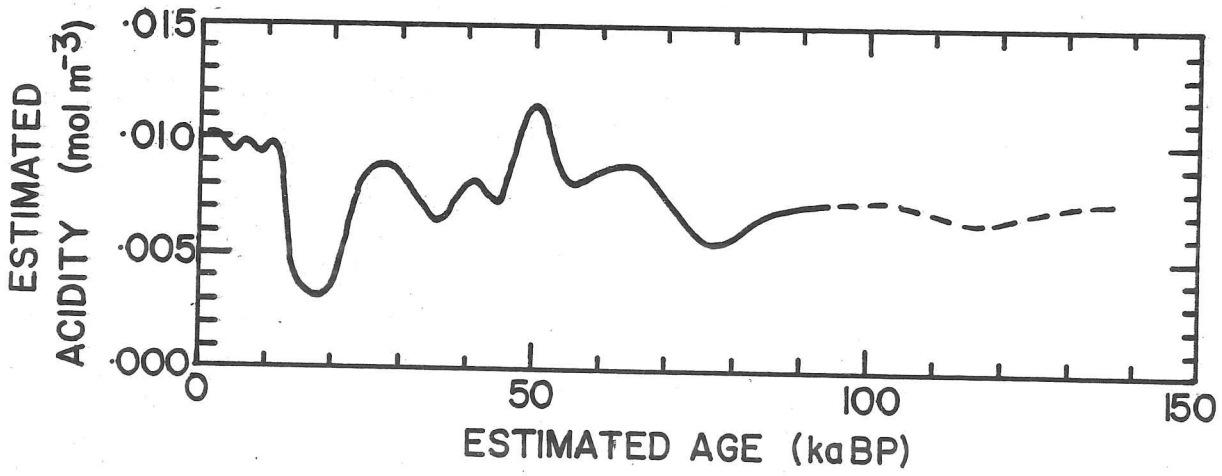

Fig. 5.9 General Antarctic acidity profile compiled from PRC vs depth data at six sites. Diagram represents the envelope of high acidity values and not the background acidity.

Fig. 5.4 (overpage) Comparison of mean annual acidities from ice core measurements at Crête (0-1500 yrs BP) and at Camp Century (>2000 yrs BP) above 0.004 molm^{-3} (vertical bars), with acidities derived from radio-echo sounding near Crête (solid line). Measured layer depths at Crête shown by upper scale, dates at Crête from model of Dansgaard & Johnsen (1969) (H = 2750 m, $\dot{A}$ = 0.285 ma^{-1}, h = 1400 m) on lower scale. Dating of Camp Century data used the model of Hammer and others (1978). Shading represents background acidity as measured on ice cores; speckled region denotes limit imposed by RES system sensitivity.

(a) acidities estimated assuming a constant ice temperature of -30°C and reflector thickness of 0.285 m

(b) acidities estimated assuming a temperature profile with a basal temperature of -10°C and reflector thickness of 0.285 m

(c) calcium concentration measured on the Camp Century core (Cragin and others 1977), dating from Hammer and others (1978) and comparable with the ice core acidity data.

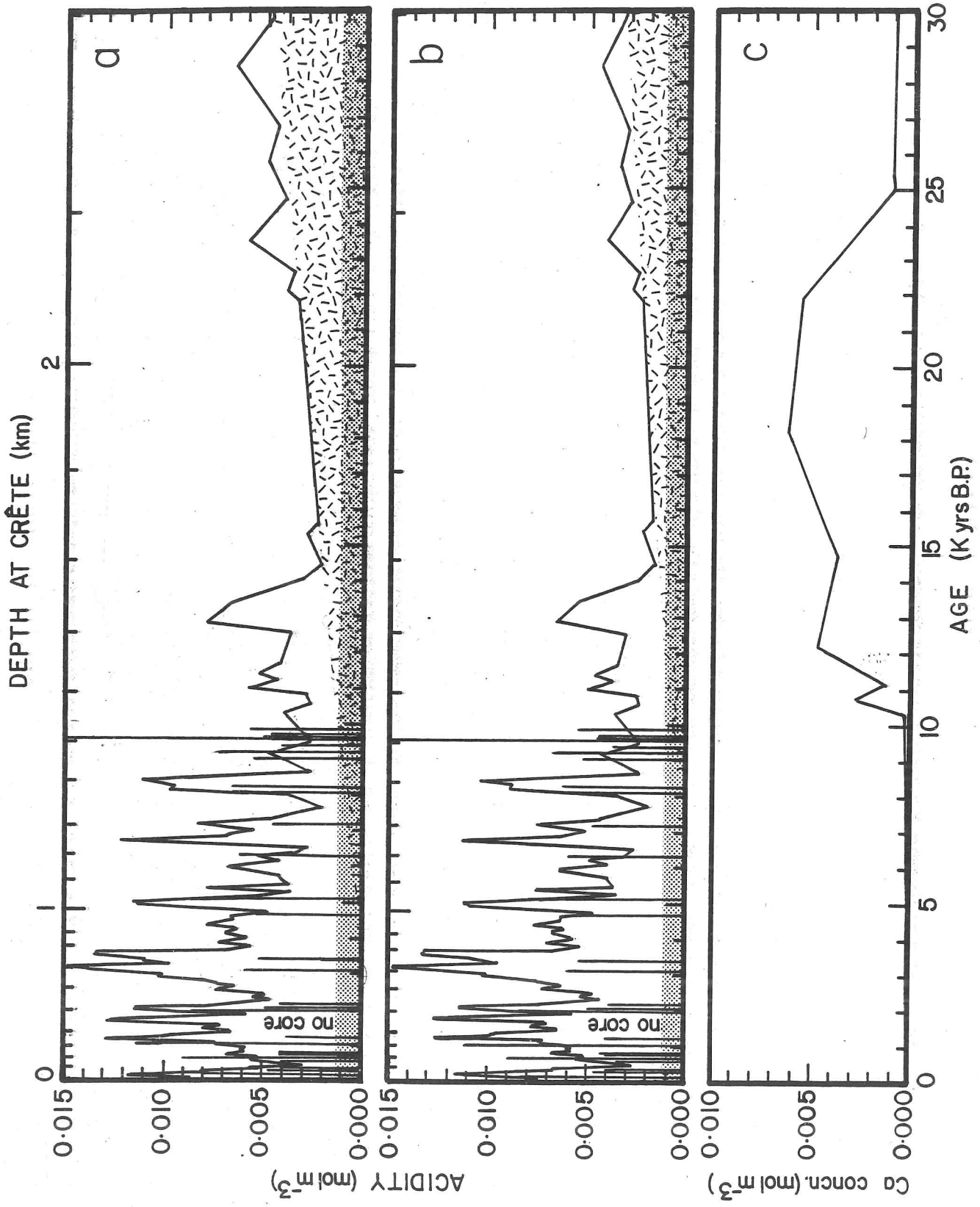

Fig. 5.4 (see preceding page for caption)

where dielectric absorption limits the technique. Hammer and others (1980) also report very poorly conducting ice at Camp Century from this period.

It seems plausible that both these observations may be explained by chemical neutralisation of any acids present by calcareous dust, possibly blown onto the ice sheet at the end of the last glaciation from areas of exposed glacial outwash or former shallow water areas, as suggested by Cragin and others (1977). Calcium concentrations of the correct level to obliterate or greatly diminish any volcanic signals between about 11-25 kaBP have been measured on the Camp Century ice core (fig. 5.4(c)). However it is difficult to think of a chemical mechanism for this neutralisation, since the calcium and acid are both thought to be present as small particles frozen into a matrix of ice. One possibility is that the neutralisation occurs in the atmosphere, with the calcareous dust acting as nucleation centres for the sulphuric acid aerosol, which then reacts with the particle. This would be easier in the atmosphere than in the ice sheet because the acid would be in the liquid phase, and sunlight would be available which might assist the reaction.

In the Antarctic, returns from density fluctuations dominate those from acidic ice layers at depths <500 m. At Crête this does not seem to be the case, as reflection coefficients show no rapid fall-off with depth near the surface, and even the shallowest layers correlate with high conductivity layers (Gudmandsen & Overgaard 1978). The explanation lies in the fact that the reflection coefficients for layers observed at Crête are typically 10-20 dB greater than for Antarctic layers. This may be seen by comparing the observed reflection coefficient vs depth profile for Crête (fig. 5.5) with those for the Antarctic sites (e.g. in fig. 3.3). This difference may in turn be associated with the disproportionate concentration of active volcanoes in the northern hemisphere (Porter 1981; Newhall & Self, in press) which probably causes greater amounts of volcanic acids to be deposited on Greenland than on the Antarctic. Generally higher accumulation rates in Greenland will also give higher

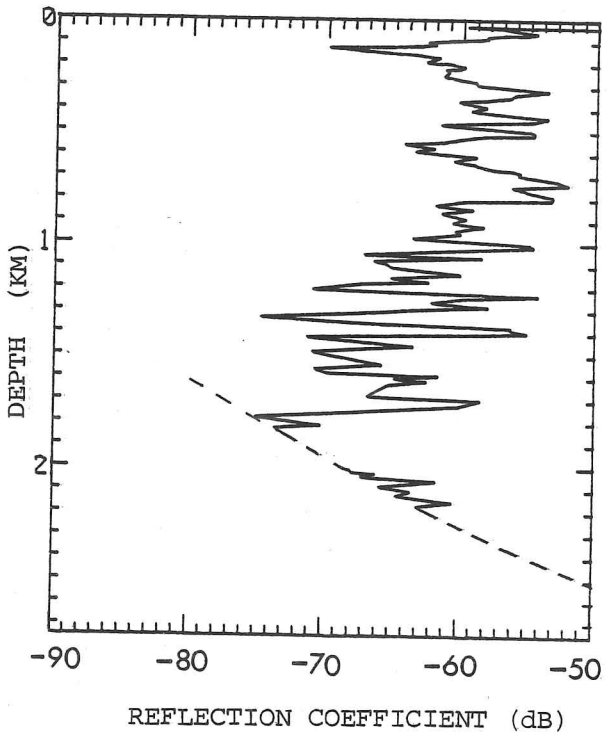

Fig. 5.5 Reflection coefficient vs depth profile at Crête, used in the estimation of the acidity profile. Detection limit denoted by dashed line.

layer reflection coefficients near to the surface, because the acidic layers will be thicker (eqn. [4.8]). Reflector thicknesses an order of magnitude greater than in the Antarctic may also be expected to affect the fading of the echoes, although this has not been measured in Greenland.

5.3 The Antarctic acidity record from radio-echo sounding

As noted in Chapter 3, layer reflectivity can vary significantly over distances of a few tens of kilometres, and it is therefore difficult to obtain values of layer PRC from a single site which are meaningful over large areas. Averaging of PRCs for individual layers over 100 km may be desirable, but many layers are not followable for such distances. The compromise taken here is to average layer PRCs over distances of 25–50 km. The layer depths are then dated using flow models and the PRCs converted into acidity estimates. The resulting acidity vs age profiles from several widely spaced sites may be compared, looking for common features and discarding those which are localised and occur at only one site. In this way an acidity vs age profile which shows only features which are observed at many locations may be obtained. Because of the atmospheric nature of the deposition of acidic impurities it is thought that the resulting profile will be of greater significance than profiles from individual sites, which may show high acidity peaks that are not important on a wider scale. It is hoped that the identification of widespread acidity events may also be of use in comparing chronologies at different sites.

Because reliable dating of the ice is difficult at sites where glaciological surface data are not available, the sites chosen for this study have been those where surface measurements have been made and ice chronologies already studied (Byrd, Vostok and Dome C), and two sites near to Dome C which can be compared with Dome C via the Z-scope layering. South Pole has also been included although the dating here is less reliable than elsewhere.

PRC vs depth profiles for these six sites are shown in fig. 5.6. Reflection coefficients for each layer identified have been measured every CBD over distances of 25-50 km along the flight-tracks, and the measurements at each CBD connected via the Z-scope record. At Vostok there is unfortunately no Z-scope data to connect the A-scope power measurements consistently to the same layers, but because of the exceptionally flat bedrock it has been assumed that layers remain at constant proportional depth to bedrock. The similarity of PRC vs depth profiles around Vostok, and Z-scope records from earlier flights (for which no A-scope data are available), suggest that this is a reasonable procedure.

The length of these profiles is limited by the depth to which strong density effects are seen near the surface, and by dielectric absorption near the bed. Absorption losses at Byrd have been estimated on the basis of the measured temperature profile (Gow 1970). At Vostok the temperature measurements to 782 m depth (Barkov 1974), and the profile estimated by Budd and others (1975) have been used. At Dome C the measured profile to ~900 m (Ritz and others, in press) has been used, and extended using eqn. [3.2] giving an estimated basal temperature of -6.5°C. The derived input parameters for eqn. [3.2] have then been used to estimate temperature profiles at the two neighbouring sites, changing only the ice thickness. For South Pole, eqn. [3.2] has been used together with input parameters from Budd and others (1971), giving an estimated basal temperature of -16°C. For the calculation of reflection coefficients by computer, eqn. [3.2] was used, and the input parameters necessary to give the above temperature profiles obtained by a least-squares fitting routine. The input data for all sites are given in Appendix 3.

The PRC vs depth profiles have been dated as follows: Byrd and Vostok - flowline model by Budd & Young (in press); South Pole - simple accumulation model (Nye 1957) with $\dot{A}$=0.08 ma^{-1}, Z=2915 m; Dome C - simple accumulation model by Lorius and others (1979); F136/608 and F136/704 - dating by simple accumulation model, related to Dome C chronology by

several internal layers that could be followed between the sites on the radio-echo records. The age vs depth relationships used at the four principal sites are shown graphically in Appendix 4. The resulting PRC vs age profiles are shown in fig. 5.7; some common features are readily apparent, particularly between the four East Antarctic sites.

Using the estimated temperature profiles, and making the assumption of a single reflecting interface for each layer echo (as in the previous section for the deeper layers at Crête), elevated acidities (Δc) were then estimated as before. The resulting elevated acidity vs age profiles are shown in fig. 5.8. It should be noted that these are elevated acidities for high acidity layers, and are not related to the background acidity of the ice. D.C. conductivity measurements along the Byrd core (Gow 1970) suggest that the background acidity remains at a uniformly low level for most of the period considered here.

Common features have been identified and used to construct a single estimated acidity vs age profile for the Antarctic (fig. 5.9), assuming a background acidity of 0.002 $molm^{-3}$, which is the mean acidity during volcanically quiet periods from measurements along the 905 m Dome C core (Legrand 1980). Because of the constant spatial resolution of the echo sounder, the temporal resolution of the profile varies with age, being ~1 ka at the beginning and rising to ~10 ka at 100 kaBP. The fact that common features can be identified between sites as far back as 100 kaBP gives confidence in the reliability of the models used for dating sites. Direct linking of remote sites via layering will be discussed in Chapter 6.

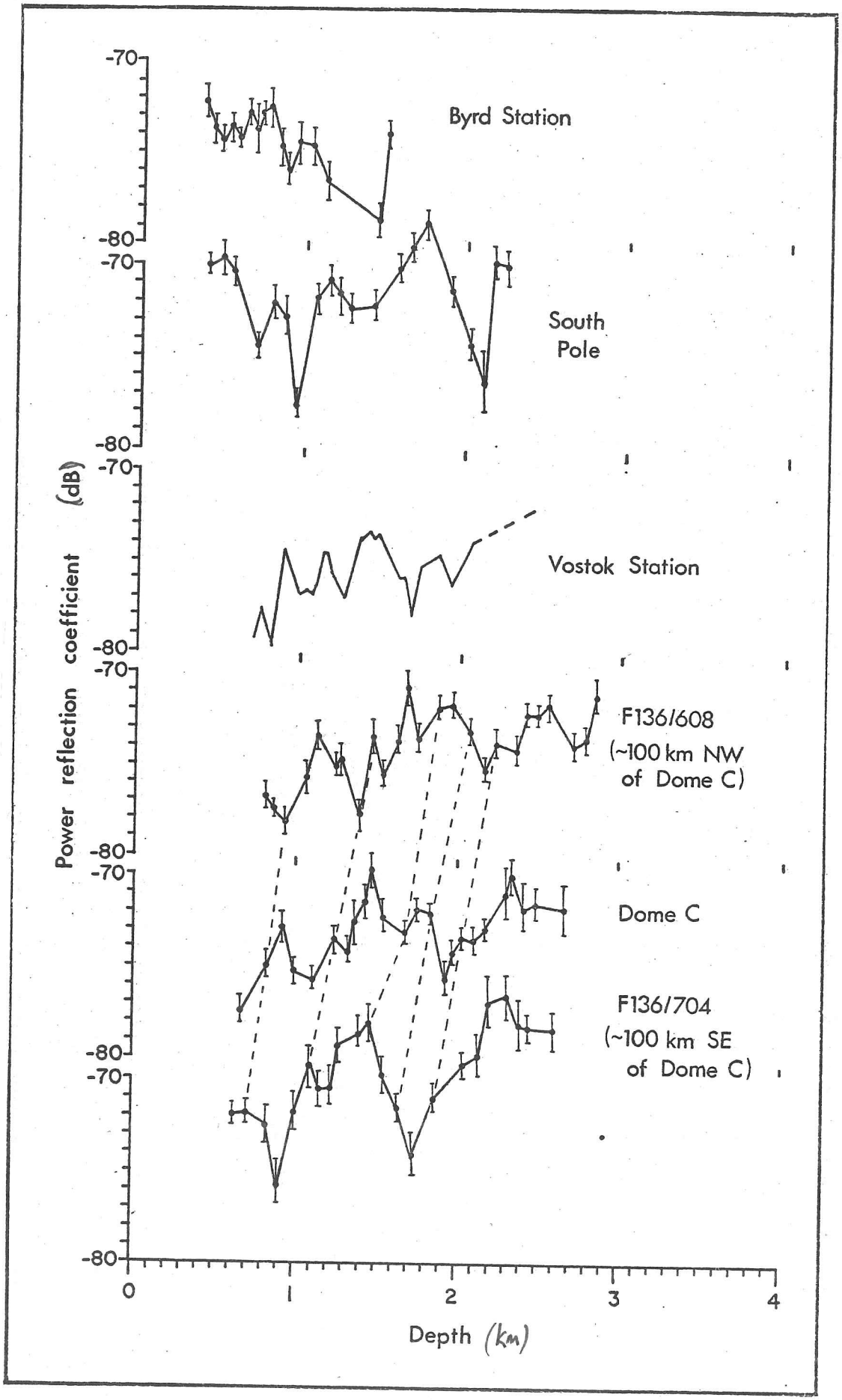

Fig. 5.6 Reflection coefficients averaged over 25-50 km vs depth at six Antarctic sites. Dashed lines connect known common horizons. Bars represent one standard error.

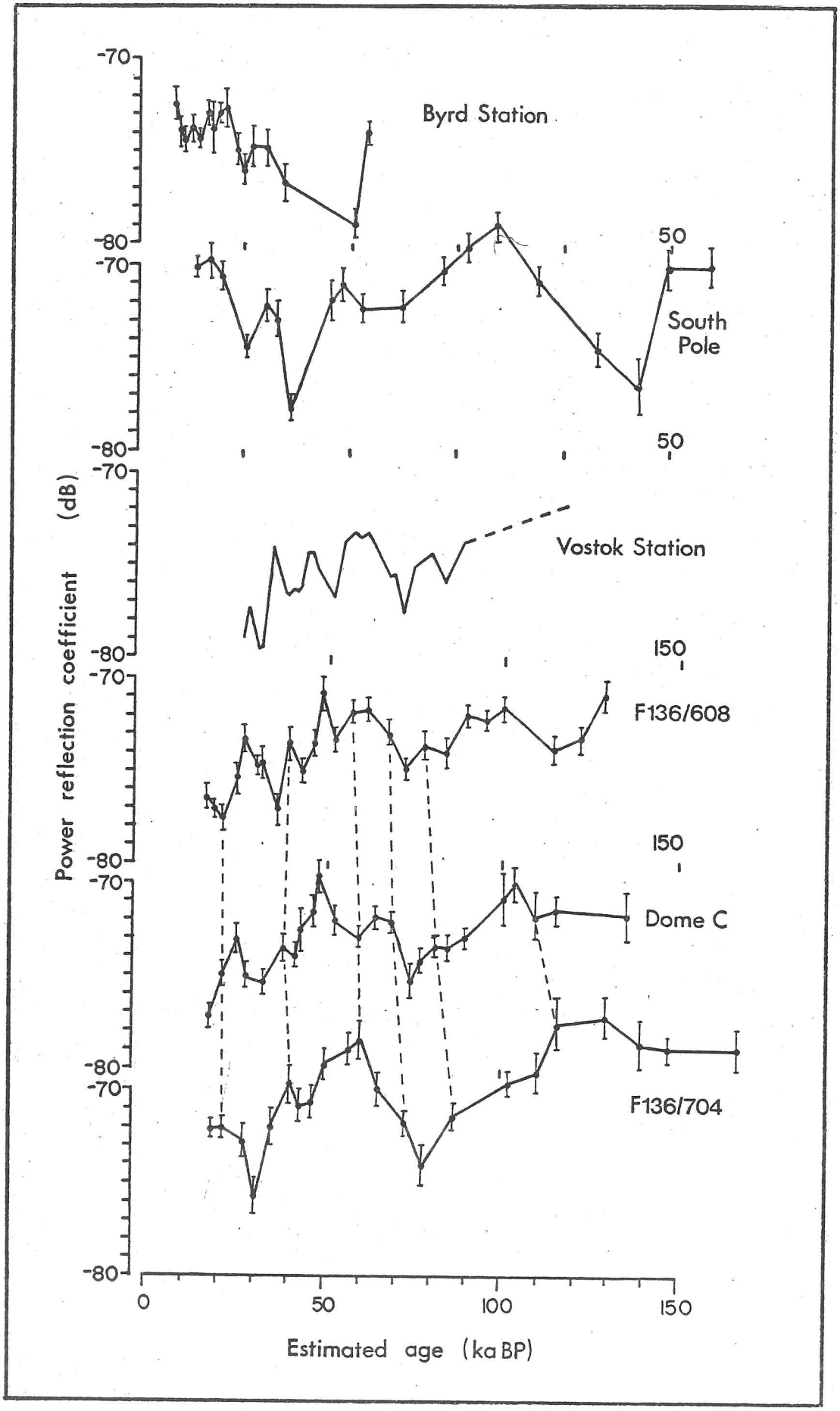

Fig. 5.7 Reflection coefficients averaged over 25-50 km vs estimated age at six Antarctic sites. Dashed lines connect known common horizons. Bars represent one standard error. Note expanded age scale for first two sites.

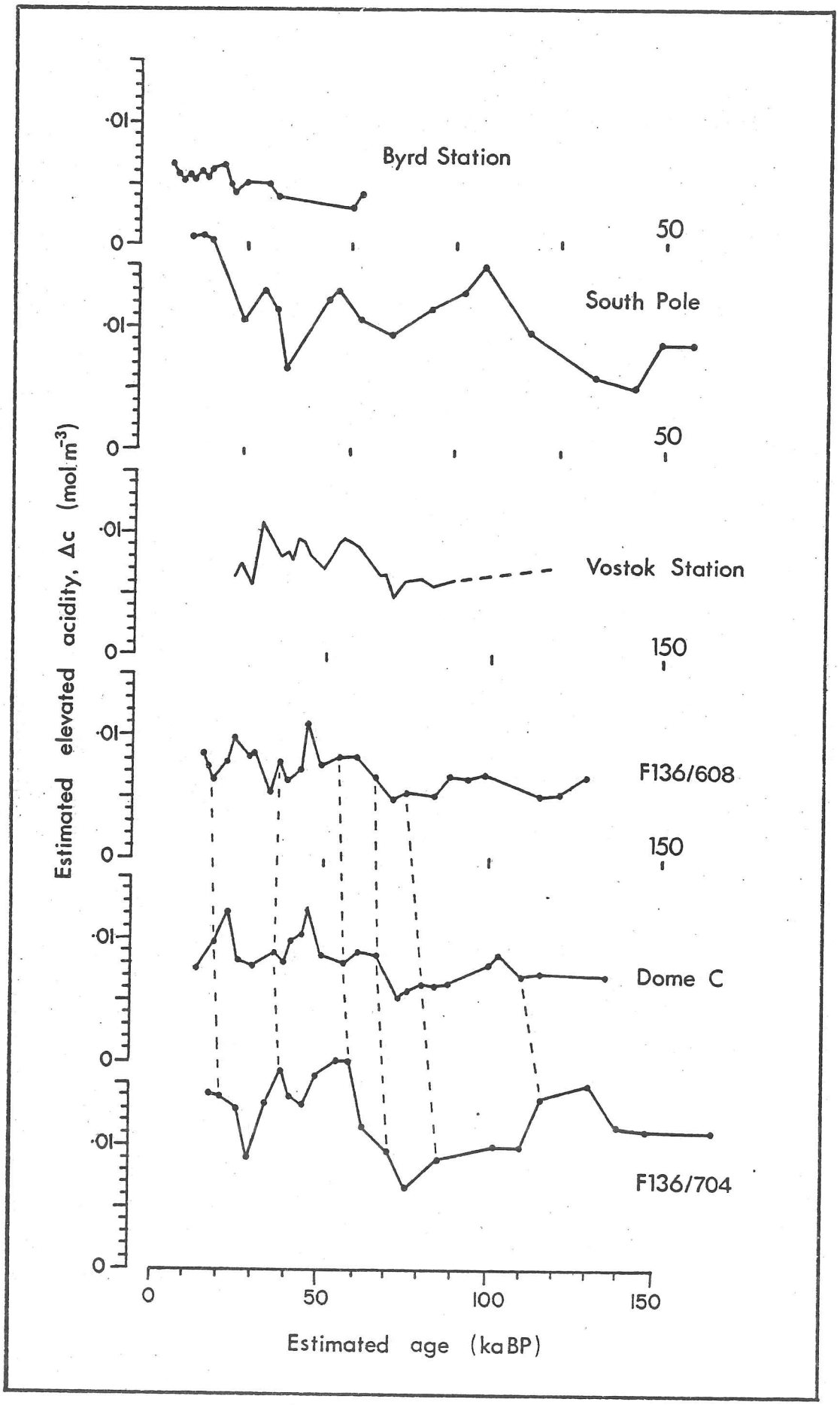

Fig. 5.8 Estimated elevated acidity vs age at six Antarctic sites. Note expanded age scale for first two sites.

5.4 Interpretation of the Antarctic acidity record

Unlike Greenland, there are no continuous conductivity records along deep Antarctic ice cores* with which to compare the results obtained in the previous section. However isolated acidity measurements have been made down the 905 m Dome C core (Legrand 1980), and isolated d.c. conductivity measurements down the Byrd deep core (Gow 1970). References to other data of interest along deep ice cores are listed in Table 5.2. In this section factors which might affect the RES acidity estimates are first considered, and the profile is then discussed with reference to other relevant data.

The discussion of the Crête acidity profile showed that large variations in the acidity may occur due to other chemical impurities (notably $CaCO_3$) or to high microparticle concentrations in the ice. The possibility that similar effects are operating in the Antarctic must obviously be considered. Calcium and microparticle measurements are available along the Byrd core (Cragin and others 1977; Thompson 1977), and microparticle data only for the Dome C core (Thompson and others 1979).

These show that although calcium levels are high between 15-30 kaBP at Byrd, the maximum concentration is only 0.0003 $molm^{-3}$, compared with 0.006 $molm^{-3}$ at Camp Century. This is less than the background acidity of the ice at Dome C and much less than the elevated acidities estimated by radio-echo sounding. Other measured elemental concentrations are similarly low, and the possibility of significant chemical neutralisation may therefore be discounted. Microparticle concentrations, although showing a peak between ~14-22 kaBP at both Byrd and Dome C, are similarly much lower than in Greenland. It is concluded that the RES acidity profile

---

* Scratch-conductivity work is in progress on the Byrd Station deep ice core (Hammer, personal communication), and acidity measurements are planned to be made on a 'liquid' core to be taken shortly at Dome C using a thermal probe (Delmas, personal communication).

TABLE 5.2 DATA AVAILABLE ALONG DEEP ANTARCTIC ICE CORES OF POSSIBLE RELEVANCE TO VOLCANIC ACTIVITY

Site	Data	Reference
Byrd	$^{18}O/^{16}O$	Johnsen and others 1972
	d.c. cond'ty	Gow 1970
	Dust bands	Gow & Williamson 1971
	Microparticles	Thompson 1977
	Na, K, Mg, Ca, Si, Al, SO_4	Cragin and others 1977
Vostok	$^{18}O/^{16}O$	Barkov and others 1977
Dome C	$^{18}O/^{16}O$	Lorius and others 1979
	Acidity	Legrand 1980
	Microparticles	Thompson and others 1979
	Zn, Cl, Na, Al, (V, Mn)	Petit and others 1981

is unaffected by other ice impurities to at least 90 kaBP (the extent of calcium measurements on the Byrd core) and probably for some time before that, since there appears to be a strong link between calcium and dust levels, and the end of the last glaciation.

The Antarctic acidity profile as an indicator of past volcanic activity will now be discussed and compared with other possible volcanic activity indices.

Since the acidity at Crête has been shown to be directly related to volcanic signals, it is thought that the Antarctic profile (fig. 5.9) represents peak acidities caused by volcanic activity averaged over the radio pulse length. The profile is unlikely to reflect directly any changes in background acidity; the Dome C core measurements (Legrand 1980) show that such changes are very small compared to the peak acidity values. Peaks on the profile can therefore be expected to indicate periods of high volcanic acid production in the southern hemisphere. Hammer (1977) showed that Greenland acidity levels were principally influenced by northern hemisphere eruptions, because there is little inter-hemispheric exchange in the lower stratosphere. Likewise it is expected that the Antarctic acidity levels will be primarily due to southern hemisphere volcanic activity .

The amount of SO_2 injected into the stratosphere by an eruption (which primarily determines the amount of acid produced) is not necessarily related to other measurements of the magnitude of the eruption, which can vary greatly in character (Stith and others 1978). The acidity profile therefore probably only represents large explosive eruptions, and will not be influenced by eruptions which may eject large amounts of material but which do not penetrate the stratosphere.

This interpretation would suggest that explosive volcanic activity was approximately one third of its present level between 13-25 kaBP,

i.e. during the end of the last glaciation, and that another slight decrease in activity occurred at about 70-80 kaBP. A marked peak occurs at about 50 kaBP. For the most part though, the level of activity appears relatively constant over the last 100 ka.

Earlier attempts to date the Antarctic layering record suggested the existence of a common gap in the Z-scope record at ~15-20 kaBP (Millar 1981). This gap appears to correspond to a minimum on the present acidity vs age record. However a clear gap in Z-scope layering is not observed at all sites, and although low acidity levels are recognisable during this period at most locations investigated, the Z-scope gap is not observed consistently enough for it to be used as a marker in the layering record. New data for South Pole have also been used to improve the PRC vs age profile over that given before.

5.5 Comparison with other estimates of past volcanicity

Isolated acidity measurements have been made down the Dome C ice core (Legrand 1980), and show approximately constant values of about 0.0025 $molm^{-3}$ to a depth of 700 m (~23 kaBP), and lower values of about 0.001 $molm^{-3}$ from 700-900 m depth (~23-32 kaBP). These results have been interpreted as an indicator of the general level of southern hemispheric volcanic activity (Petit and others 1981). If so, then this would appear to agree with the RES acidity results for the past 30 ka. However the ice core measurements were made on samples only a few centimetres long at isolated points along the core. Detailed acidity profiles from Crête, Camp Century and short sections of the Dome C core would suggest that with such a small sample size it is extremely unlikely that any high conductivity peaks are included. The measurements may therefore be considered to refer to background values, which are thought to be largely due to sulphuric acid and CO_2-induced ions (Hammer 1977), probably of marine and atmospheric origin (Delmas & Boutron 1978). The decreased values below 700 m are

therefore possibly due to lower sea-surface temperatures rather than to a decrease in volcanism.

Other ice properties which have been measured and which might be influenced by volcanic activity include d.c. conductivity, decreases in the $^{18}O/^{16}O$ ratio (via the atmospheric cooling associated with large or sustained eruptions (Newell 1971)), and increased concentrations of certain volatile elements released to the atmosphere in large amounts by eruptions (Boutron & Lorius 1977; Boutron 1980).

Unfortunately the only available d.c. conductivity profile (from the Byrd core, Gow 1970), was again based on widely spaced measurements on very small sections of core and probably refers to background conductivity, which is not thought to be influenced by volcanic activity. The profile shows uniform values of about 200 μSm^{-1} for the whole of its length.

Detailed oxygen isotope profiles are available for cores from Byrd, Vostok and Dome C (Johnsen and others 1972; Barkov and others 1975; Lorius and others 1979). A comparison of these profiles with Z-scope layer echo depths (fig. 5.10), PRC vs depth profiles, and the general Antarctic acidity profile, reveals no significant correlation in any case, however. This may well be because any atmospheric cooling (due to dust thrown into the atmosphere by the eruption), is too small or short-lived to show up as a change in isotopic ratio.

Boutron & Lorius (1977) have suggested Pb, Cd, Cu, Zn and Ag as indicators of volcanic activity for Antarctic snow samples, as volcanic aerosols are strongly enriched in these elements with enrichment factors close to those determined at Dome C (Mroz & Zoller 1975; Buat-Menard & Arnold 1978). A profile of Zn concentration along the Dome C core shows higher values during the end of the last glaciation (Petit and others 1981), however the crustal enrichment factor (with reference to Al) is very low (~1) during this period. Values higher than 100 are observed in

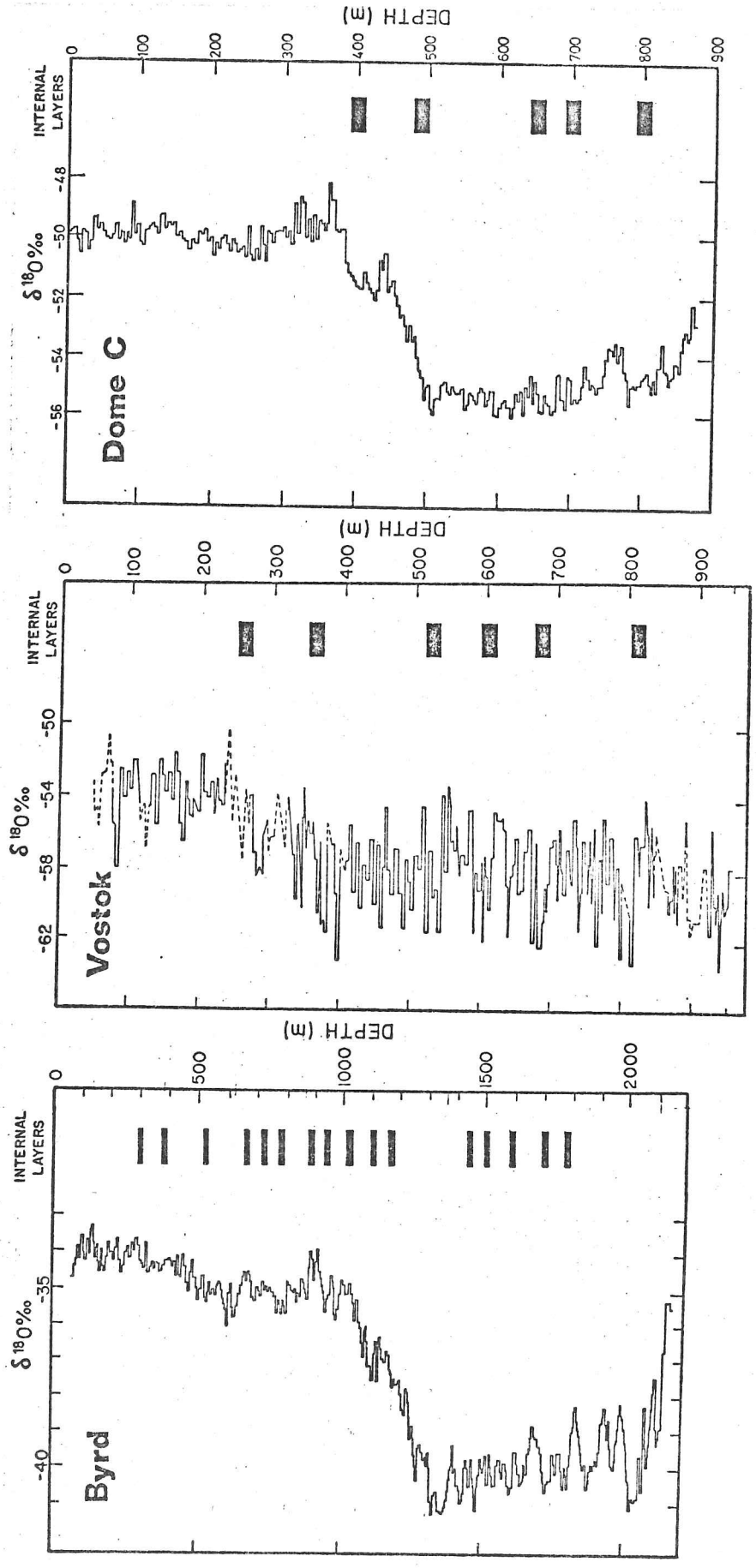

Fig. 5.10 Comparison of oxygen isotope profiles and depths of prominent radio-echo layers. Thickness of layer bars is equivalent to half a pulse length in ice (20 m).

surface samples corresponding to periods including volcanic events (Boutron 1980). This suggests that the higher Zn concentrations during the end of the glacial period are not due to enhanced volcanic activity but are of continental origin. However the average crustal enrichment factor for Zn since the glaciation is about 10, suggesting higher volcanic activity since the glaciation rather than during it. This is in agreement with the RES acidity record, which shows elevated acidities in the period after the glaciation which are roughly double those during the latter part of the ice age.

Apart from this partial corroboration for the more recent part of the profile, it is evident that there is as yet no suitable data from Antarctic ice cores which might provide an independent measure of past volcanic activity. The only other sources of information are dated ash layers from individual eruptions, which are found in marine cores and land deposits (Huang and others 1973; Bryson & Goodman 1980). Because material is mainly deposited near to the source, such methods yield only a local record of past volcanicity, so studies are needed at many sites in order to build up a hemispheric record. Unfortunately only a very small proportion of past eruptions are known (Rampino and others 1979; Newhall & Self, in press), and these are often concentrated disproportionately in areas which have been well studied. Table 5.3 lists known large explosive southern hemisphere eruptions during the period of interest. It is clear that there is not sufficient information from this source to draw any conclusions about past general levels of explosive volcanicity.

TABLE 5.3 KNOWN LARGE EXPLOSIVE SOUTHERN HEMISPHERE ERUPTIONS

Date (kaBP)	Eruption	Bulk volume of deposit* (km^3)
0.067	Krakatoa (Indonesia)	~18
0.135	Tambora (Indonesia)	<150
1.82	Taupo (New Zealand)	>30
2.00	Sunda (Indonesia)	>10?
3.80	Waimihia (New Zealand)	≫15
20.5	Oruanui (New Zealand)	~150
28.4	Roseau (Dominica)	>40
30.0	Mangaeone (New Zealand)	>20
41.7±3.5	Rotoehu-Rotoiti ash (New Zealand)	>100
75.0	Toba (Sumatra)	~2000
75.0	Y6 ash (Gulf of Mexico)	>50?
85.0±5.0	Los Chocoyos (Y8 ash, Gulf of Mexico =D ash, east Pacific)	>400?

* Estimates from Rampino and others (1978).

Chapter 6

DEEP ICE DYNAMICS FROM LAYER ECHO STUDIES

6.1 Introduction

This chapter attempts to collect together and describe observations from radio-echo sounding and data from other sources which have relevance to the study of ice flow at depth. It does not attempt to provide a exhaustive examination of the applications of internal layering in flow studies. As depositional (and hence isochronous) surfaces, radio-echo layers can provide unique information on the flow of ice at depth over large areas. Valuable comparisons have previously been made (Robin and others 1969; Whillans 1976) between internal layers and isochronous surfaces calculated from models. Layering is used here to investigate the effect of rough bedrock topography on the uniformity of the vertical strain rate. This shows that the simple ice flow model used is generally a good approximation to the flow of the ice sheet, but situations where the approximation is not so good are also identified. Layering near isolated peaks is also examined to try to see how the ice flows around such obstacles.

Layering is frequently not detected in the basal zone of the ice. This has been noted before by Robin and others (1977), and the suggestion made that its absence at the lowest levels may be due to complex deformation of the ice over rough relief. Power measurements are used here to confirm that this 'basal layer-free zone' is often due to the absence of suitable reflecting surfaces, rather than to insufficient system sensitivity, and its thickness and extent are studied over a wider area than has previously been attempted. Taking into consideration relevant observations from other glaciological sources, suggestions are made as to its cause.

Finally, the use of layering in comparing ice core chronologies at widely separated sites is discussed.

6.2 Internal layering and models of ice flow

Radio-echo layering is potentially an invaluable tool for studying the flow of ice sheets at depths which are otherwise inaccessible except at isolated points via boreholes. The previous chapters have established that the deeper layers are due to impurities deposited over short periods from the atmosphere, and hence represent isochronous surfaces. Comparing layers with isochrones calculated from ice flow models in areas with different bedrock roughnesses and ice velocities can indicate how reliable those models are in various situations.

A frequent assumption of simple ice flow theories (Nye 1957; Paterson 1969) is that the vertical strain rate, $\dot{\varepsilon}_z$, remains constant down the ice column, which implies that isochronous surfaces should remain at constant fractional depths to bedrock along a flowline as the ice thickness varies, if the accumulation rate is also constant along the section. The possibility that the upper surface of the basal echo-free zone represents a boundary where the vertical strain rate becomes non-uniform will also be considered.

A number of radio-echo profiles lying approximately parallel or perpendicular to surface flowlines (as determined from surface contours) have been examined to see how good the approximation of a constant vertical strain rate is; locations of sections chosen as examples are shown on fig. 6.1. The sections are generally less than 50 km long, so changes in accumulation rate along them are not expected to be significant. Fig. 6.2 shows sections, expressed both as true depths and fractional depths to bedrock, of selected internal horizons, including the shallowest and deepest observed; Table 6.1 summarises fractional depths

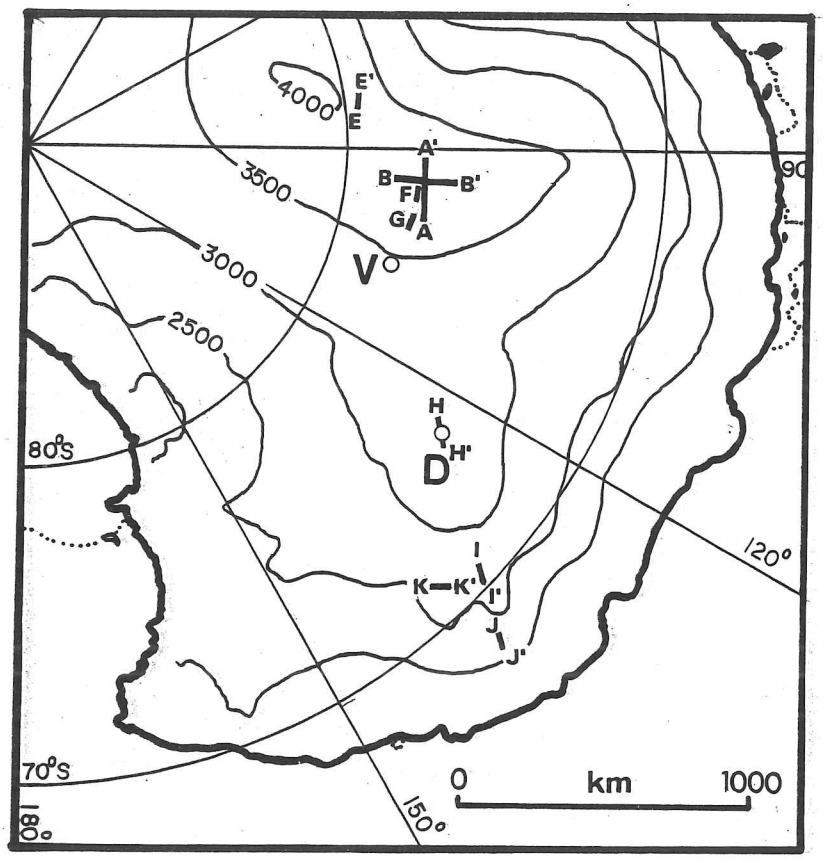

Fig. 6.1 Location of profiles discussed in chapter 5

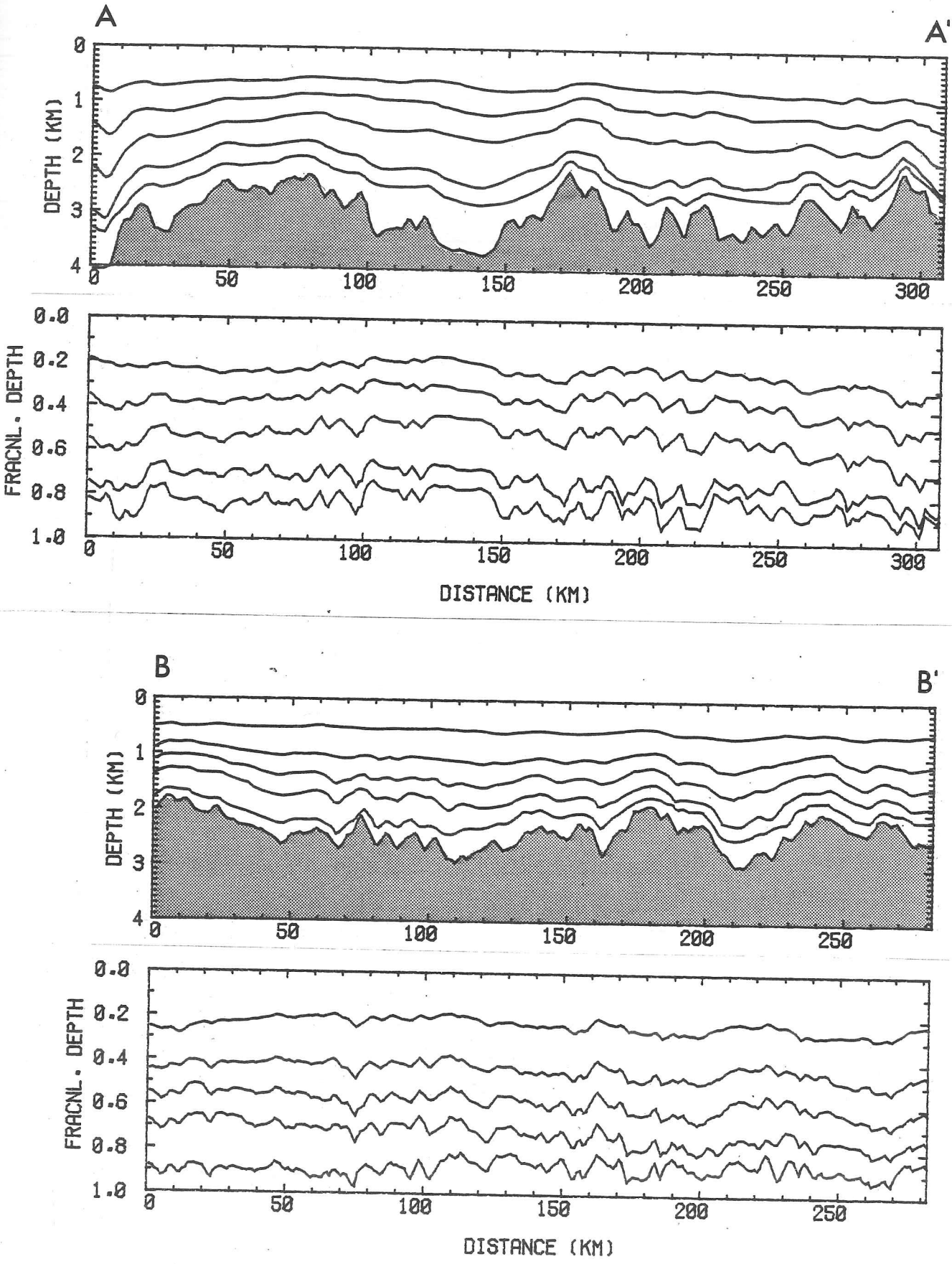

Fig. 6.2 Radio echo profiles with layering: upper diagrams show ice thickness profile, lower diagrams show fractional depths of internal layers to bedrock. Shallowest and deepest detectable layers included. Note horizontal scale for AA' and BB' is four times that for other profiles.

Fig.6.2 contd.

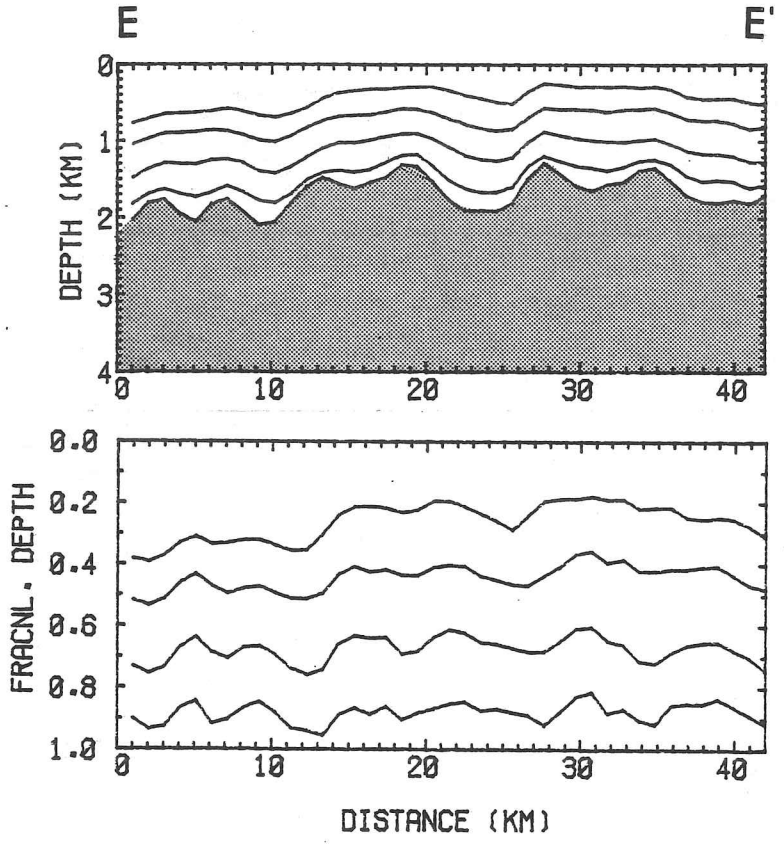
E
E'
DEPTH (KM)
0
1
2
3
4
0
10
20
30
40
FRACNL. DEPTH
0.0
0.2
0.4
0.6
0.8
1.0
DISTANCE (KM)

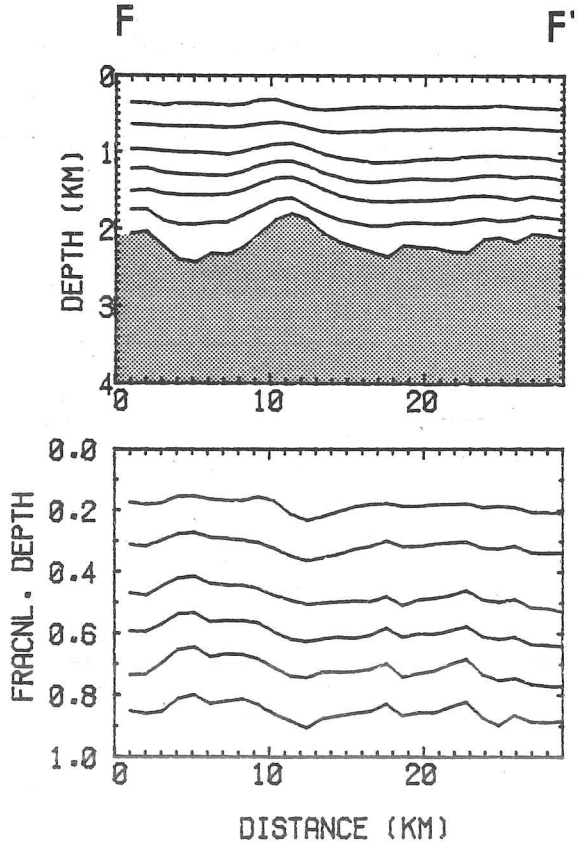
F
F'
DEPTH (KM)
0
1
2
3
4
0
10
20
FRACNL. DEPTH
0.0
0.2
0.4
0.6
0.8
1.0
DISTANCE (KM)

Fig. 6.2 contd.

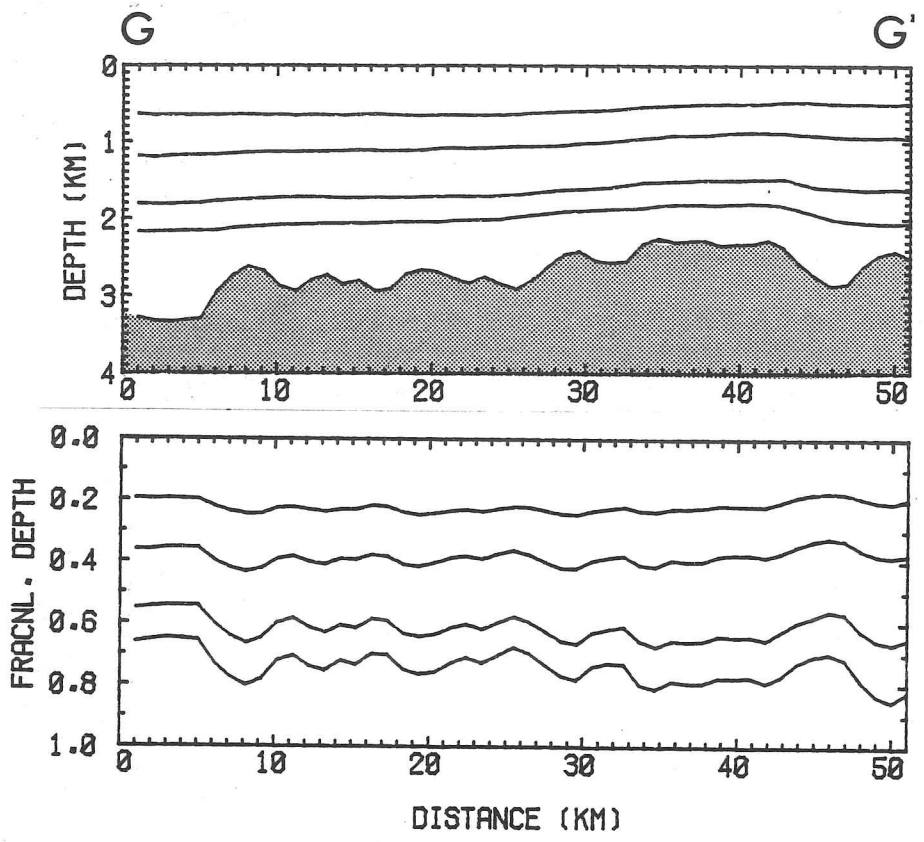
G
G'
DEPTH (KM)
0
1
2
3
4
0
10
20
30
40
50
FRACNL. DEPTH
0.0
0.2
0.4
0.6
0.8
1.0
DISTANCE (KM)

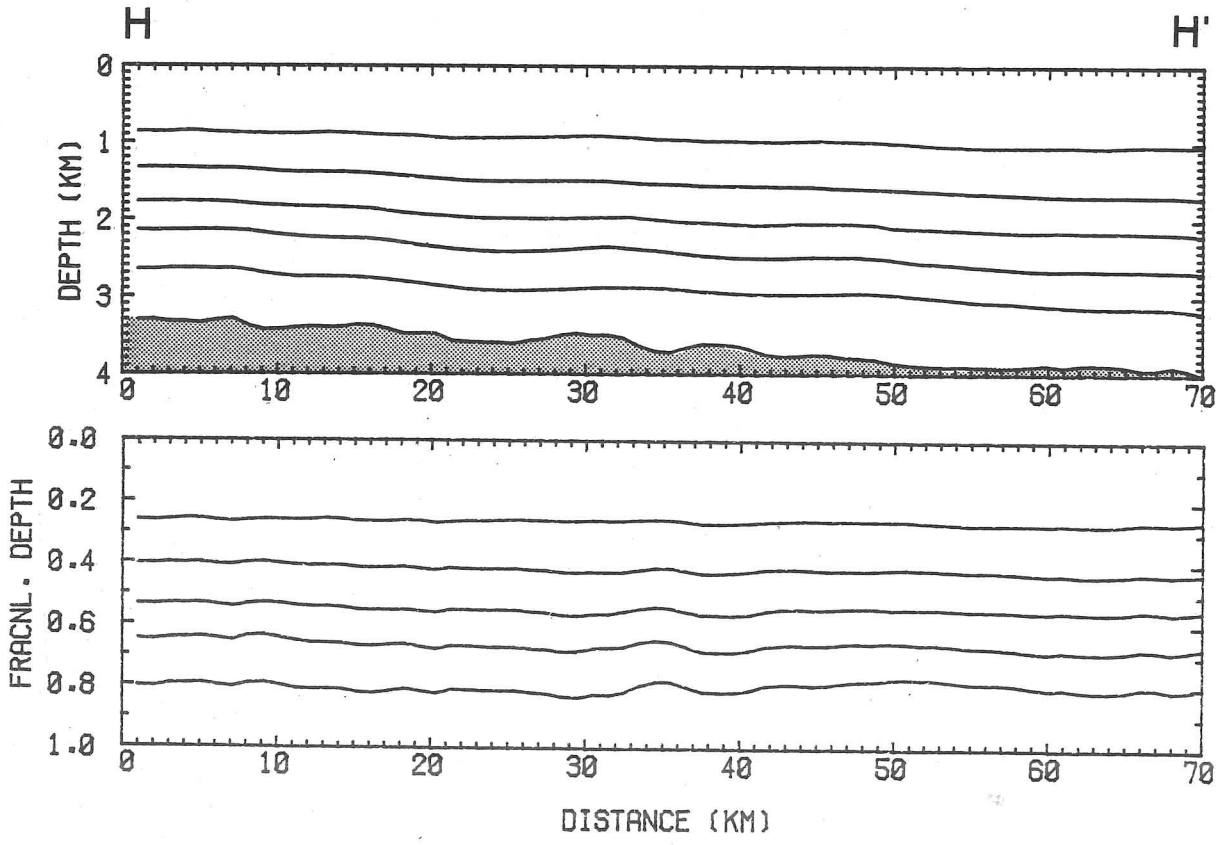
H
H'
DEPTH (KM)
0
1
2
3
4
0
10
20
30
40
50
60
70
FRACNL. DEPTH
0.0
0.2
0.4
0.6
0.8
1.0
DISTANCE (KM)

Fig. 6.2 contd.

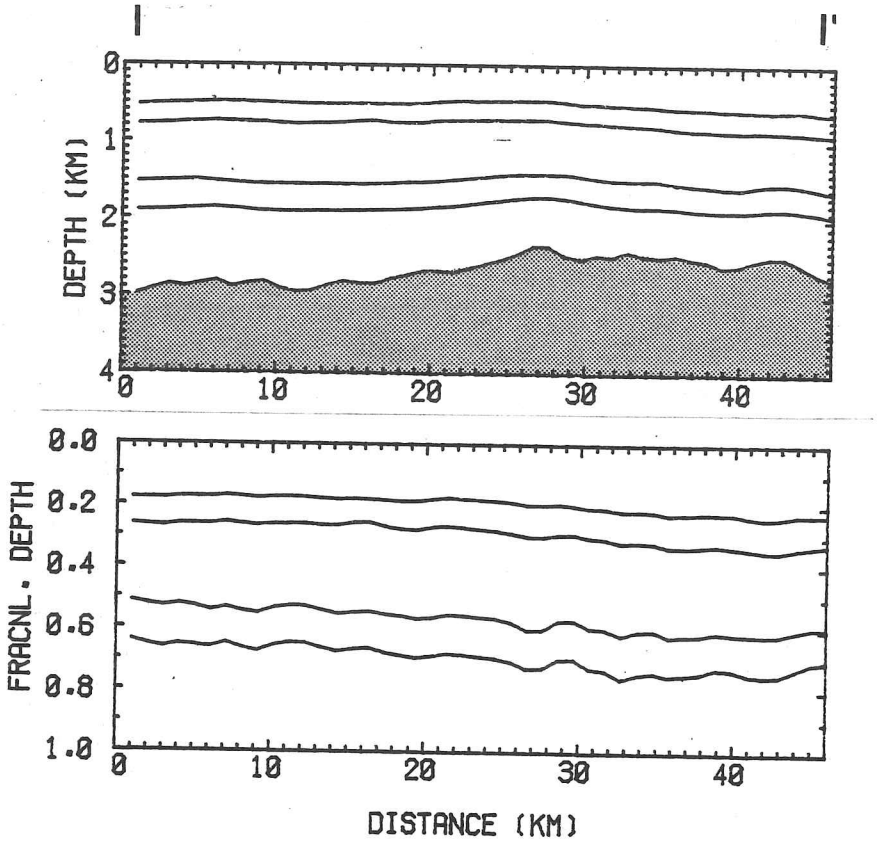
I
I'
DEPTH (KM)
0
1
2
3
4
0
10
20
30
40
FRACNL. DEPTH
0.0
0.2
0.4
0.6
0.8
1.0
DISTANCE (KM)

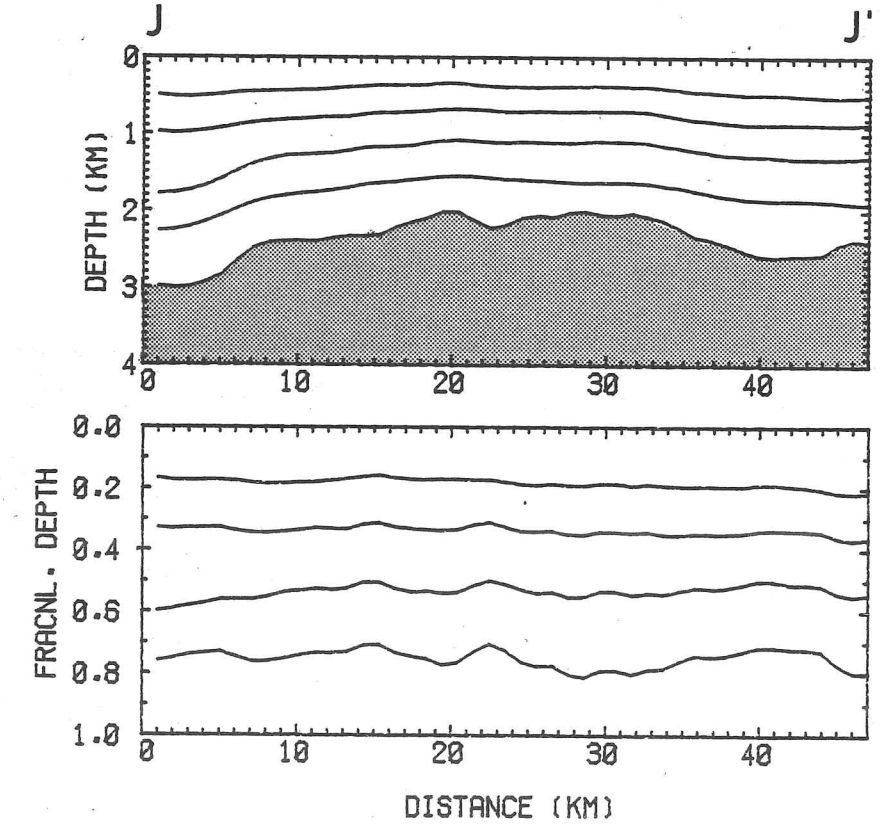
J
J'
DEPTH (KM)
0
1
2
3
4
0
10
20
30
40
FRACNL. DEPTH
0.0
0.2
0.4
0.6
0.8
1.0
DISTANCE (KM)

TABLE 6.1 FRACTIONAL SEPARATION MEASUREMENTS FOR INTERNAL LAYERS ALONG PROFILES

Profile	Location	$\bar{z}$ m	σ_z m	Layer nr.	$\bar{\xi}_{bed}$	σ_{bed}	$\bar{\xi}_{BLFZ}$	σ_{BLFZ}	mean ξ sepn.	σ_{sepn} (%)
									.238	16.3
AA'	F123/832-720 (flowline)	2981	398	1	.238	.039	.283	.035	.133	16.1
				2	.370	.052	.441	.046	.165	10.8
				3	.536	.062	.639	.051	.197	29.7
				4	.735	.052	.879	.032	.101	26.9
				5	.836	.047	1.000	0.000	.167	40.0
				BED	1.000	0.000	-	-		
									.236	12.9
BB'	F121/970-750 (contour)	2372	268	1	.236	.027	.268	.029	.201	10.9
				2	.438	.033	.498	.034	.152	21.6
				3	.589	.041	.669	.044	.133	49.9
				4	.727	.044	.826	.051	.159	47.9
				5	.881	.032	1.000	0.000	.119	27.0
				BED	1.000	0.000	-	-		
									.263	23.9
EE'	F9/1410-1432 (centre of outflow)	1687	218	1	.263	.063	.298	.066	.179	16.3
				2	.442	.043	.502	.038	.234	10.8
				3	.677	.041	.768	.026	.204	10.2
				4	.880	.093	1.000	0.000	.120	27.4
				BED	1.000	0.000	-	-		
									.186	10.9
FF'	F9/891-907 (flowline)	2164	154	1	.186	.020	.218	.018	.130	6.2
				2	.316	.023	.370	.017	.165	9.4
				3	.481	.031	.562	.022	.115	5.2
				4	.596	.031	.698	.017	.122	8.4
				5	.718	.037	.840	.021	.136	11.1
				6	.854	.028	1.000	0.000	.146	19.3
				BED	1.000	0.000	-	-		

Table 6.1 contd.

Profile	Location	$\bar{z}$ m	σ_z m	Layer nr.	$\bar{\xi}_{bed}$	σ_{bed}	$\bar{\xi}_{BLFZ}$	σ_{BLFZ}	mean ξ sepn.	σ_{sepn} (%)
									.220	8.9
GG'	F9/803-830 (flowline)	2691	292	1	.220	.020	.299	.025		
									.156	33.0
				2	.384	.025	.529	.074		
									.242	26.4
				3	.618	.037	.834	.018		
									.108	21.9
				4	.740	.048	1.000	0.000		
									.275	41.9
				BED	1.000	0.000	-	-		
									.265	1.8
HH'	F136/670-640 (flowline)	3616	211	1	.265	.005	.329	.008		
									.154	5.5
				2	.418	.011	.521	.014		
									.133	4.7
				3	.551	.010	.686	.011		
									.114	5.3
				4	.666	.014	.829	.015		
									.138	9.7
				5	.803	.016	1.000	0.000		
									.197	7.8
				BED	1.000	0.000	-	-		
									.198	11.5
II'	F135/940-920 (flowline)	2667	181	1	.198	.023	.284	.020		
									.093	9.5
				2	.291	.031	.417	.025		
									.282	4.4
				3	.573	.034	.823	.011		
									.123	5.1
				4	.696	.036	1.000	0.000		
									.304	11.8
				BED	1.000	0.000	-	-		
									.179	16.6
JJ'	F135/804-784 (flowline)	2355	280	1	.183	.013	.262	.112		
									.157	20.2
				2	.336	.012	.448	.014		
									.199	11.6
				3	.535	.022	.715	.028		
									.197	28.5
				4	.749	.028	1.000	0.000		
									.268	42.5
				BED	1.000	0.000	-	-		

N.B.: $\bar{z}$ mean ice thickness

σ_z standard deviation in $\bar{z}$

$\bar{\xi}_{bed,\ BLFZ}$ mean fractional depth to bed, basal layer-free zone, of layer

$\sigma_{bed,\ BLFZ}$ standard deviation in $\bar{\xi}$

and separations between successive horizons along the profiles.

Where bedrock relief is small (standard deviation of ice thickness <250 m), e.g. profile HH', proportional layer separations remain almost constant along the profile, often with standard deviations of <5% in the upper regions, and the basal layer-free zone varies little in thickness. This suggests that the assumption of a constant vertical strain rate through the ice column is adequate. Sites where this applies include Vostok and Dome C.

Where the range of bedrock relief is greater (standard deviation >250 m), e.g. section AA', the layer separations vary more, and in particular the proportional thickness of the basal layer-free zone becomes very variable, with a standard deviation of up to 50%. In such cases significant errors may be introduced by the assumption of a constant vertical strain rate, and even the assumption of a constant vertical strain rate to the lowest detectable layer is little better. As the ice velocity increases between sites with similar basal roughness (e.g. from FF' to GG') the lowest layer follows the bed less closely and the basal layer-free zone increases in proportional thickness, however the variability of the basal layer-free zone thickness increases only slightly. Robin and others (1977) studied the separation of three layers along section AA' at ten points, and found standard deviations in layer separations similar to those obtained here.

In summary, in the upper parts of the ice (above the basal layer-free zone), the variability of the vertical strain rate, as deduced from layer separations, seems to be strongly dependent upon bedrock relief, with standard deviations of ~5-10% for an ice thickness s.d. of <250 m, and ~20-30% for an ice thickness s.d. of >250 m. For sites with rough bedrock the variability of the basal layer-free zone becomes very large, ~50%.

6.3 Ice flow near to bedrock

The nature of ice flow near to bedrock, where the presence of subglacial peaks and large basal slopes can have important effects on ice movement, is poorly understood. Evidence comes from several sources, but the deformation of radio-echo layering is probably the most unequivocal. Relevant observations from ice fabric studies, seismic reflection work and isotope profiles are also considered here however.

Near the base of the ice a zone of a few hundred metres in thickness has been widely observed in East Antarctica (and probably also exists in West Antarctica) in which layering is not seen. Provided that the absence of layering is genuine and not due to inadequate system performance, this basal echo-free zone must be due to an absence of suitable reflecting surfaces, and complex ice deformation near to bedrock resulting in significant bending of internal surfaces is suggested as the most likely cause. Since the upper surface of the echo-free zone is not found to be of constant age at all locations, it is unlikely that the lack of layering is caused by chemical neutralisation of acidic ice layers, as appears to be the case for the widespread gap in layering observed in Greenland at ~13-23 kaBP (Gudmandsen 1975; Millar, in press). The thickness of the echo-free zone also depends on bedrock relief, suggesting again that it is an ice-flow feature. Sites where layering is observed to deform in the vicinity of subglacial peaks are also of great help in understanding the way in which bedrock obstacles disturb ice flow.

These two types of layering feature will first be described together with relevant data from other sources, and conclusions about the deformation of ice in the vicinity of the bedrock are then presented.

(a) basal radio echo-free zone

The absence of layering close to bedrock despite adequate system performance has been noted before by Robin and others (1977) and Drewry (1979). At sites where the presence of a true echo-free zone (rather than excessive absorption limiting detection) is in doubt, reflection coefficient vs depth profiles are useful in determining whether the absence of layers is due a lack of system performance or to a lack of reflecting surfaces.

Near Byrd, fig. 3.3 shows that layering extends as far as the detection limit of the echo sounder at ~1800 m. At the South Pole, by contrast, layering ceases 250 m above bedrock and short of the theoretical detection limit (fig. 6.3), indicating a true echo-free zone of ~250 m thickness. A particularly unambiguous example of the existence of the echo-free zone is seen on section AA' (figs. 6.4 and 6.5). The PRC vs depth profile recorded over a deep valley at F123/779 (fig. 6.6) shows internal echoes ceasing at a depth of ~2800 m in 3700 m-thick ice, ~500 m above the system detection limit.

Note the different form of the cut-off in the power return at these sites: at Byrd there is a sloping cut-off of reflection coefficient with depth (as for the estimated absorption limit), whereas at the South Pole and the site above Vostok (F123/779) layers cease abruptly and independently of the PRC. A simple way of deciding whether or not absorption limiting is occurring is to compare the depths of the deepest layers seen on the A-scope and Z-scope records. Because the sensitivity of the Z-scope record is ~15 dB greater than that of the A-scope (due to the integrating effect of the film, Skou & Sondergaard (1976)), echoes will be seen to a greater depth on the Z-scope than on the A-scope where absorption limiting occurs. This can provide a quick method of checking whether the detection limit has been reached without the necessity for estimating a temperature profile or measuring returned power levels. The

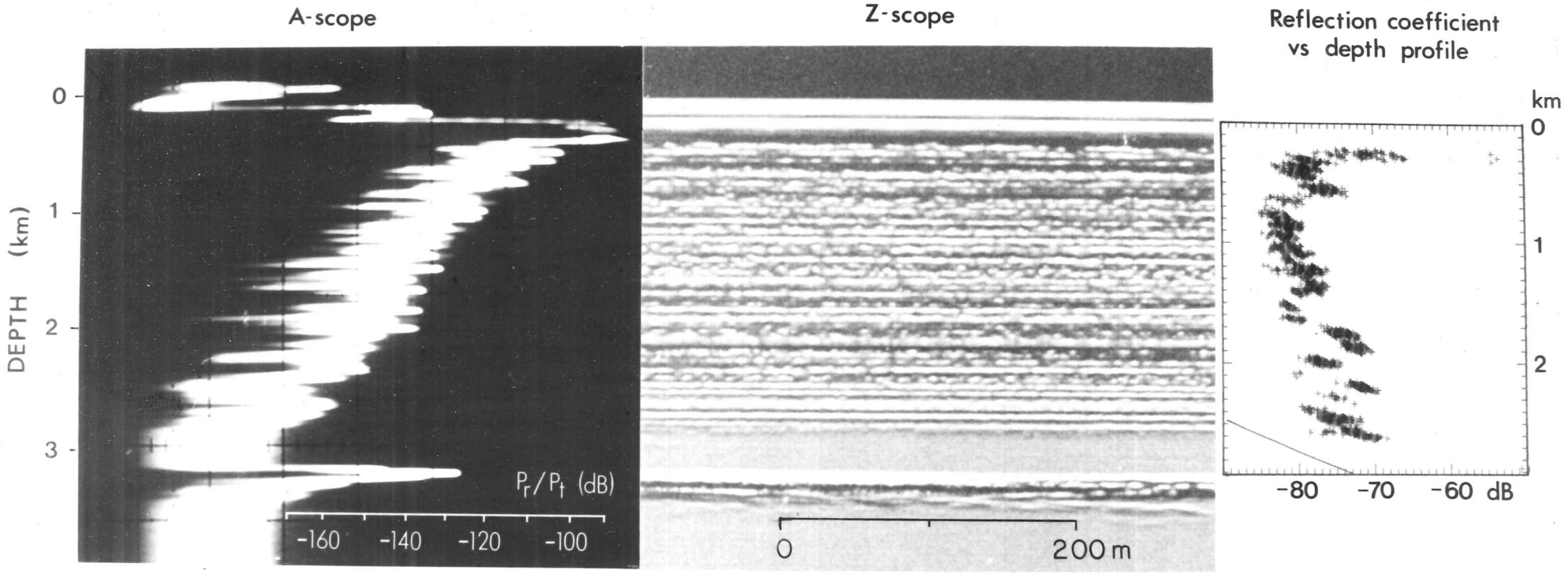

Fig. 6.3 Layer-free zone near to bedrock at South Pole, as seen on A- and Z-scope records and the reflection coefficient vs depth profile.

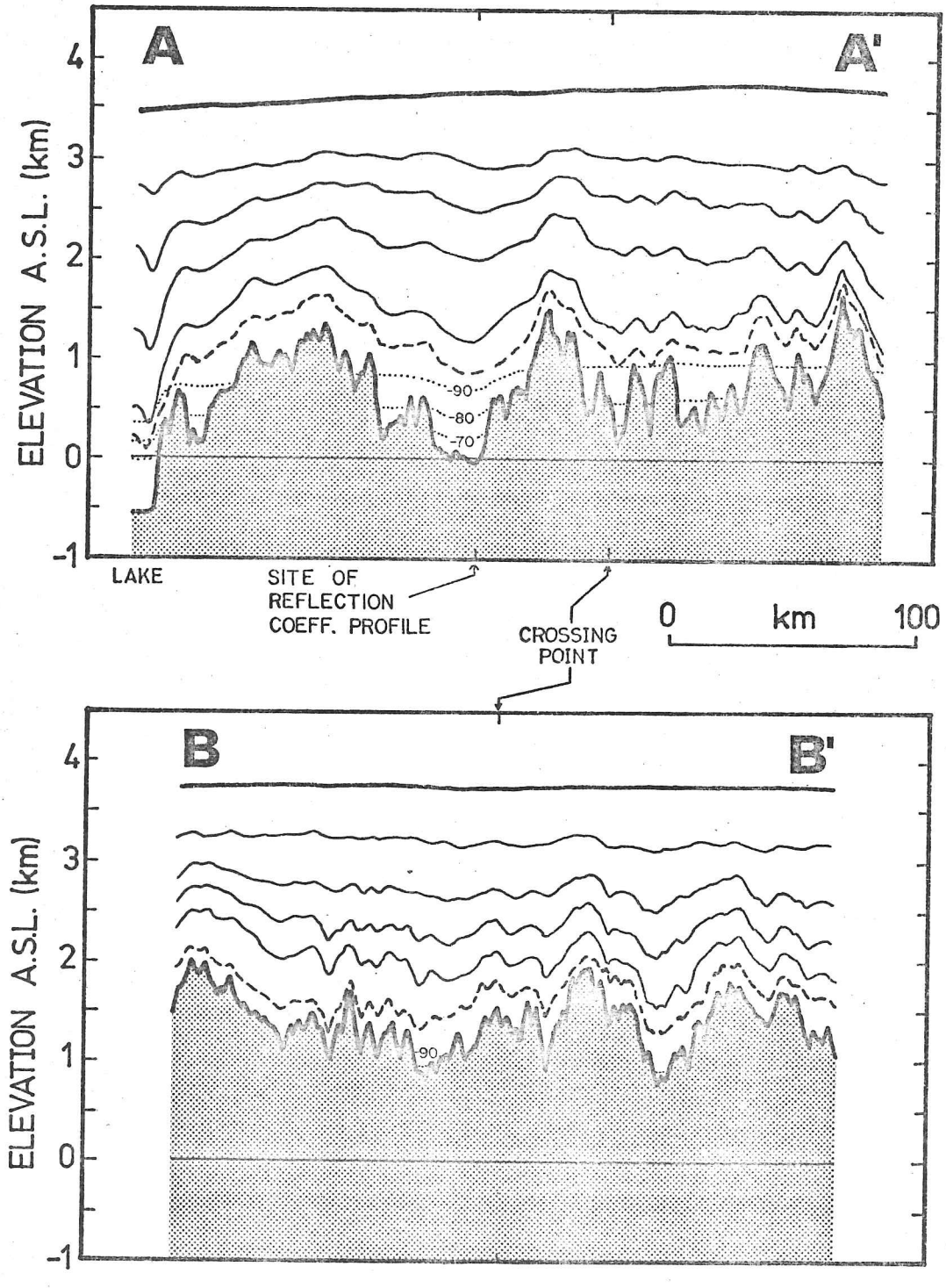

Fig. 6.4 Profiles showing positions of selected internal layers and surface and bedrock along lines down a flowline from the ice divide above Vostok (AA') and along the crest of the ice divide (BB'). Dashed line represents lowest visible layer, dotted lines represent calculated maximum depths to which surfaces with reflection coefficients of -70, -80 and -90 dB may be seen with the 60 MHz system.

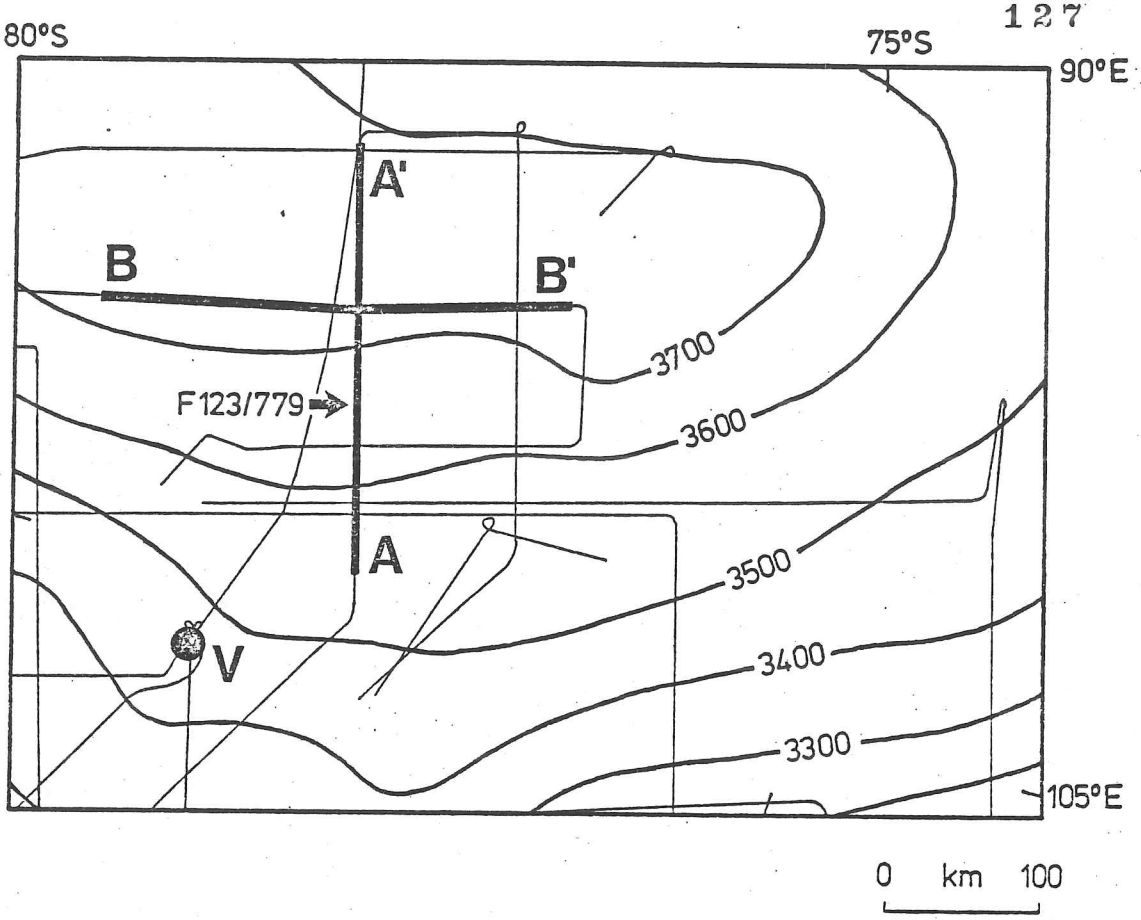

Fig. 6.5 Location of sections AA' and BB', with surface topography (contours in masl). Thin lines represent RES flightlines, bold lines are sections.

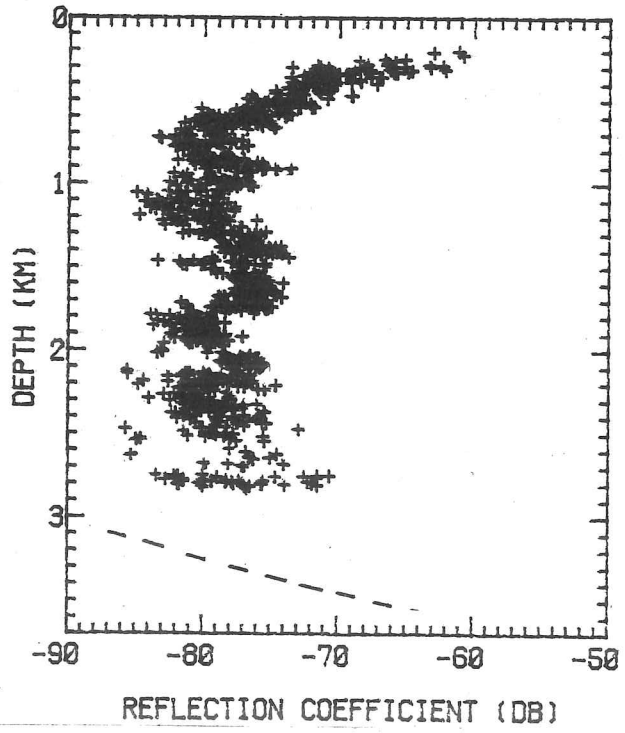

Fig. 6.6 Reflection coefficient vs depth profile at site F123/779 on section AA'. Dashed line is A-scope detection limit.

echo-free zone also tends to retain an approximately constant thickness along the flight-line, whereas when absorption limiting is present the deepest layers detected normally lie at approximately constant depth from the surface rather than height above the bedrock.

At many locations near the centre of the ice sheet, where an echo-free zone is present, a transition zone of 100-200 m thickness may also be observed between it and the layering above it. This zone contains apparently 'broken-up' layer echoes with very short horizontal continuity, and focussing features (Harrison 1971). These features indicate the presence of bent or tilted surfaces above the basal echo-free zone (fig. 6.7). Far from ice divides these features tend to disappear, possibly because after repeated deformation during a long period of flow the layering is too distorted to produce recognisable cusps. The existence of this zone would suggest that the internal surfaces become increasingly bent or tilted in three dimensions as they approach the bedrock, so that although the surfaces still exist, they return power at different angles and eventually cease to give a recognisable layer echo. Because of the narrow antenna beamwidth along the track and the smoothness of the reflecting surface, only a small amount of sideways tilt may be necessary in order to 'lose' the echo.

Having seen that the echo-free zone is a genuine feature and not an equipment artifact, and therefore indicates the absence of suitable reflecting surfaces, the effect of bedrock topography and ice movement on the zone is now described.

The simplest ice flow situation is near to a centre of outflow where the horizontal component of ice movement is small. Fig. 6.8 shows layering extending to bedrock over Dome B, East Antarctica, and illustrates that in such cases the basal ice must be deforming very slowly and that layering is not broken up by the rough bedrock. This is observed at all major centres of outflow for which RES coverage is available, and generally

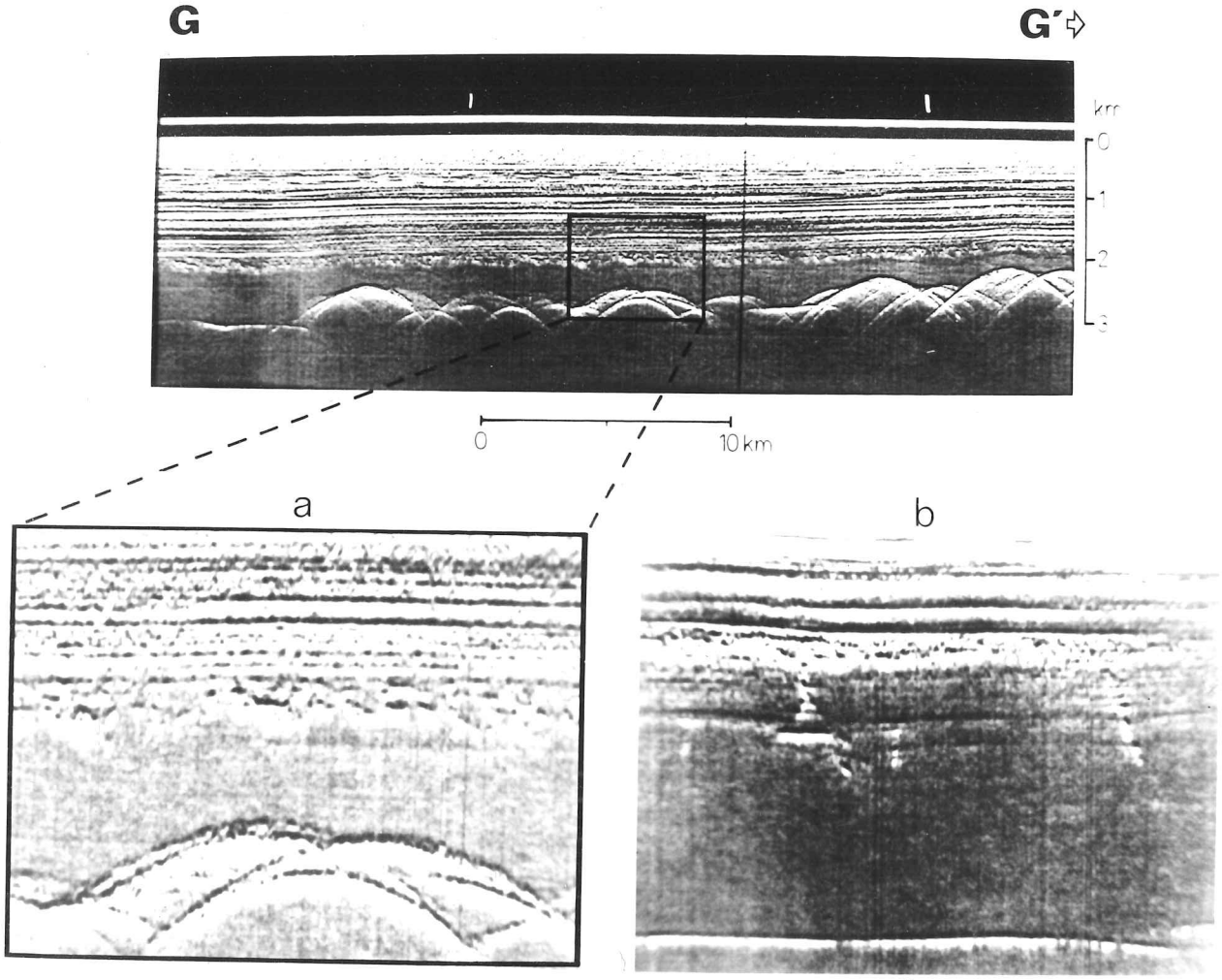

Fig. 6.7 Part of section GG' (on flowline above Vostok), showing well-developed basal layer-free zone, and transition zone containing broken-up layering (a), and cusps due to focussing (b, on same flight nearer to Vostok).

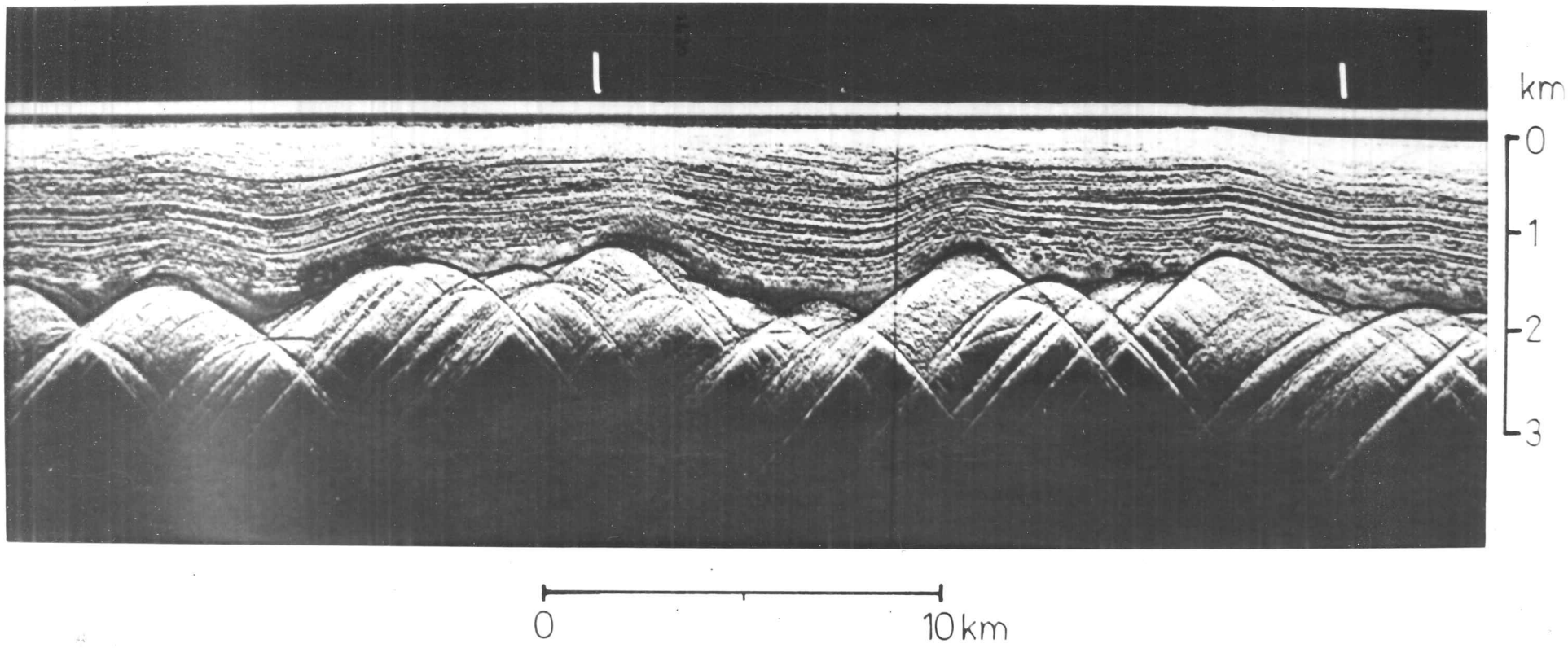

Fig. 6.8 Layering near to a centre of outflow, Dome B (section EE').

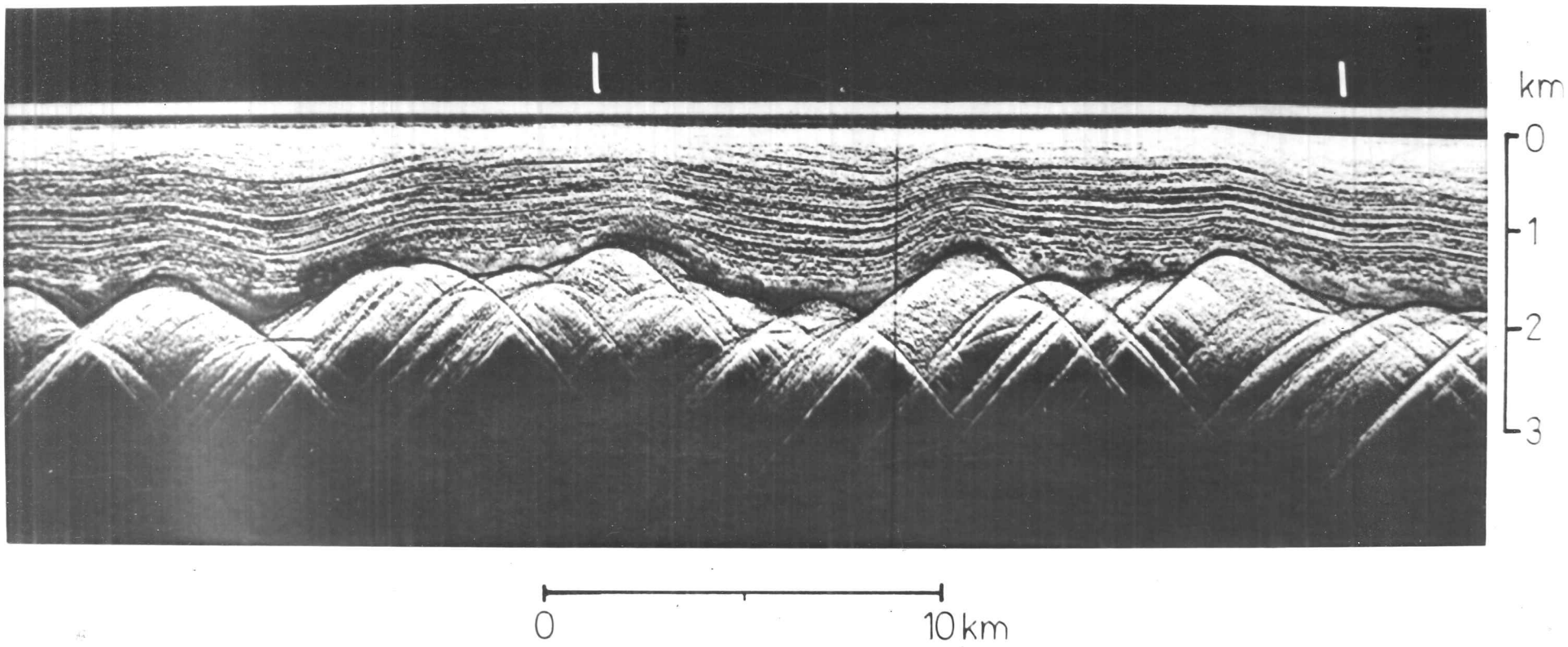

Fig. 6.8 Layering near to a centre of outflow, Dome B (section EE').

extends for ~50 km away from the highest point. Dome C, on the other hand, has an echo-free zone ~300 m thick beneath it, suggesting that ice is (or was in the past) moving horizontally near to bedrock (see fig. 6.9). The ice sheet surface topography in this area (Steed 1980) also suggests that Dome C is an ice divide rather than a true dome.

Moving away from a centre of outflow or ice divide the ice velocity increases and we might expect greater deformation to occur in the basal layers of the ice sheet. The effect of this on the layering may be illustrated by the two sections above Vostok (fig. 6.4), one extending downstream from the ice crest to a large subglacial lake near Vostok (section AA'), and the other (BB') running parallel to the ice crest. Surface, bedrock and selected internal layers (including the shallowest and deepest detectable horizons) are shown. Deepest internal reflections are indicated by dashed lines, and the maximum depth to which surfaces of given reflection coefficient may in theory be detected are shown by dotted lines. From fig. 6.6 we see that most layers below ~600 m have reflection coefficients of -70 to -80 dB, so it is clear that the deepest layers lie well above the detection limit. The basal echo-free zone therefore has a thickness here varying from ~50 m (about one radio pulse length) over subglacial peaks to about 900 m over some valleys.

The thickness of the zone is strongly dependent on bedrock relief and ice velocity, the lowest layers following the bedrock more closely when ice movement is small in the direction perpendicular to the main subglacial valleys and ridges (cf. AA' and BB'). Moving down AA' towards Vostok the ice velocity increases to about 3 ma^{-1} (Liebert & Leonhardt 1974) and the echo-free zone generally increases in thickness.

To demonstrate the wide extent of the basal layer-free zone in the Antarctic, a 1500 km section XX' from south of Dome C to the coast at Dumont d'Urville is presented (fig. 6.9). At intervals along this section PRC vs depth profiles have been measured (fig. 6.10). It is seen that the

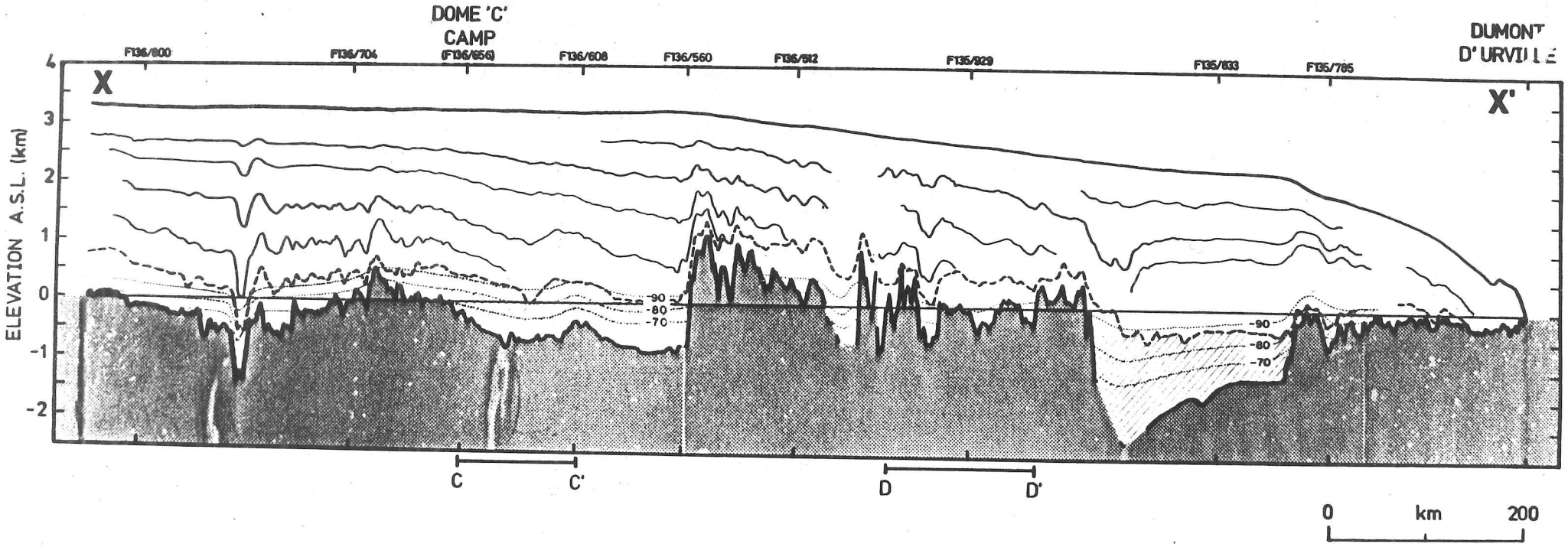

Fig. 6.9 1500 km section from above Dome C to the coast at Dumont d'Urville, showing surface, selected internal horizons, and bedrock. Sites where power measurements made are indicated. Dashed line represents boundary of basal layer-free zone. Dotted lines indicate maximum depth to which reflectors of given PRC may be detected. Shaded areas indicate where lack of layers is due to heavy dielectric absorption.

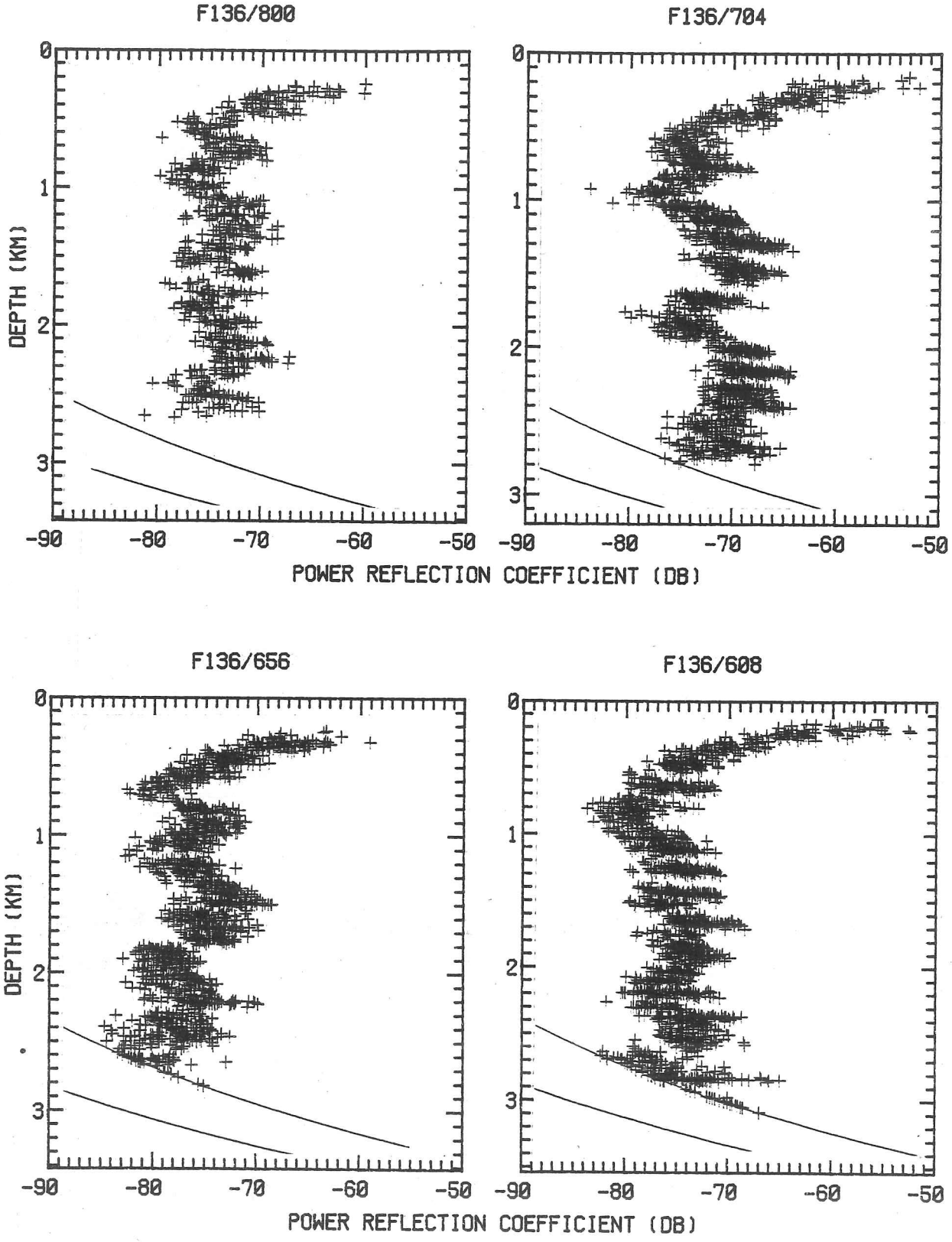

Fig. 6.10 Reflection coefficient vs depth profiles at nine sites along section XX'. Thin lines represent estimated detection limits for A- (upper curves) and Z-scope formats (lower curves).

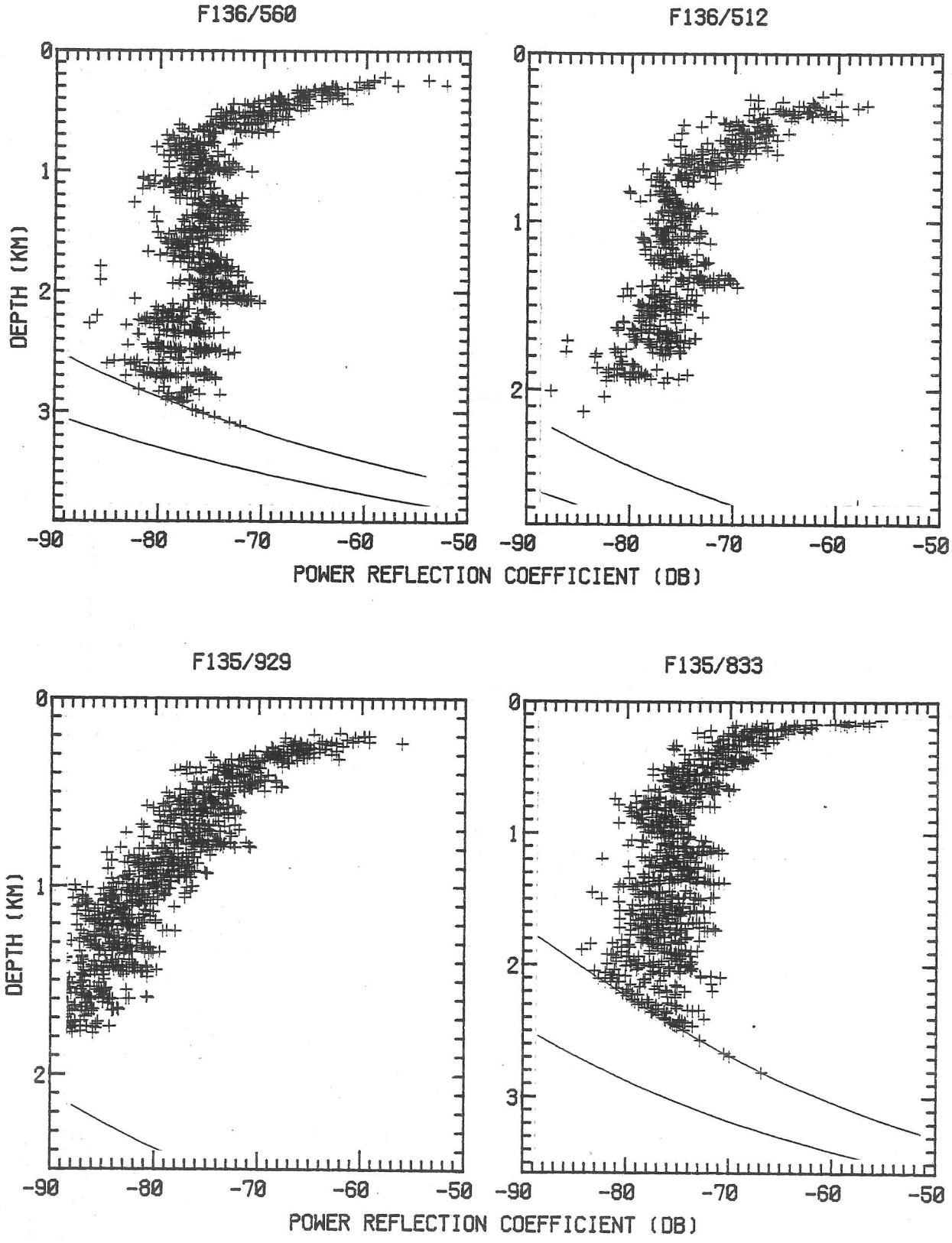

Fig. 6.10 contd.

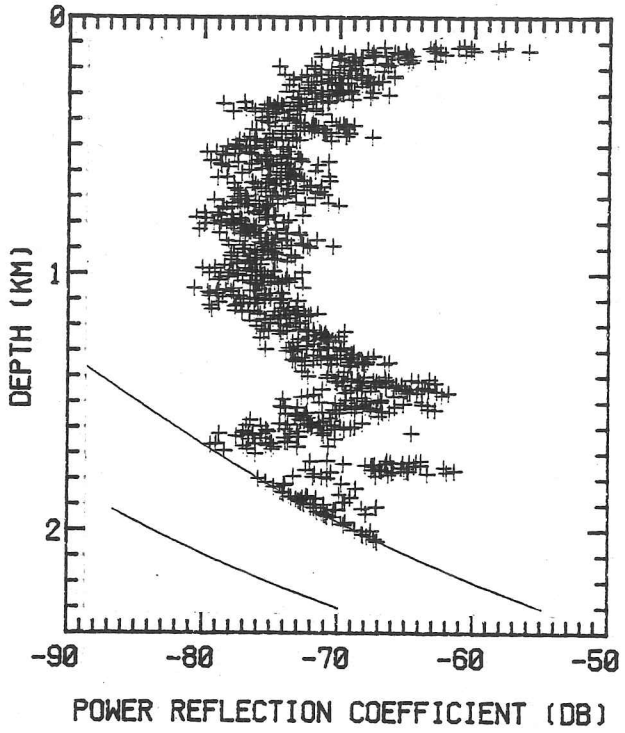

Fig. 6.10 contd.

echo-free zone is present at all locations except where excessive absorption prevents its observation, and that (apart from in the immediate vicinity of peaks) its thickness is generally about 500 m, which is comparable with the range of bedrock relief. However even at locations with a smooth bedrock, such as the South Pole, a minimum zone thickness of ~200-300 m is maintained. Close to the coast (<50 km) the zone disappears.

In conclusion, the lack of layering in the lowest levels appears to be related to bedrock relief and ice velocity, and this, together with features such as focussing effects seen just above the deepest layers, suggests that the lack of reflections is due to increased tilting of the internal surfaces in three dimensions, resulting in little power being returned normally.

An alternative explanation is that acidic impurities within the ice may become concentrated at grain boundaries, where they may have a diminished effect on the dielectric properties of the ice (Paren & Walker 1971). This concentration of impurities perhaps arises as a result of the combination of higher temperatures and greater deformation near to bedrock.

(b) radio-echo layer deformation near subglacial peaks

The deformation of ice around bedrock peaks is a process which takes place throughout the ice to some extent, even layering near to the surface being bent slightly over large peaks (e.g. in fig. 6.4). Near isolated peaks layering is sometimes seen to deform uniformly over the peak (e.g. fig. 6.11(a)) in a manner suggesting that there is little flow sideways around the peak. More often, the layering is deformed relatively little, suggesting that a significant amount of the flow must be laterally around the peak (e.g. fig. 6.11(b)). The end result of this type of flow around bedrock obstacles can be seen in fig. 6.12, which lies perpendicular to the direction of flow of the ice and has a generally smooth bedrock; the

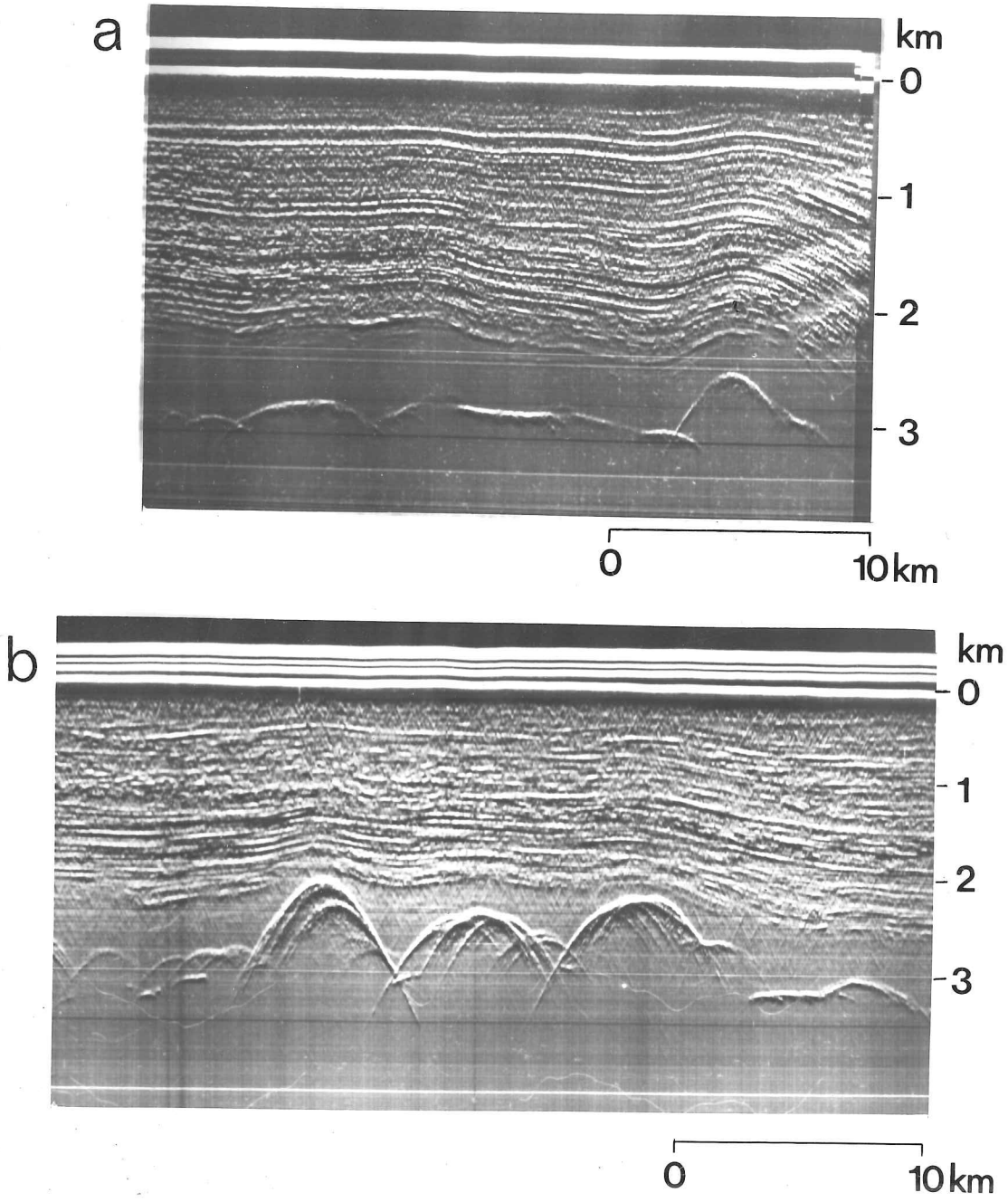

Fig. 6.11 Examples of flow over subglacial peaks:

(a) uniform deformation, suggesting little lateral flow
(b) non-uniform deformation, with large change in fractional depth to bedrock of lowest layer, suggesting that some flow occurs around the obstacle at lower levels

Both sections lie approximately along flowlines.

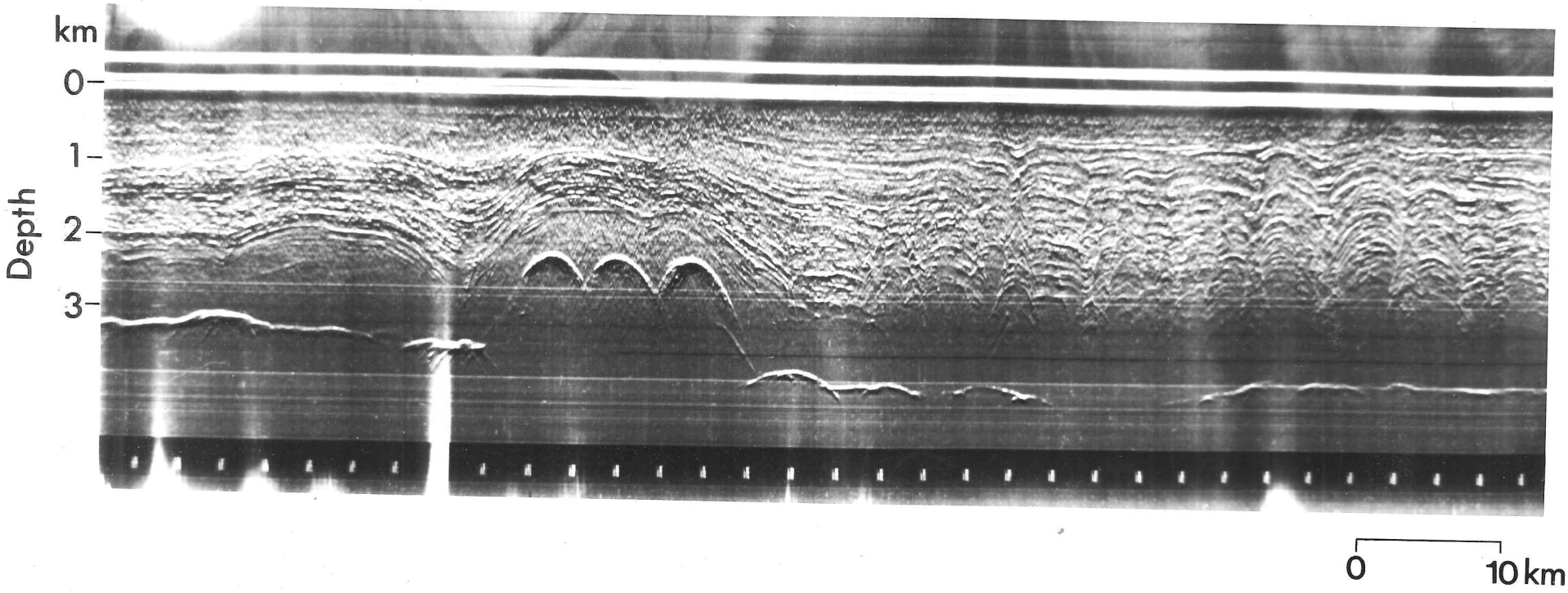

Fig. 6.12 Layering across a flowline downstream of an area of rough bedrock topography, showing resulting 'buckling' of layering (section KK').

large amount of 'buckling' in the layering here, typically of a few hundred metres in height and a kilometre in width, is believed to result from stronger deformation of the ice upstream where ice has flowed over peaks. Note that this would not occur to such an extent if the ice moved uniformly over the peak with no lateral flow, because the uniformity of the layering should be preserved downstream of the peak and no lasting buckling would be seen.

Normally the Antarctic RES Program flightlines were spaced ~50 km apart to fit into a grid pattern flown for the construction of surface and bedrock topography maps, and this means that no information is generally available on the three-dimensional layering structure of the ice. However in the vicinity of Byrd Station there is a much more detailed RES coverage, and this has enabled the three-dimensional structure of internal surfaces to be studied within a distance of ~20 km from the station. Byrd Station itself is located on the upper flanks of a subglacial high which rises to -450 masl; ~5 km to the north is a bedrock trough extending to -1200 masl. Figs. 6.13(a) and (b) show the topography of the bed and of the deepest radio-echo layer which was traceable over the whole area (~1350 m depth at Byrd). In these diagrams the direction of ice surface movement at Byrd lies directly down the page with a velocity of 12.7 ma^{-1} (Whillans 1977). Comparison of the two maps indicates that at this level in the ice the deepest internal layer deforms closely over the bedrock highs, but that there is a delay of about 8 km before it begins to sink into the main bedrock trough. This delay suggests the possible existence of a zone of slowly moving ice at the head of the valley.

It is not possible to infer from these data the direction of ice flow at depth, but a resurvey of the inclination of the Byrd borehole seven years after it was drilled (Garfield & Ueda 1976) has enabled the deformation of the hole to be investigated to a depth of 1474 m. The derived velocity vs depth profile (fig. 6.14) shows that in the upper 1300 m the flow direction is slightly to the south side of the main

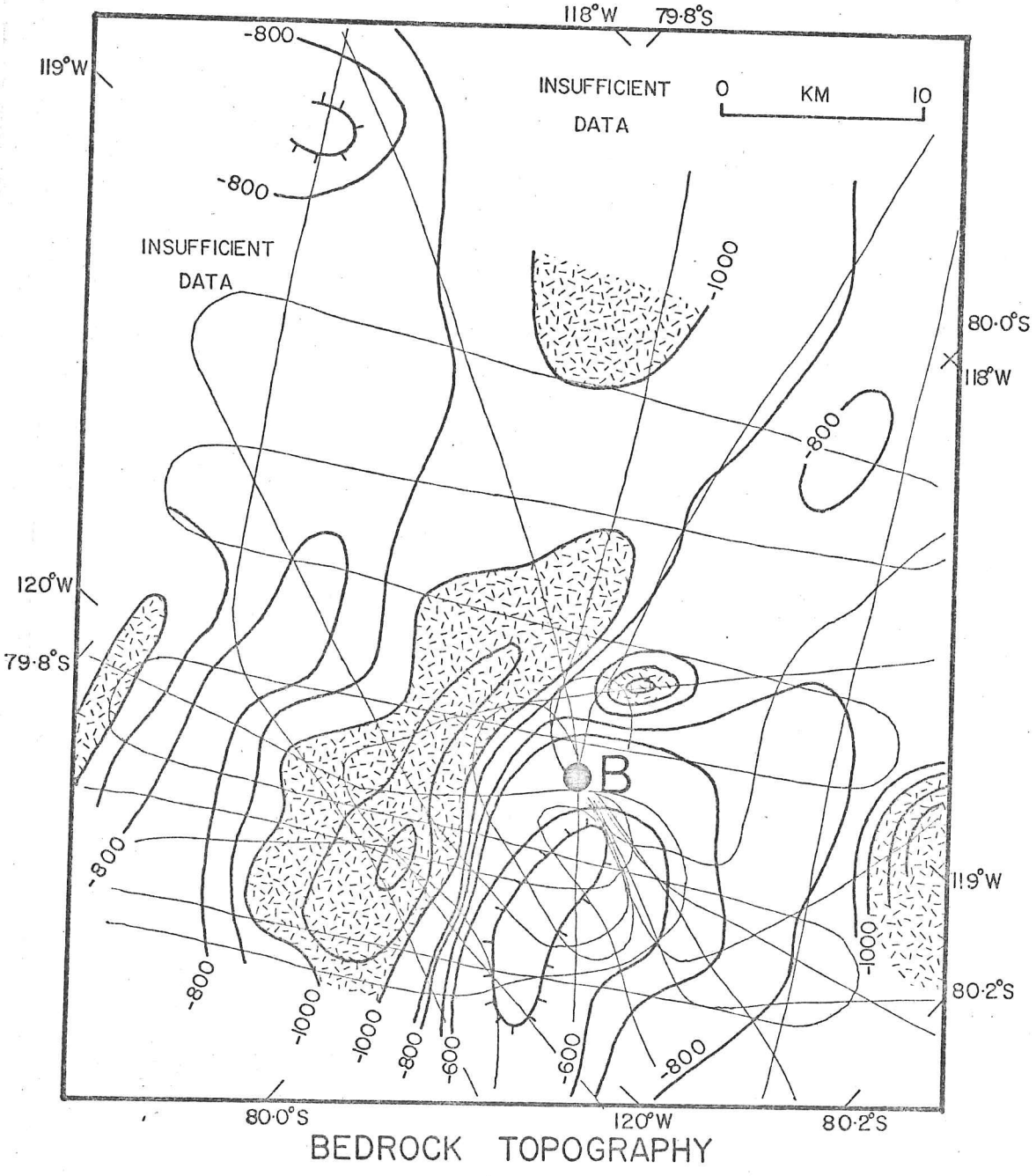

Fig. 6.13(a) Bedrock topography in vicinity of Byrd Station. Area below -1000 masl shaded. Principal flight-lines indicated by thin lines.

Surface velocity lies directly down the page.

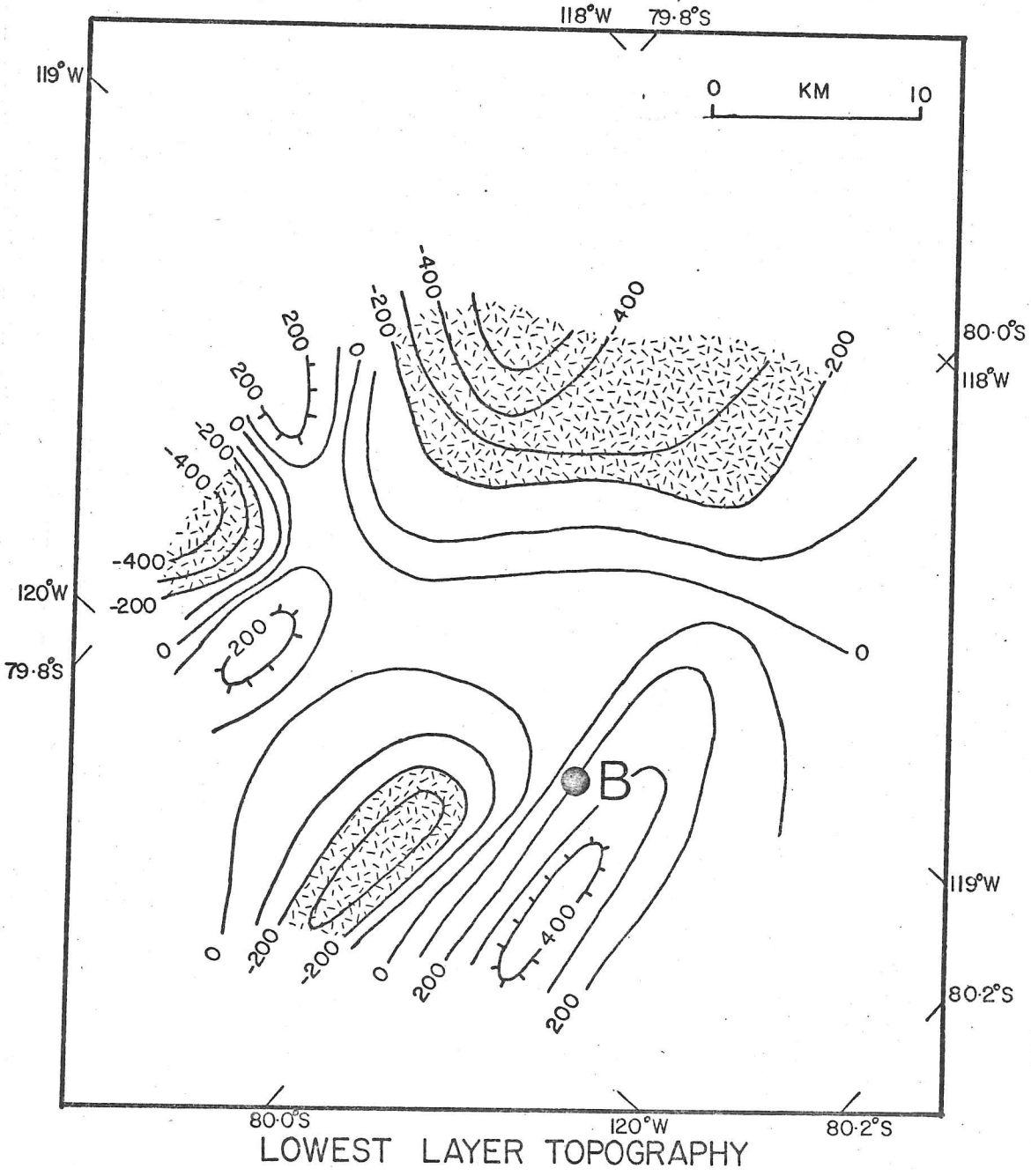

Fig. 6.13(b) Topography of lowest detected layer in vicinity of Byrd Station. Area below -200 masl shaded.

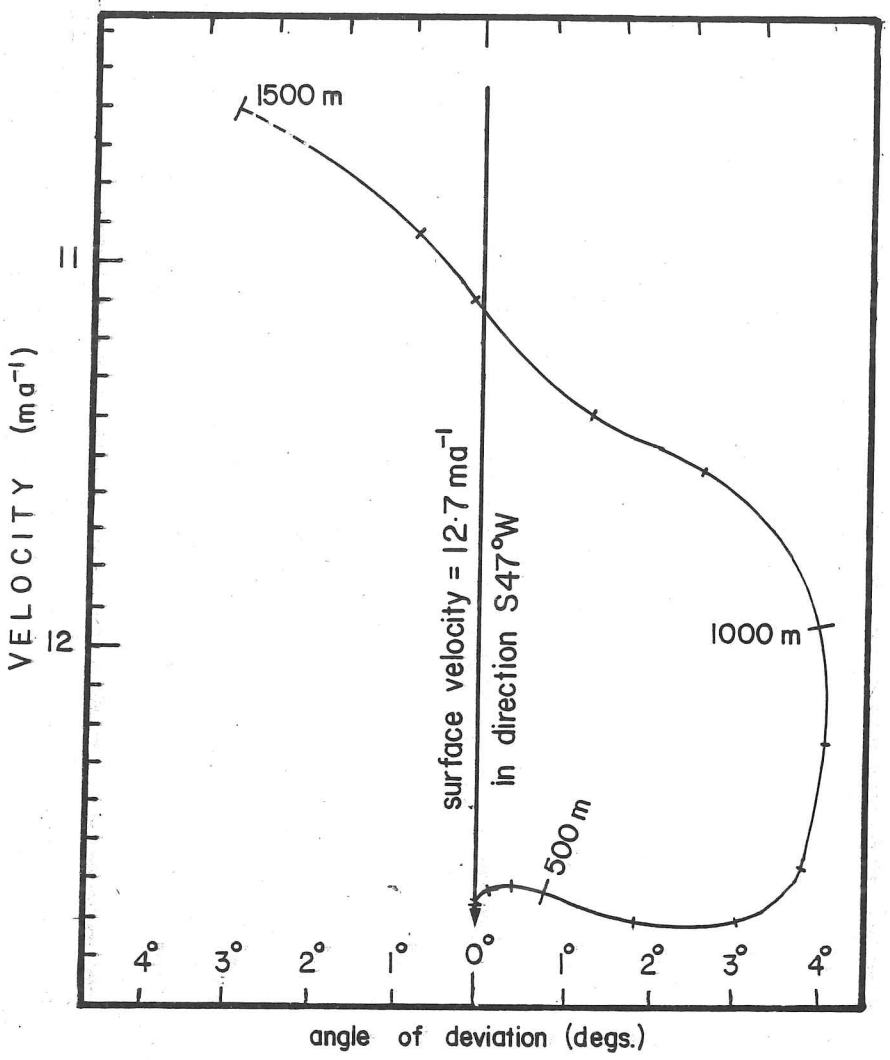

Fig. 6.14 Velocity vs depth profile at Byrd Station from borehole deformation measurements of Garfield & Ueda (1976).

bedrock high, but that at greater depths the flow direction moves increasingly northwards, towards the bedrock trough. If this deviation is sustained at lower depths then there must be a twisting motion where the deeper ice has a tendency to be diverted around the hill into the valley (which lies at an angle of about 20° to the direction of surface movement), as well as some flow occurring over the bedrock high. The small angle of deviation of the flow would suggest that the bulk motion of the ice is similar to that at the surface, and that the component of sideways motion is relatively small. These results are in agreement with the conclusions already drawn above at other locations, i.e. that at lower depths there is a component of flow around bedrock obstacles as well as over them, and that the effects of this are transmitted through the whole thickness of the ice.

Analysis of reflections from the bedrock may also tell us something about the flow at the base of the ice sheet. If pressure-melting occurs due to higher pressures on the upstream faces of bedrock obstacles, the water may be trapped at the bed and a high reflection coefficient (-3 to -10 dB) may be observed, whereas at a dry ice/rock interface a much lower reflectivity (<-30 dB) is to be expected. Measurement of basal reflectivity in areas where ice is flowing past a subglacial peak might therefore show whether the excess pressure upstream of the obstacle is sufficient to cause detectable pressure-melting.

Basal reflectivity measurements around Byrd (fig. 6.15) were made with this in mind. Although there are some interesting variations, it is not possible to interpret the measurements unambiguously. The variations may well be due to varying amounts of moraine in the basal ice. Even if pressure-melting is occurring over a wide area (borehole measurements show that it is at Byrd Station itself), the resulting water is not likely to be trapped at the base but may be drained away because of the bedrock slope.

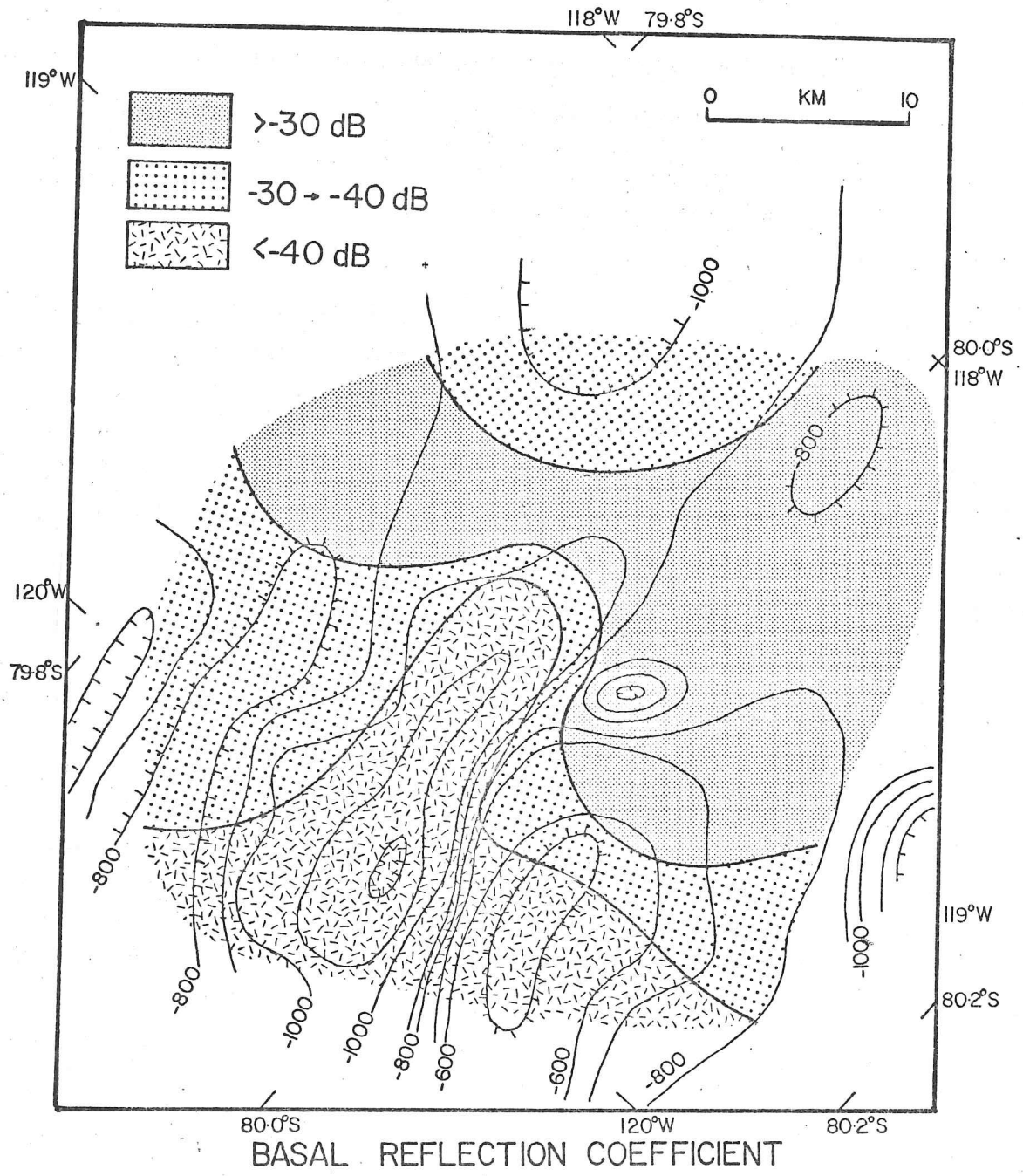

Fig. 6.15 Basal reflection coefficient in vicinity of Byrd Station. Bedrock topography also shown.

(c) near-basal seismic reflecting zone

A phenomenon which may be closely related to the basal echo-free zone observed on RES records is a low amplitude seismic reflecting layer reported by Bentley (1971) to be widespread in West Antarctica. His seismic reflection profiles often show weak reflections from a layer several hundred metres above the bed, and at times weaker reflections closer to bedrock within the layer. Unfortunately it has not been possible to make a direct comparison of the thickness of this layer with the RES echo-free zone because at the sites where the seismic layer is observed the high dielectric absorption prevents the detection of a RES echo-free zone if it exists, however the thicknesses of the two types of layer are similar.

Bentley proposed three alternative explanations for the phenomenon; moraine within the ice, changes in ice fabric, or a layer of isothermal ice at the pressure-melting point. The first was his preferred explanation, however the Byrd ice core subsequently showed that moraine was confined to the lowest few metres of the ice, whereas at Old Byrd Station (15 km distant) the seismic reflecting layer extended to 460 m above bedrock in 2480 m-thick ice. Temperature measurements in the Byrd borehole do not show a layer of isothermal ice near to bedrock either, and so ice fabric changes seem to be the best explanation. Robin & Millar (in press) show that a seismic wavelength of 40 m, together with a change in P-wave velocity of 100 ms^{-1} over 5-10 m (which, from the P-wave velocity measurements of Gow & Kohnen (1979) on the Byrd core, seems plausible), should produce a reflection of 11.5% of the incident wave amplitude. Measured amplitude ratios lay in the range 0.3-13%. If this is the correct explanation for the seismic reflections then it is possible that the seismic reflecting layer and RES echo-free zone have the same origin. The RES zone has been observed to be connected with changes in the pattern of deformation of the ice, so it may be that a change in ice fabric is also present.

(d) ice fabric studies

The development of a strongly oriented ice fabric with vertical c-axes occurs in the Byrd ice core between ~950-1810 m (Gow & Williamson 1976), below which the cores are composed entirely of coarse-grained ice in which the fabrics are all of the multiple-maximum type. Ultrasonic velocity measurements on the ice core from Byrd Station (Gow & Kohnen 1979) also indicate the existence of a strong vertical alignment of c-axes in the lower half of the ice sheet.

On the Law Dome, Russell-Head & Budd (1979) found the highest horizontal shear rates at the lowest level of a zone containing a high concentration of vertical c-axes, and concluded that 'the shear stress must decrease towards the bed after reaching a maximum in the region of the high shear layer located at about two-thirds of the ice thickness'. It is thought (as demonstrated by Goodman and others (1981), for example) that ice deformation in the region where a strong single pole fabric is observed is dominated by proton-rearrangement controlled glide, whereas at greater depths recrystallisation occurs, which is largely attributed by Gow & Williamson (1976) to the effects of age and rapidly increasing temperature. Goodman and others show that at the depth where the single pole fabric gives way to a multipole fabric at ~1800 m in the Byrd core, grain-boundary melting probably becomes important and that this accelerates creep.

Russell-Head & Budd note from their work on Law Dome that there appears to be a widespread, rather immobile (or stagnant) layer at the base of the ice sheet, and suggest that this may be related to the RES echo-free zone.

(e) conclusions

The following hypothesis for the nature of deformation of the ice is based on the observations above. In the upper part of the ice sheet (above the echo-free zone) flow is enhanced by a near-horizontal easy glide plane with a high concentration of near vertical c-axes. Below this a multipolar fabric is caused by recrystallisation which arises partly because of the higher temperature of the ice, but principally because of changing stress fields produced by varying bedrock slopes. If the interface between the two fabrics is sharp enough, it may produce the seismic reflections observed by Bentley over wide areas of West Antarctica, and also mark the level at which internal horizons become heavily deformed and radio-echo layering disappears.

The layering indicates that deformation in the lowest ice occurs both over and around the subglacial peaks, and that the effects of this are frequently visible on even near-surface layering, suggesting that the deformation takes place throughout the ice column to some extent.

6.4 Implications for ice core chronologies

In addition to providing a check on ice flow models along flowlines, radio-echo layering may be used to compare accepted or proposed ice core chronologies at widely separated stations. This should give an improved estimate of dating errors along ice cores, and hence enable a more reliable comparison between sites of parameters measured on cores.

Despite the very extensive flight coverage available for the Antarctic it has not been possible to connect any of the major scientific stations (Byrd, South Pole, Vostok and Dome C) by internal layering. Although this is principally due to a lack of connecting flights, the poor continuity of the layering between most sites may prevent a reliable

comparison even if suitable flights had been made (see fig. 2.2).

In Greenland, Gudmandsen (1975) has made a comparison between Crête and Camp Century, stating that a layer at about 1900 m depth at Crête is a continuation of one seen at 1100 m at Camp Century. The best chronology available for Camp Century is that of Hammer and others (1978), which is based on measured annual layer thicknesses along the deep ice core. This gives a date of 9±1 kaBP for a depth of 1100±25 m. At Crête a chronology with an accuracy of ±1 yr is available along the 404 m core, but in the deeper ice dating can only be made by models. Using the model by Dansgaard & Johnsen (1969) and the measurements by Reeh and others (1978) provides a date of ~13±2 kaBP at 1900 m at Crête. The model should be reliable here because Crête is located on an ice divide, and accumulation and vertical strain rates have been measured from the 404 m core. The discrepancy between these dates is probably due to an error in following the same layer between stations, as the Z-scope record on which the layering was followed is of poor quality (see figs. 8 and 9, Gudmandsen 1976).

An alternative to following individual layers is to use the PRC vs depth measurements, as reported in Chapter 5. Although these do not give as high a resolution as following individual layers might, they confirm that there are no significant errors in dating of the principal Antarctic sites, using the chronologies given in Appendix 4. Vostok and Dome C are seen in fig. 5.8 to be comparable back to ~100 kaBP, and the dating for South Pole and Byrd are consistent back to ~20 kaBP. Due to the strong reflections from density fluctuations in the upper layers no reliable comparison can be made between South Pole and Vostok or Dome C.

Finally, the basal layer-free zone indicates a lack of vertical continuity in the ice at the lowest levels. Clearly the flow models used for dating do not apply in this zone, and the basal layer-free zone can therefore be used to identify the depths at which these dating models break down. For the four principal sites these are, using the chronologies

in Appendix 4:

STATION	DEPTH (m)	AGE (kaBP)	REMARK
Byrd	>1800	>34	Absorption limit
South Pole	2650	~90	Layer-free zone
Vostok	>3000	>225	Absorption limit
Dome C	~2900	~170	Layer-free zone

It is interesting to note that at the only site where a core below these depths is available, i.e. Byrd Station, the oxygen isotope profile (Johnsen and others 1972) shows a number of sharp excursions below ~1900 m depth, which could be interpreted as indicating complex folding of the lowest ice layers (Boulton, in press).

Chapter 7

CONCLUSIONS

This brief section reiterates some of the conclusions drawn in earlier chapters.

(a) reflection mechanisms

On the basis of reflection coefficient vs depth profiles at many sites, two reflection mechanisms have been suggested to account for the observations. In approximately the upper 500 m in the Antarctic ice sheet reflections appear to arise from fluctuations in ice density; at greater depths layers of ice containing high concentrations of volcanogenic acid impurities account for the reflections seen. In Greenland all echoes appear to originate from such acidity variations, probably because thicker annual layers and higher volcanic acid input to the ice sheet dominate any density effects.

The spacing of individual reflectors appears to be of the order of a few metres, however the echoes observed with the present equipment probably originate from unresolved groups of reflectors. Individual reflectors of particularly high acidity are thought to provide structure and horizontal continuity. Layer spacings are generally similar to the pulse length used when this is >10 m. Short period fading of layering indicates that the reflecting surfaces are extremely smooth, and measured roughness parameters support the hypothesis that they are depositional surfaces.

(b) acidity levels in ice sheets

Having established that layer echoes arise from changes in acidity within the ice, a method of estimating acidities from measured reflection coefficients has been developed. Where data are available, the results agree well with direct ice core acidity measurements. Acidity profiles derived from RES have been presented for Crête (Greenland) and six representative Antarctic sites.

These have been interpreted to provide information on past explosive volcanic activity to ~30 kaBP in Greenland and ~100 kaBP in the Antarctic. In Greenland very low acidities are observed between ~14-23 kaBP, and are believed to be due to neutralisation by calcareous dust. In the Antarctic low acidity levels are found between ~13-25 kaBP, and between ~70-80 kaBP. A peak in ice sheet acidity occurs at ~50 kaBP. These are thought to reflect levels of southern hemisphere explosive volcanic activity, and agree with estimates based on volcanogenic zinc levels at Dome C to ~30 kaBP. Before this time no estimates of volcanic activity are available for the southern hemisphere from other sources.

(c) deep ice dynamics

Observations of layering in a variety of ice flow situations have been described and illustrated. In particular, a near-basal zone where layering is not detected despite adequate system performance has been widely observed. This is thought to be caused by layering becoming bent or tilted in three dimensions as it approaches the bedrock, so that although individual surfaces still exist, they return little power to the receiver.

It has been proposed that this basal layer-free zone may be related to a seismic reflecting zone observed near to bedrock in West Antarctica, and to changes in ice fabric observed in deep ice cores. Near centres of outflow there is little horizontal movement and layering is usually

observed to bedrock.

In the vicinity of subglacial peaks layering is distorted due to the disturbance in ice flow, and this suggests that there is a significant component of flow around the obstacle as well as over it.

In the upper ice layering has been used to estimate the variability in vertical strain rate along flowlines, and a strong dependence on the range of bedrock relief found.

Appendix 1

THE ROUTE OF VOLCANIC ACIDS INTO POLAR SNOW

Eruption plumes inject very large amounts of sulphur dioxide, hydrogen sulphide, hydrogen chloride and other gases, together with small amounts of acidic droplets, into the lower stratosphere (Lazrus and others 1979; Arnold & Fabian 1980). Chemical conversion of sulphur dioxide is thought (Sze & Ko 1979) to be dominated by the reaction sequence:

$$O_3 \longrightarrow O_2 + O(^1D) \longrightarrow 2OH$$

$$OH + SO_2 + M \longrightarrow H_2SO_3 + M$$

$$H_2SO_3 + OH \longrightarrow H_2SO_4$$

where M refers to some gaseous species which removes energy from the exothermic second stage. The time constant for this sequence has been estimated to be about 100 days (Castleman and others 1974), which is in good agreement with the observed times taken for the Junge layer (the aerosol-rich zone of the stratosphere at about 20 km altitude) to display a peak aerosol concentration after an eruption. By considering the particularly well-documented eruption of Gunung Agung in 1963 we can follow the stratospheric formation and transport of this aerosol.

Gunung Agung is located at 8°25'S 115°30'E on the island of Bali, and erupted violently on 17 March 1963. Cadle and others (1976) estimate that $\sim 1.2 \times 10^7$ tonnes of SO_2 were ejected. No other major explosive eruption occurred in the world for over two years, so the formation and dispersion of the subsequent aerosol could be directly measured. Mossop (1964)

studied the increase in aerosol concentration at a height of 20 km for over a year after the eruption, and found that the aerosol concentration increased from less than one particle per standard cubic metre (SCM) before the eruption to over 160 particles/SCM during the period 70–140 days afterwards (fig. 1). It was observed that the particles consisted mainly of sulphuric acid, and that almost every aerosol particle contained at least one small solid particle, of radius 0.02–0.15 μm. These solid cores are probably volcanic dust particles which act as condensation nuclei for the acid aerosol. Castleman and others (1974) studied several aerosol collections made during this time, and showed that in the southern hemisphere (0°–43°S) the sulphate concentration in the Junge layer had increased from about 0.04–0.15 μg/SCM before the eruption, to a maximum of about 40 μg/SCM a year later. In the northern hemisphere (0°–34°N) the increase was not so marked, but the sulphate level increased from a background level of 0.1–0.2 μg/SCM to a peak value of 10–15 μg/SCM about 6–18 months later. This supports the conclusion of Hammer (1977) that southern hemisphere eruptions deposit little acid onto the Greenland ice sheet.

The stratospheric aerosol gradually spread over the southern hemisphere, reaching South Africa and Australia in April, Chile in May and the South Pole in November, eight months after the eruption. The aerosol was located in a relatively thin layer around the 50 mb surface at a height of 21–25 km over Australia and 19–20 km over the South Pole. The presence of the material over the Antarctic was first detected via a sharp reduction in the amount of direct solar radiation at the South Pole (Viebrock & Flowers 1968). Initially the aerosol entered the circumpolar vortex in the form of impulses or clouds, but by the middle of December it had spread evenly throughout the region. The direct solar radiation level remained relatively constant throughout the remainder of the austral summer following the arrival of the aerosol; by the following summer the amount of direct solar radiation had increased significantly, but again remained constant during the summer, indicating no depletion of aerosol at

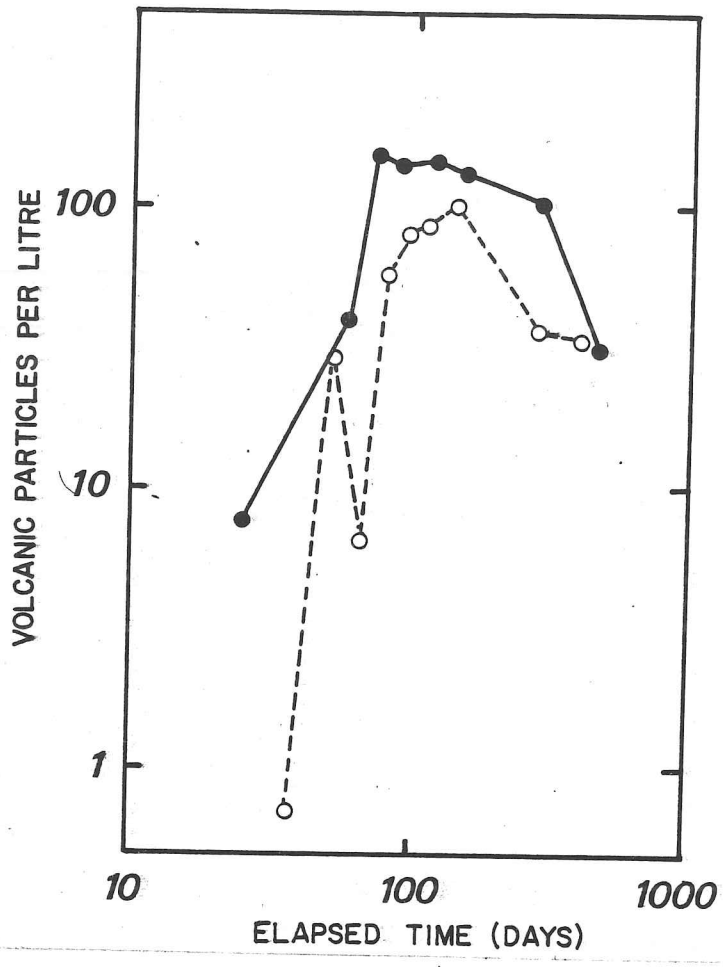

Fig. 1 Change of concentration of volcanic dust particles with time elapsed since the 1963 eruption of Agung, at an altitude of 20km. Full line indicates data from northerly sampling flights, broken line southerly (from Mossop 1964).

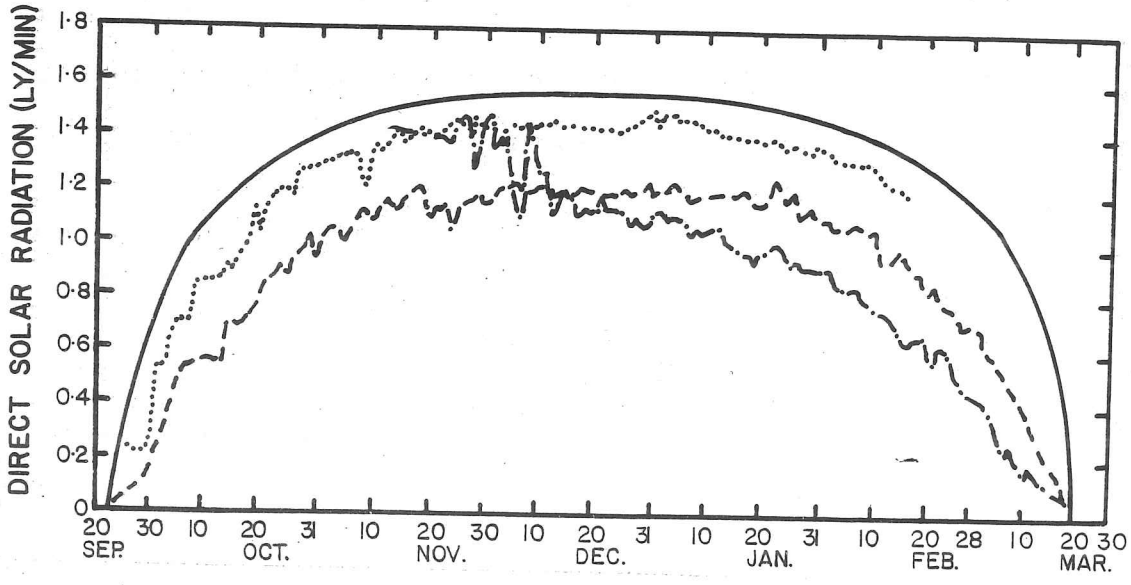

Fig. 2 Direct solar radiation data for Amundsen-Scott (South Pole) Station. Solid line, mean 1957-62; pecked line, 1963-64; dashed line, 1964-65; dotted line, 1965-66. (from Viebrock & Flowers 1968)

that time. The same sharp increase in solar radiation following the austral winter was observed for the following two years as the solar radiation level gradually returned to normal (fig. 2). This indicates that the depletion of the aerosol over the Antarctic occurred largely during the winter. A strong inversion forms near the ice surface during the polar winter and breaks occurring in this inversion, which are accompanied by katabatic winds, can transport the aerosol from above the inversion downwards and deposit it on the snow surface. In addition the particles probably act as condensation nuclei for ice crystals and are precipitated in snow.

Analyses of snow samples from pits dug at Dome C and the South Pole have revealed a sharp peak in sulphate level during 1964-65 (Delmas & Boutron 1980; see fig. 3). This corresponds well with the depletion of the aerosol in the Antarctic stratosphere, which must have occurred mainly between March-September, 1964. Sulphate analysis of snow samples from Dome C covering the last hundred years shows that the Agung sulphate peak is the largest since that due to Krakatoa in 1883. Delmas & Boutron (1980) have also shown that the contribution of Antarctic volcanoes to the snow sulphate level is probably unimportant; transport must occur stratospherically as the residence time of sulphur dioxide in the troposphere is only a few days. They suggest that in future it will be possible to date snow pit stratigraphy by using the high sulphate levels from major eruptions such as Agung and Krakatoa as reference horizons.

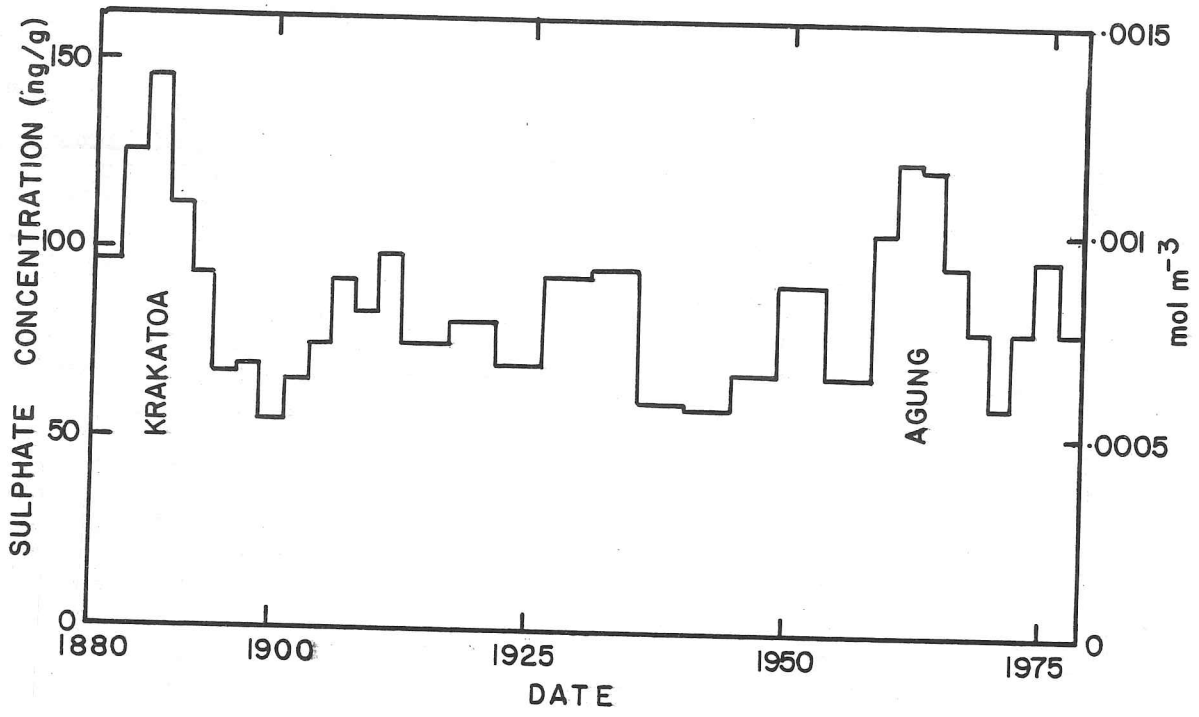

Fig. 3 Sulphate concentration in snow at Dome C on thirty-two samples covering the last hundred years. Peaks due to known volcanic eruptions indicated.
(after Delmas & Boutron 1980)

Appendix 2

DATA AVAILABILITY AND SUMMARY OF MEASUREMENTS AT PRINCIPAL SITES

(a) data availability

Byrd Station

80°01'S 119°30'W
1530 masl elevation
2160 m ice thickness

Season	Flight/CBD	60 MHz film	Type*	Remarks
1974/75	137/766	Z+A	O/F	Station clutter
	137/773	Z+A	O/F	Reasonable
	137/1220	Z+A	O/F	Aircraft banking
	137/1233	Z+A	O/F	Station clutter
	147/1215	Z+A	O/F	Banking & clutter
	147/1227	Z+A	O/F	Good
	147/1285	Z+A	O/F	Good
	148/17-19	Z+A	T/O	No surface echo
	148/537	Z+A	O/F	Station clutter
1977/78	5/2060-70	Z+A	L	No surface echo
	13/2215	Z+A	O/F	Station clutter
	13/2260-75	Z+A	L	No surface echo
1978/79	35/827	Z+A	O/F	Station clutter
	36/2210	Z	L	Banking & clutter
	37/1937	Z	L	Station clutter
	39/1765-90	Z	L	No surface echo

* where O/F denotes direct overflight, T/O taxiing and take-off, and L landing.

Nearest Super 8 data recorded at F147/1318 (1974/75), approximately 15.5 km NE of Byrd, and connected to Byrd via layering on F147 and F148.

South Pole

90°S
2810 masl elevation
2915 m ice thickness

Season	Flight/CBD	60 MHz film	Type	Remarks
1974/75	111/1275	Z	O/F	Good
	111/1289-1301	Z	L	Good
	112/8-12	Z+A	T/O	Good
	121/1540-48	Z+A	L	Good
	133/1289	Z+A	O/F	Good
	133/1305-22	Z+A	L	Good
1978/79	30/2344-49	Z+A	L	Good
	33/1957-76	Z+A	L	Good
	34/2634-58	Z+A	T/O	Good; pulse changes
	39/0-100	Z	T/O	Good

Nearest Super 8 data over station at F133/1286 (200 m terrain clearance), and taxiing on runway at F133/1309.

Vostok Station

78°27'S 106°48'E
3490 masl elevation
3770 m ice thickness

Season	Flight/CBD	60 MHz film	Type	Remarks
1974/75	130/557	A	O/F	No Z film
1977/78	9/698-732	Z	O/F	Good

Super 8 data recorded during overflight at F130/557.

Dome C Camp

74°40'S 123°50'E
3200 masl elevation
3420 m ice thickness

Season	Flight/CBD	60 MHz film	Type	Remarks
1974/75	136/656	Z+A	O/F	Good
1977/78	11/643	Z+A	O/F	Good Z, poor A
	11/2074-2120	Z+A	O/F	Variable Z, poor A
1978/79	40/579, 812, 1027	Z+A	O/F	Reasonable

Super 8 data recorded during overflight at F136/656.

(b) summary of measurements

Byrd Station

Z-scope data			A-scope data				
Depth m	Age[1] kaBP	Age[2] kaBP	Depth m	Age[1] kaBP	R dB	E dB	Δc molm^{-3}
309	2.8	2.6					
394	3.6	3.5	384	3.5	-72.5	1.0	.0065
			441	4.0	-73.9	0.8	.0054
			492	4.4	-74.5	0.7	.0051
528	4.9	4.9	538	5.0	-73.7	0.8	.0056
			594	5.7	-74.4	0.5	.0052
			651	6.5	-72.9	0.6	.0061
672	6.7	6.4	691	6.9	-73.9	1.4	.0054
728	7.5	7.1	738	7.6	-72.9	0.6	.0061
789	8.3	7.8	789	8.3	-72.6	1.4	.0065
			855	9.3	-75.0	0.7	.0048
895	9.9	9.1	896	9.9	-76.2	0.7	.0041
951	10.6	9.7	954	10.7	-74.7	1.2	.0050
1030	11.8	11.1	1040	12.0	-74.8	0.9	.0049
1114	13.5	12.6	1127	13.7	-76.7	1.1	.0038
1187	14.8	14.0					
1450	20.4	21.2	1445	20.2	-78.9	0.2	.0020
1509	21.8	23.3	*1500	21.5	-74.0	-	.0040
1601	24.6	27.4					
1705	28.8	32.7					
1788	33.5	38.0					
2157							

Notes:
(1) dating from Budd & Young (in press) flowline model
(2) dating from Whillans (1979) model
(3) Z-scope data from F137/1233 and F147/1227, 1285
(4) A-scope data averaged along F148/528-535
* additional value from Super 8 record at F147/1318
(5) R, mean power reflection coefficient; E, standard error
(6) Δc, elevated acidity estimated as in Chapter 4
(7) where Z-scope and A-scope layer depths were within half a pulse length (20 m) they are placed on the same line. Because layer depths are averaged from several flights, A- and Z-scope data do not always coincide. A-scope reflection coefficients are averaged along 25-50 km of flight track.

South Pole

Z-scope data		A-scope data				
Depth m	Age kaBP	Depth m	Age kaBP	R dB	E dB	Δc molm^{-3}
434	5.9	414	5.6	-70.1	0.5	.0172
489	6.7	494	6.8	-69.7	1.0	.0174
555	7.7	562	7.8	-70.5	0.7	.0170
695	9.9	707	10.2	-74.5	0.5	.0104
		817	12.1	-72.1	0.9	.0130
867	12.9	887	13.3	-73.0	1.3	.0115
		949	14.4	-77.8	0.7	.0065
		1074	19.1	-71.9	1.6	.0120
1138	18.1	1147	18.3	-70.9	0.9	.0130
1194	19.3					
1276	21.1	1279	21.2	-72.4	0.8	.0105
1319	22.1					
1359	23.0					
		1426	24.6	-72.2	0.9	.0092
1567	28.3	1587	28.8	-70.2	0.8	.0115
1647	30.5	1665	31.1	-68.9	0.7	.0128
1773	34.3	1756	33.8	-67.7	0.9	.0150
1865	37.4	1873	37.7	-70.8	0.7	.0096
1930	39.8					
2005	42.7	2020	43.3	-74.5	0.8	.0060
2124	47.8	2108	47.1	-76.5	1.6	.0050
		2167	49.8	169.8	1.2	.0087
2209	51.9					
		2240	53.6	-70.0	-	.0087
2300	57.0					
2383	62.3					
2465	68.5					
2549	76.0					
2915						

Notes: (1) dating from simple accumulation model (Nye 1957), with 0.08 ma^{-1} accumulation rate and 2915 m ice thickness
(2) Z-scope data from F111/1275 and F133/1289
(3) A-scope data from F133/1305-10

Vostok Station

A-scope data			
Depth m	Age kaBP	R dB	Δc $molm^{-3}$
712	28.3	-79.1	.0064
761	30.2	-77.5	.0075
822	32.9	-79.7	.0057
834	33.4	-79.7	.0057
889	36.1	-75.1	.0099
903	36.8	-74.3	.0107
990	41.1	-76.8	.0080
1033	42.7	-76.5	.0080
1070	44.0	-76.7	.0080
1097	45.0	-76.2	.0076
1137	46.8	-74.5	.0093
1157	47.9	-74.6	.0092
1189	49.5	-75.4	.0081
1271	53.6	-76.9	.0068
1368	57.7	-73.8	.0090
1407	59.4	-73.4	.0095
1441	61.5	-73.7	.0092
1482	63.9	-73.6	.0087
1612	69.6	-75.8	.0065
1642	71.1	-75.8	.0065
1686	73.3	-77.9	.0045
1749	76.9	-75.2	.0060
1847	81.4	-74.5	.0062
1934	84.7	-76.1	.0055
2070	90.8	-73.9	.0067
2453	118.7	-72.1	.0070
3770			

Notes: (1) dating from Budd & Young (in press)
(2) data from F130/562-582
(3) no simultaneously recorded A- and Z-scope data was available at this site, and it was not therefore possible to ensure that successive A-scope power measurements refered to the same internal layer. Taking advantage of the smooth bedrock, A-scope power maxima were related by assuming that they maintained a constant fractional depth.

F136/704

A-scope data				
Depth m	Age kaBP	R dB	E dB	Δc $molm^{-3}$
624	22.0	-72.0	0.4	.0142
707	25.4	-71.9	0.5	.0140
829	30.5	-72.5	0.8	.0130
900	33.6	-75.9	0.9	.0088
1000	38.1	-71.9	0.9	.0132
1103	43.0	-69.2	0.8	.0162
1146	45.1	-70.6	0.7	.0140
1230	49.3	-70.5	0.7	.0131
1273	51.6	-68.2	0.7	.0180
1410	59.1	-67.5	0.9	.0170
1463	62.1	-66.9	0.9	.0170
1543	66.9	-69.8	0.5	.0115
1649	73.7	-71.5	0.4	.0095
1740	82.9	-74.0	0.6	.0065
1858	88.4	-71.1	0.4	.0090
2037	103.0	-69.2	0.5	.0100
2128	111.3	-68.7	0.9	.0100
2192	117.6	-65.8	1.2	.0140
2306	130.0	-65.4	1.0	.0150
2380	138.7	-67.0	1.3	.0116
2444	147.0	-67.2	0.6	.0114
2585	168.0	-67.3	0.8	.0112
3200				

Notes: (1) dating by simple accumulation model, Z=3200 m, $\dot{A}$=0.0315 ma^{-1}
(2) data from F136/700-720

Dome C Camp

Z-scope data			A-scope data				
Depth m	Age[1] kaBP	Age[2] kaBP	Depth m	Age[2] kaBP	R dB	E dB	Δc molm^{-3}
410	11.4	11.8					
498	14.4	14.6					
662	21.6	19.9	657	19.8	-77.4	0.5	.0076
714	23.8	21.7					
810	28.1	25.0	809	24.9	-75.0	0.6	.0098
920	32.0	29.0	914	28.7	-72.8	0.5	.0122
994	36.0	31.8	973	30.9	-75.1	0.6	.0083
1072	39.4	34.8	1097	35.8	-75.6	0.5	.0078
1121	41.6	36.8					
1192	44.8	39.7					
1256	47.9	42.4	1234	41.4	-73.4	0.7	.0089
1333	51.6	45.7	1313	44.8	-74.1	0.3	.0080
			1345	46.2	-72.5	1.2	.0098
1392	54.6	48.4					
1438	57.0	50.5	1419	49.5	-71.3	0.7	.0103
1474	58.9	52.2	1457	51.3	-69.5	0.6	.0124
			1528	54.7	-72.2	0.5	.0087
1563	62.7	56.6					
1664	69.5	61.8	1665	61.7	-73.0	0.3	.0080
1762	75.5	67.1	1737	65.5	-71.8	0.3	.0090
			1818	70.5	-72.0	0.4	.0086
1851	81.2	72.2					
			1918	76.5	-75.6	0.6	.0052
1951	88.1	78.4	1963	78.9	-74.2	0.4	.0056
2003	91.8	81.7	2027	83.0	-73.3	0.4	.0063
2043	94.8	84.4					
			2080	86.6	-73.5	0.6	.0062
2108	99.8	88.9					
			2140	90.8	-73.0	0.5	.0064
2171	104.9	93.5					
			2288	102.2	-70.8	1.4	.0079
			2327	105.4	-69.9	0.8	.0087
2358	121.9	108.7					
2422	128.4	114.5	2394	111.3	-71.7	1.2	.0070
			2456	117.0	-71.4	0.6	.0072
2495	136.3	121.6					
2606	149.7	133.7	2636	136.2	-71.7	1.2	.0070
2677	159.3	142.3					
2842	185.8	166.1					
3420							

Notes: (1) dating from Lorius and others (1979) 'isotopic' chronology extended with a simple accumulation model
(2) dating from simple accumulation model, Z=3400 m, $\dot{A}$=0.037 ma^{-1}
(3) Z-scope data from F136/656 and F11/643
(4) A-scope data from F136/653-660

F136/608

A-scope data

Depth m	Age kaBP	R dB	E dB	Δc $molm^{-3}$
799	20.3	-76.7	0.6	.0086
863	22.1	-77.5	0.4	.0070
922	23.9	-78.1	0.3	.0063
1044	27.7	-75.8	0.5	.0078
1115	29.9	-73.4	0.5	.0097
1229	33.8	-75.1	0.2	.0082
1268	35.1	-74.6	0.5	.0087
1377	39.0	-77.7	0.6	.0052
1463	42.2	-73.4	0.4	.0079
1522	44.6	-75.6	0.2	.0060
1629	48.8	-73.8	0.5	.0072
1676	50.8	-70.7	0.5	.0107
1741	53.6	-73.6	0.3	.0073
1867	59.4	-71.9	0.5	.0082
1943	63.1	-71.7	0.4	.0083
2053	68.7	-73.1	0.2	.0068
2149	74.0	-75.3	0.4	.0047
2229	78.7	-73.8	0.7	.0054
2346	86.1	-74.2	0.8	.0050
2421	91.3	-72.2	0.4	.0065
2486	96.0	-72.3	0.4	.0065
2549	100.9	-71.7	0.5	.0068
2710	115.0	-74.0	0.7	.0050
2778	121.6	-73.6	0.7	.0051
2848	129.4	-71.0	0.8	.0067
3540				

Notes: (1) dating by simple accumulation model, Z=3540 m, $\dot{A}$=0.0447 ma^{-1}
(2) data from F136/600-616

LOCATION OF MEASUREMENT SITES AND INPUT DATA FOR CALCULATING TEMPERATURE PROFILES

Site	Location	Elev.	TCL	z	Ȧ	V	α	λ_e	θ_s	γ_g	θ_b	D_{total}
		masl	m	m	ma^{-1}	ma^{-1}		$^oCm^{-1}$	^oC	$^oCm^{-1}$	^oC	dB
Byrd	80°01'S 119°30'W	1530	-	2160	.12	10.0	.002	.02	-28.3	.0275	-2.1	69.0
F147/1318	79°52'S 119°11'W	1600	580	2520	.12	10.0	.002	.02	-28.3	.0275	-1.7	76.0
South Pole	90°S	2800	-	2915	.06	3.0	.001	.01	-50.8	.020	-15.7	42.0
F123/779	77°52'S 99°08'E	3670	740	3715	.022	1.0	.0012	.005	-57.5	.018	-5.9	72.0
Vostok	78°27'S 106°48'E	3490	-	3770	.022	1.0	.0014	.005	-57.2	.018	-4.9	76.0
F136/800	76°40'S 114°45'E	3250	695	3420	.023	4.0	.001	.01	-57.0	.018	-9.4	58.0
F136/704	75°22'S 121°29'E	3230	760	3200	.035	0.0	.000	.02	-53.5	.020	-6.0	69.0
Dome C Camp	74°40'S 123°50'E	3200	-	3420	.035	0.0	.000	.02	-53.5	.020	-6.5	66.0
F136/608	73°50'S 126°23'E	3220	800	3540	.035	0.0	.000	.02	-53.5	.020	-6.0	69.0
F136/560	73°04'S 128°39'E	3220	875	3910	.04	2.0	.000	.02	-53.0	.02	-4.2	78.0
F110/542	71°27'S 127°26'E	2510	385	2520	.08	3.0	.0015	.014	-46.0	.025	-10.8	46.0
F136/512	72°15'S 130°31'E	3015	915	2800	.08	3.0	.0015	.013	-48.0	.025	-10.4	47.0
F135/929	70°42'S 133°50'E	2660	335	2500	.13	5.0	.0015	.015	-43.0	.025	-15.1	40.0
F135/833	68°56'S 136°45'E	2370	685	3575	.20	10.0	.0005	.02	-35.0	.025	-8.3	38.0
F135/785	68°02'S 138°01'E	1995	430	2400	.25	10.0	.0010	.02	-28.0	.025	-9.0	52.0
Crete	71°07'N 37°19'W	3170	500	3000	.20	0.0	.000	.00	-30.0	.02	-10.0	78.0

NB: Site F133/1286 is at South Pole, with zero terrain clearance, F133/1309 is at South Pole with 200 m terrain clearance; F130/557 is at Vostok, terrain clearance=850 m; F136/656 is at Dome C Camp, terrain clearance=745 m.

ICE CORE CHRONOLOGIES AT PRINCIPAL STATIONS

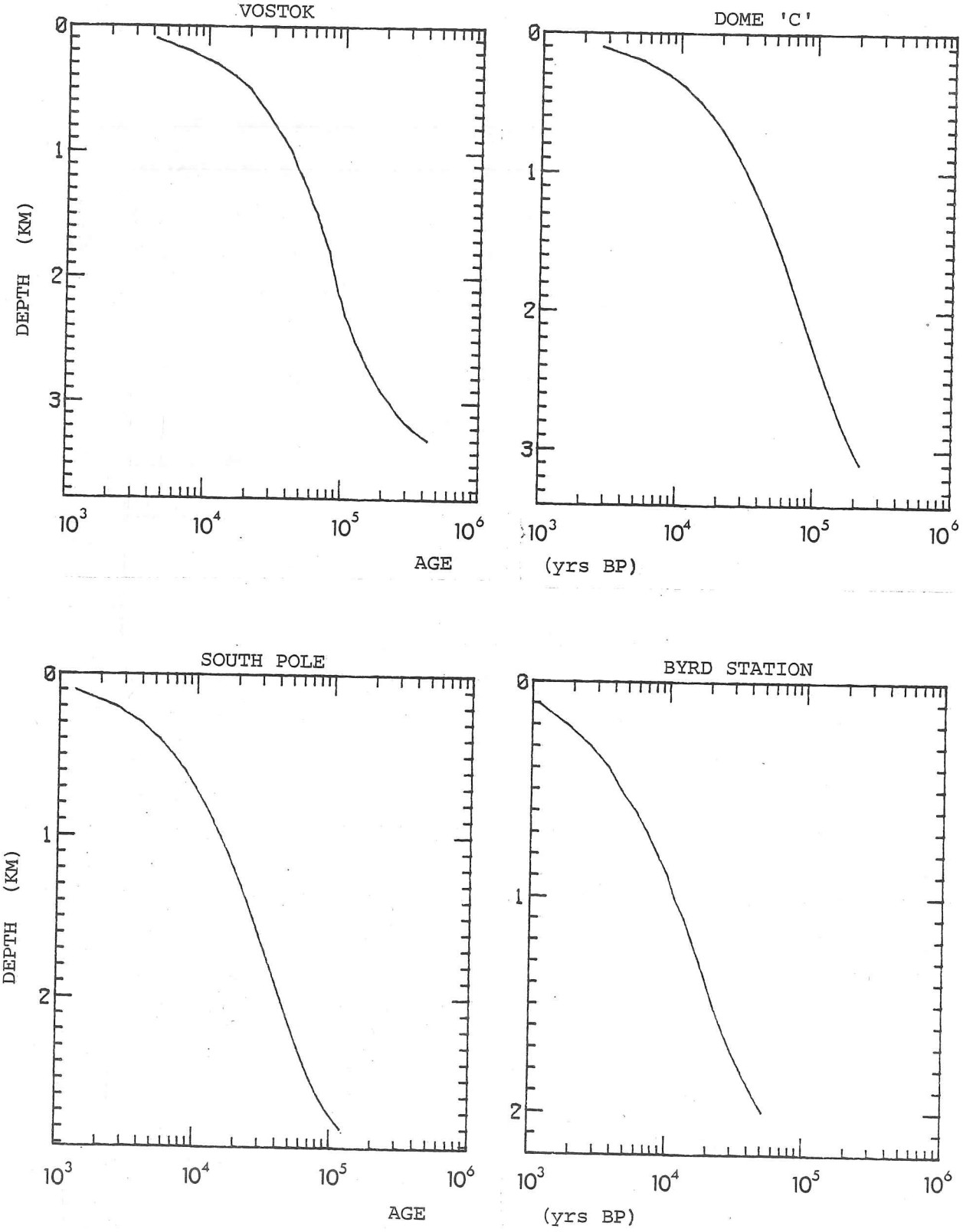

For details of models used and references, see p.100.

REFERENCES

ACKLEY, S.F. and KELIHER, T.E. 1979 'Ice sheet internal radio-echo reflections and associated physical property changes with depth' Journal of Geophysical Research, 84, Nr. B10, 5675-5680

ARNOLD, F. and FABIAN, R. 1980 'First measurements of gas phase sulphuric acid in the stratosphere' Nature, 283, Nr. 5742, 55-57

BAILEY, J.T., EVANS, S. and ROBIN, G. de Q. 1964 'Radio echo sounding of polar ice sheets' Nature, 204, Nr. 4957, 420-421

BARKOV, N.I. 1974 'Ice temperatures to the depth of 782 m from the drill hole at Vostok Station' Materialy Glyatsroleyicheskikh Issledovany Khrononika Obssnzhdeniya, Vypush 24, 257-259

BARKOV, N.I., KOROTKEVICH, E.S., GORDIENKO, F.G. and KOTLYAKOV, V.M. 1975 'The isotope analysis of ice cores from Vostok Station (Antarctica), to the depth of 950 m' Proceedings, Isotopes & Impurities in Snow & Ice Symposium, Grenoble, 1975, IASH Publn. Nr. 118, 382-387

BECKMANN, P. and SPIZZICHINO, A. 1963 'The scattering of electromagnetic waves from rough surfaces' Electromagnetic Waves Series, Vol. 4, Pergamon Press

BENTLEY, C.R. 1971 'Seismic evidence for moraine within the basal Antarctic ice sheet' Antarctic Snow & Ice Studies II, American Geophysical Union Antarctic Research Series, Vol. 16, 89-129

BOULTON, G.S. (in press) Chapter III(j), In: G. de Q. Robin (ed.) Publication of the Cambridge Workshop on Isotope & Temperature Profiles in Polar Ice Sheets, Cambridge University Press

BOUTRON, C. 1980 'Respective influence of global pollution and volcanic eruptions on the past variations of the trace metals content of Antarctic snows since 1880's' Journal of Geophysical Research, 85, Nr. C12, 7426-7432

BOUTRON, C. and LORIUS, C. 1977 'Trace element content in east Antarctic snow samples' Proceedings, Isotopes & Impurities in Snow & Ice Symposium, Grenoble, 1975, IASH Publn. Nr. 118, 164-171

BOUTRON, C. and LORIUS, C. 1979 'Trace elements in Antarctic snows since 1914' Nature, 277, Nr. 5697, 551-554

BROOKS, R.L, CAMPBELL, W.J., RAMSEIER, R.O., STANLEY, H.R. and ZWALLY, H.J. 1978 'Ice sheet topography by satellite altimetry' Nature, 274, Nr. 5671, 539-543

BRYSON, R.A. and GOODMAN, B.M. 1980 'Volcanic activity and climatic changes' Science, 207, 1041-1044

BUAT-MENARD, P. and ARNOLD, M. 1978 'The heavy metal chemistry of atmospheric particulate matter emitted by Mount Etna volcano' Geophysical Research Letters, 5, Nr. 4, 245-248

BUDD, W.F. 1969 'The dynamics of ice masses' ANARE Scientific Reports, Series A(IV) Glaciology, Publn. Nr. 108

BUDD, W.F. and CARTER, D.B. 1971 'An analysis of the relation between the surface and bedrock profiles of ice caps' Journal of Glaciology, 10, Nr. 59, 197-209

BUDD, W.F., JENSSEN, D. and RADOK, U. 1971 'Derived physical characteristics of the Antarctic ice sheet' ANARE Interim Reports, Series A (IV) Glaciology, Publn. Nr. 120

BUDD, W.F., JENSSEN, D. and YOUNG, N.W. 1975 'Computation of the temperature profile from drill data at Vostok Station' Soviet Antarctic Expedition Information Bulletin, 90, 50-58

BUDD, W.F. and YOUNG, N.W. (in press) Chapter V(e), In: G. de Q. Robin (ed.), Publication of the Cambridge Workshop on Isotope & Temperature Profiles in Polar Ice Sheets, Cambridge University Press

BUSENBERG, E. and LANGWAY, C.C. 1979 'Levels of ammonium, sulphate, chloride, calcium and sodium in snow and ice from southern Greenland' Journal of Geophysical Research, 84, Nr. C4, 1705-1709

CADLE, R.D., KIANG, C.S. and LOUIS, J-F. 1976 'The global scale dispersion of the eruption clouds from major volcanic eruptions' Journal of Geophysical Research, 81, Nr. 18, 3125-3132

CAMPLIN, G.C., GLEN, J.W. and PAREN, J.G. 1978 'Theoretical models for interpreting the dielectric behaviour of HF-doped ice' Journal of Glaciology, 21, Nr. 85, 123-142

CASTLEMAN, A.W., MUNKELWITZ, H.R. and MANOWITZ, B. 1974 'Isotopic studies of the sulphur component of the stratospheric aerosol layer' Tellus, 26, 222-234

CHRISTENSEN, E.L. 1970 'Radioglaciology 300 MHz radar' Electromagnetics Inst., Technical University of Denmark, Lyngby, Report R93

CLOUGH, J.W. 1977 'Radio-echo sounding: reflections from internal layers in ice sheets' Journal of Glaciology, 18, Nr. 78, 3-14

CLOUGH, J.W. and BENTLEY, C.R. 1970 'Measurements of electromagnetic wave velocity in the east Antarctic ice sheet' Proceedings, International Symposium on Antarctic Glaciological Exploration, Hanover, 1968, IASH Publn. Nr. 86, 115-128

CRAGIN, J.H., HERRON, M.M., LANGWAY, C.C. and KLOUDA, G. 1977 'Interhemispheric comparison of changes in the composition of atmospheric precipitation during the late Cenozoic era' Proceedings, Polar Oceans Conference, Montreal, 1974, 617-631

DANSGAARD, W. and JOHNSEN, S.J. 1969 'A flow model and a time scale for the ice core from Camp Century, Greenland' Journal of Glaciology, 8, Nr. 53, 215-223

DELMAS, R. and BOUTRON, C. 1978 'Sulphate in Antarctic snow: spatio-temporal distribution' Atmospheric Environment, 12, 723-728

DELMAS, R. and BOUTRON, C. 1980 'Are the past variations of the stratospheric sulphate burden recorded in central Antarctic snow and ice layers?' Journal of Geophysical Research, 85, Nr. C10, 5645-5649

DREWRY, D.J. 1979 'Ice sheet glaciology' Progress in Physical Geography, 3, Nr. 3, 313-328

DREWRY, D.J. and MELDRUM, D.T. 1978 'Antarctic airborne radio echo sounding, 1977-78' Polar Record, 19, Nr. 120, 267-278

EISENBERG, D. and KAUZMANN, W. 1969 'The structure and properties of water' Oxford University Press, London.

ENDO, Y. and FUJIWARA, K. 1973 'Characteristics of the snow cover in east Antarctica along the route of the JARE South Pole Traverse and factors controlling such characteristics' JARE Scientific Reports, Series C, Nr. 7

EVANS, S. 1963 'Radio techniques for the measurement of ice thickness', Polar Record, 11, Nr. 73, 406-410

EVANS, S. 1965 'Dielectric properties of ice and snow - a review' Journal of Glaciology, 5, Nr. 42, 773-792

EVANS, S. and SMITH, B.M.E. 1969 'A radio echo equipment for depth sounding in polar ice sheets' Journal of Scientific Instruments (Journal of Physics E), Series 2(2), 131-136

FEDOROV, B.A. 1967 'Radar sounding of Antarctic ice' Soviet Antarctic Expedition Information Bulletin, 6, Nr. 4, 337-340

FITZGERALD, W.J. and PAREN, J.G. 1975 'The dielectric properties of Antarctic ice' Journal of Glaciology, 15, Nr. 73, 39-48

GARFIELD, D.E. and UEDA, H.T. 1976 'Resurvey of the Byrd Station, Antarctica, drill hole' Journal of Glaciology, 17, Nr. 75, 29-34

GLEN, J.W. and PAREN, J.G. 1975 'The electrical properties of snow and ice' Journal of Glaciology, 15, Nr. 73, 15-38

GOODMAN, D.J., FROST, H.J. and ASHBY, M.F. 1981 'The plasticity of polycrystalline ice' Philosophical Magazine, Series A, Vol. 43, Nr. 3, 665-695

GOW, A.J. 1970 'Preliminary results of studies of ice cores from the 2164 m deep drill hole, Byrd Station, Antarctica' Proceedings, International Symposium on Antarctic Glaciological Exploration, Hanover, 1968, IASH Publn. Nr. 86, 78-90

GOW, A.J. and WILLIAMSON, T. 1971 'Volcanic ash in the Antarctic ice sheet and its possible climatic implications' Earth & Planetary Science Letters, 13, 210-218

GOW, A.J. and KOHNEN, H. 1979 'The relationship of ultrasonic velocities to c-axis fabrics and relaxation characteristics of ice cores from Byrd Station, Antarctica' Journal of Glaciology, 24, Nr. 90, 147-154

GOW, A.J. and WILLIAMSON, T. 1976 'Rheological implications of the internal structure and crystal fabrics of the West Antarctic ice sheet as revealed by deep core drilling at Byrd Station' Geological Society of America Bulletin, 87, Nr. 12, 1665-1677

GUDMANDSEN, P. 1975 'Layer echoes in polar ice sheets' Journal of Glaciology, 15, Nr. 73, 95-101

GUDMANDSEN, P. 1976 'Studies of ice by means of radio echo sounding' Electromagnetics Inst., Technical University of Denmark, Lyngby, Report R162

GUDMANDSEN, P. and OVERGAARD, S. 1978 'Establishment of time horizons in polar ice sheets by means of radio echo sounding' Electromagnetics Inst., Technical University of Denmark, Lyngby, Report P312

HAMMER, C.U. 1977 'Past volcanism revealed by Greenland ice sheet impurities' Nature, 270, Nr. 5637, 482-486

HAMMER, C.U. 1980 'Acidity of polar ice cores in relation to absolute dating, past volcanism and radio-echoes' Journal of Glaciology, 25, Nr. 93, 359-372

HAMMER, C.U., CLAUSEN, H.B. and DANSGAARD, W. 1980 'Greenland ice sheet evidence of post-glacial volcanism and its climatic impact' Nature, 288, Nr. 5788, 230-235

HAMMER, C.U., CLAUSEN, H.B., DANSGAARD, W., GUNDESTRUP, N., JOHNSEN, S.J. and REEH, N. 1978 'Dating of Greenland ice cores by flow models, isotopes, volcanic debris, and continental dust' Journal of Glaciology, 20, Nr. 82, 3-26

HARGREAVES, N.D. 1977 'Radio echo studies of the dielectric properties of ice sheets' Unpublished Ph.D. thesis, University of Cambridge

HARRISON, C.H. 1971 'Radio-echo sounding: focussing effects in wavy strata' Geophysical Journal of the Royal Astronomical Society, 24, 383-400

HARRISON, C.H. 1972 'Radio propagation effects in glaciers' Unpublished Ph.D. thesis, University of Cambridge.

HARRISON, C.H. 1973 'Radio echo sounding of horizontal layers in ice' Journal of Glaciology, 12, Nr. 66, 383-397

HERRON, M.M., HERRON, S.L., and LANGWAY, C.C. 1981 'Climatic signal of ice melt features in southern Greenland' Nature, 293, Nr. 5831, 389-391

HERRON, M.M. and LANGWAY, C.C. 1980 'Firn densification: an empirical model' Journal of Glaciology, 25, Nr. 93, 373-386

HOBBS, P.V. 1974 'Ice Physics' Clarendon Press, Oxford

HUANG, T.C., WATKINS, N.D., SHAW, D.M. and KENNETT, J.P. 1973 'Atmospherically transported volcanic dust in south pacific deep sea sedimentary cores at distances over 3000 km from the eruptive source' Earth & Planetary Science Letters, 20, 119-124

JACCARD, C. 1959 'Etude theorique et experimentale des proprietes electriques de la glace' Helvetica Physica Acta, 32, Fasc. 2, 89-128

JIRACEK, G.R. 1967 'Radio sounding of Antarctic ice' University of Wisconsin, Geophysical & Polar Research Centre, Research Report Series, 67-1

JOHARI, G.P. and CHARETTE, P.A. 1975 'The permittivity and attenuation in polycrystalline and single crystal ice Ih at 35 and 60 MHz' Journal of Glaciology, 14, Nr. 71, 293-303

JOHNSEN, S.J., DANSGAARD, W., CLAUSEN, H.B. and LANGWAY, C.C. 1972 'Oxygen isotope profiles through the Antarctic and Greenland ice sheets' Nature, 235, Nr. 5339, 429-434

KUNST, M. and WARMAN, J.M. 1980 'Proton mobility in ice' Nature, 288, Nr. 5790, 465-467

KYLE, P.R., JEZEK, P.A., MOSLEY-THOMPSON, E. and THOMPSON, L.G. (unpublished) 'Tephra layers in the Byrd Station ice core and the Dome C ice core, Antarctica, and their climatic importance' Presented at the 17th General Assemby of the International Union of Geodesy & Geophysics, Canberra, 1979.

LANGWAY, C.C. 1970 'Stratigraphic analysis of a deep ice core from Greenland' Geological Society of America, Special Paper Nr. 125

LAZRUS, A.L., CADLE, R.D., GANDRUD, B.W., GREENBERG, J.P., HUEBERT, B.J. and ROSE, W.I. 1979 'Sulfur and halogen chemistry of the stratosphere and of volcanic eruption plumes' Journal of Geophysical Research, 84, Nr. C12, 7869-7875

LEGRAND, M. 1980 'Mesure de l'acidite et de la conductivite electrique des precipitations Antarctiques' Centre National de la Recherche Scientifique, Laboratoire de Glaciologie et Geophysique de l'Environment, Publn. Nr. 316

LIEBERT, J. and LEONHARDT, G. 1974 'Astronomical observations for determining ice movement in the Vostok Station area' Soviet Antarctic Expedition Information Bulletin, 8, Nr. 10, 569-570

LORIUS, C., MERLIVAT, L., JOUZEL, J. and POURCHET, M. 1979 'A 30,000-yr isotope climatic record from Antarctic ice' Nature, 280, Nr. 5724, 644-648

MÄLZER, H. 1964 'Das Nivellement uber das gronlandische Inlandeis der Internationalen Glaziologischen Gronland-Expedition 1959' Meddelelser om Gronland, Bd. 173, Nr. 7.

MILLAR, D.H.M. 1981 'Radio-echo layering in polar ice sheets and past volcanic activity' Nature, 292, Nr. 5822, 441-443

MILLAR, D.H.M. (in press) 'Acidity levels in ice sheets from radio-echo sounding' Accepted by Annals of Glaciology, 3

MOSSOP, S.C. 1964 'Volcanic dust collected at an altitude of 20 km' Nature, 203, Nr. 4947, 824-827

MROZ, E.J. and ZOLLER, W.H. 1975 'Composition and atmospheric particulate matter from the eruption of Heimaey, Iceland' Science, 190, Nr. 4213, 461-464

NEAL, C.S. 1976 'Radio echo power profiling' Journal of Glaciology, 17, Nr. 77, 527-530

NEAL, C.S. 1977 'Radio echo studies of the Ross Ice Shelf' Unpublished Ph.D. thesis, University of Cambridge.

NEWELL, R.E. 1971 'The global circulation of atmospheric pollutants' Scientific American, 224,Nr. 1, 32-42

NEWHALL, C.G. and SELF, S. (in press) 'The volcanic explosivity index (VEI): an estimate of explosive magnitude for historical volcanism' Submitted to Journal of Geophysical Research

NYE, J.F. 1957 'The distribution of stress and velocity in glaciers and ice sheets', Proc. Roy. Soc. A, 239, Nr. 1216, 113-133

ONSAGER, L. 1973 Introductory Lecture, Proceedings, Physics & Chemistry of Ice Symposium, Ottawa, 1972, 7-12

OSWALD, G.K.A. 1975 'Radio echo sounding of polar glacier beds' Unpublished Ph.D. thesis, University of Cambridge.

PAREN, J.G. 1973 'The electrical behaviour of polar glaciers' Proceedings, Physics & Chemistry of Ice Symposium, Ottawa, 1972, 262-267

PAREN, J.G. 1981 'Reflection coefficient at a dielectric interface' Journal of Glaciology, 27, Nr. 95, 203-204

PAREN, J.G. and ROBIN, G. de Q. 1975 'Internal reflections in polar ice sheets' Journal of Glaciology, 14, Nr.14, 251-259

PAREN, J.G. and WALKER, J.C.F. 1971 'Influence of limited solubility on the electrical and mechanical properties of ice' Nature, 230, Nr. 12, 77-79

PATENAUDE, R.W., MARSHALL, E.W. and GOW, A.J. 1959 'Deep core drilling in ice, Byrd Station, Antarctica' Snow, Ice & Permafrost Research Establishment, Technical Report Nr. 60

PATERSON, W.S.B. 1969 'The physics of glaciers' Pergamon Press, Oxford.

PETIT, J-R., BRIAT, M. and ROYER, A. 1981 'Ice age aerosol content from East Antarctic ice core samples and past wind strength' Nature, 293, Nr. 5831, 391-394

PETRIN, M.F. 1975 'A computer model of radar echo sounding of multi-layer stratified media' M.S. thesis, University of New Hampshire.

PORTER, S.C. 1981 'Recent glacier variations and volcanic eruptions' Nature, 291, Nr. 5811, 139-142

RAMPINO, M.R., SELF, S. and FAIRBRIDGE, R.W. 1979 'Can rapid climatic change cause volcanic eruptions?' Science, 206, 826-828

REEH, N., CLAUSEN, H.B., DANSGAARD, W., GUNDESTRUP, N., HAMMER, C.U. and JOHNSEN, S.J. 1978 'Secular trends of accumulation rates at three Greenland stations' Journal of Glaciology, 20, Nr. 82, 27-30

REYNOLDS, J.M. and PAREN, J.G. 1980 'Recrystallisation and the electrical behaviour of glacier ice' Nature, 283, Nr. 5742, 63-64

RITZ, C., LLIBOUTRY, L. and RADO, C. (in press) 'Analysis of a 870 m deep temperature profile at Dome C' Accepted by Annals of Glaciology, 3

ROBIN, G. de Q. 1975 'Velocity of radio waves in ice by means of a bore-hole interferometric technique' Journal of Glaciology, 15, Nr. 73, 151-159

ROBIN, G. de Q., DREWRY, D.J. and MELDRUM, D.T. 1977 'International studies of ice sheet and bedrock' Phil. Trans. Roy. Soc. B, 279, 185-196

ROBIN, G. de Q., EVANS, S. and BAILEY, J. 1969 'Interpretation of radio echo sounding in polar ice sheets' Phil. Trans. Roy. Soc. A, 265, Nr. 1166, 437-505

ROBIN, G. de Q. and MILLAR, D.H.M. (in press) 'Flow of ice sheets in the vicinity of subglacial peaks' Accepted by Annals of Glaciology, 3

ROBIN, G. de Q, SWITHINBANK, C.W.M. and SMITH, B.M.E. 1970 'Radio echo exploration of the Antarctic ice sheet' Proceedings, International Symposium on Antarctic Glaciological Exploration, Hanover, 1968, IASH Publn. Nr. 86, 472-487

ROBINSON, E.S. 1964 'On the relationship of ice-surface topography to bed topography on the south polar plateau' Journal of Glaciology, 6, Nr. 43, 43-54

ROSE, K.E. 1978 'Radio echo sounding studies of Marie Byrd Land, Antarctica' Unpublished Ph.D. thesis, University of Cambridge.

RUSSELL-HEAD, D.S. and BUDD, W.F. 1979 'Ice-sheet flow properties derived from bore-hole shear measurements combined with ice-core studies' Journal of Glaciology, 24, Nr. 90, 117-130

SHABTAIE, S., BENTLEY, C.R., BLANKENSHIP, D.D., LOVELL, J.S. and GASSETT, R.M. 1981 'Dome C geophysical survey, 1979-80' Antarctic Journal of the United States, 15, Nr. 5, 2-5

SKOU, N. and SONDERGAARD, F. 1976 'A 60 MHz ice sounder system' Electromagnetics Inst., Technical University of Denmark, Lyngby, Report R169

SMITH, B.M.E. 1971 'Radio echo studies of glaciers' Unpublished Ph.D. thesis, University of Cambridge.

SONDERGAARD, F. 1975 'Radioglaciology: surface soundings near DYE-3' Electromagnetics Inst., Technical University of Denmark, Lyngby, Report D258

STEED, R.H.N. 1980 'Geophysical investigations of Wilkes Land, Antarctica' Unpublished Ph.D. thesis, University of Cambridge

STITH, J.L., HOBBS, P.V. and RADKE, L.F. 1978 'Airborne particle and gas measurements in the emissions from six volcanoes' Journal of Geophysical Research, 83, Nr. C8, 4009-4017

SULLIVAN, W. 1981 'Ancient ice yielding secrets of climate' The New York Times, 130, Nr. 45,035, 1 & 24

SZE, N.D. & KO, M.K.W. 1979 'CS_2 and COS in the stratospheric sulphur budget' Nature, 280, Nr. 5720, 308-310

THOMPSON, L.G. 1977 'Variations in microparticle concentration, size distribution and elemental composition found in Camp Century, Greenland, and Byrd Station, Antarctica, deep ice cores' Proceedings, Isotopes & Impurities in Snow & Ice Symposium, Grenoble, 1975, IAHS Publn. Nr. 118, 351-364

THOMPSON, L.G., MOSLEY-THOMPSON, E. and PETIT, J-R. 1979 'Glaciological interpretation of microparticle concentrations from the French 905-m Dome C, Antarctica core' Proceedings, Sea Level, Ice, and Climatic Change Symposium, Canberra, 1979, IAHS Publn. Nr. 131, 227-234

VIEBROCK, H.J. and FLOWERS, E.C. 1968 'Comments on the recent decrease in solar radiation at the South Pole' Tellus, 20, 400-411

WESTPHAL, J.A. 1963 Personal communication in Robin and others (1969)

WHILLANS, I.M. 1976 'Radio-echo layers and the recent stability of the West Antarctic ice sheet' Nature, 264, Nr. 5582, 152-155

WHILLANS, I.M. 1977 'The equation of continuity and its application to the ice sheet near Byrd Station, Antarctica' Journal of Glaciology, 18, Nr. 80, 359-371